# SURFACE-ENHANCED RAMAN SPECTROSCOPY INVESTIGATIONS OF INTERFACIAL CHEMISTRY UNDER POTENTIAL CONTROL

by

Chaoxiong Ma

A dissertation submitted to the faculty of
The University of Utah
in partial fulfillment of the requirements for the degree of

Doctor of Philosophy

Department of Chemistry

The University of Utah

December 2011

# The University of Utah Graduate School

## STATEMENT OF DISSERTATION APPROVAL

The dissertation of **Chaoxiong Ma**

has been approved by the following supervisory committee members:

| | | |
|---|---|---|
| **Joel M. Harris** | , Chair | **7/14/2011** Date Approved |
| **John C. Conboy** | , Member | **7/14/2011** Date Approved |
| **Henry S. White** | , Member | **7/14/2011** Date Approved |
| **Michael D. Morse** | , Member | **7/14/2011** Date Approved |
| **Jan Miller** | , Member | **7/14/2011** Date Approved |

and by **Henry S. White** , Chair of the Department of **Chemistry**

and by Charles A. Wight, Dean of The Graduate School.

# ABSTRACT

Surface-enhanced Raman scattering (SERS) spectroscopy is a sensitive tool that can be used to probe chemistry at metal-solution interfaces. To control the interfacial activity of ionic species at the metal surface, the metal-surface potential is controlled with a potentiostat, while SERS provides an *in situ* method to observe the interfacial chemistry. In this work, SERS studies are carried out with potential control to investigate monolayer self-assembly, acid-base chemistry, ion-pair interactions, and reduction of electroactive anions at chemically-modified silver surfaces.

Adsorption and self-assembly of 11-mercaptoundecanoic acid on silver was monitored by SERS. The time-dependent profiles of Raman spectra indicate a multistep self-assembly process, which involves participation of both thiol and carboxylate groups in the adsorption process and depends on the solvent, solution pH, and surface potential. The acid-base chemistry of 2-mercaptobenzoic acid (2-MBA) immobilized on a silver surface was also investigated. The benzoate form and benzoic acid form of 2-MBA could be identified spectroscopically to determine the relative populations of the bound ligand. In addition, shifts in the carboxylate stretching mode of 2-MBA revealed interactions between the benzoate group and the silver surface, which could be displaced by other anions in solution. It was found that applied potential has significant effects on the proton dissociation equilibrium of immobilized 2-MBA, an effect arising from the changes in the interfacial pH relative to bulk solution.

Adsorption of cetylpyridinium ($CP^+$) and its interaction with nitrobenzenesulfonate ($NB^-$) on a 1-dodecanthiol ($C_{12}$) modified silver surface was also studied. The binding of $NB^-$ to the $C_{12}$ surface relies on its ion-pairing with $CP^+$. Adsorption of $CP^+$ and ion-pair stability on the $C_{12}$ surface can be modulated by electrolyte concentration. The results provide understanding of surfactant adsorption and ion interactions involved in ion-interaction chromatography. SERS and cyclic voltammetry were used to investigate reduction of $NB^-$ on bare and $C_{12}$-modified silver surfaces in the presence of $CP^+$. The reduction was identified by the disappearance of the $NO_2$ symmetric stretching mode and frequency shifts in the ring breathing mode. Ion-pair accumulation of $NB^-$ can be observed on $C_{12}$ surface, and its repeatable reduction was studied by cyclic voltammetry and SERS.

TABLE OF CONTENTS

# ACKNOWLEDGMENTS

I would like to take this opportunity to thank all those people who helped me to finish my research and dissertation over the years.

First of all, I would like to thank my advisor, Dr. Joel Harris for his guidance and support. His enthusiasm and love for science, generosity, patience and willingness to help have always impressed me. His insight and broad knowledge of chemistry have been a tremendous help in my research and have made my graduate study enjoyable. I was extremely fortunate to have him as my mentor during my graduate study and as an advisor for my future career.

Secondly, I am so grateful to everybody in the Harris group for their kindness and support. Eric Peterson provided helpful instruction using the coating system. He was somebody I could count on whenever the system was down or when I encountered a problem in the lab. Emily Heider and Jennifer Ramirez are such encouraging people, giving me a lot of support in my writing. It was such a wonderful experience to have run a marathon with them. Jonathan Schaefer and Grant Myers were always open to help whenever I had a question. Doug Kriech and Jay Kitt helped machining parts and setting up the green laser. Appreciation is also given to Moussa Barhoum, Justin Cooper, Christopher Fox, Joshua Wayment, and all other group members who have been helpful, stimulating and supportive of my research.

I also would like to express my thanks to Jiewen Xiong and Dr. Henry White for their help with the cyclic voltammetry measurements.

Finally, I would like to thank my family for their support of my career. Special thanks are given to my wife, Qili Shen, for her support, understanding and patience through all these years.

This research was supported in part with funds from the U.S. Department of Energy under Grant DE-FG03-93ER14333.

# CHAPTER 1

# INTRODUCTION

## 1.1 Background

Chemistry at liquid/solid interfaces is of increasing interest in research because it is fundamental to many chemical and biochemical systems.[1-21] Adsorption, desorption, and reactions at interfaces are involved in numerous analytical methods[1-6] and heterogeneous catalysis,[12-14] which generally require immobilizing target molecules to the solid surface. Therefore, understanding the chemistry that governs surface reactions and the ability to control the chemical and structural properties of surfaces contribute to advances in chromatography,[1-4, 19, 21] chemical and biological sensing,[1-11] catalysis, and many other techniques. The structure and properties at interfacial regions differ significantly from those in bulk solution, and accordingly, exhibit unique physical processes and chemical reactions compared with the homogeneous phase.[1-5, 20]

The special characteristic of the interface originates largely from the substrates that are used for the immobilization of ligands or other target molecules. Numerous substrates including metals,[1, 2, 5-8] metal oxides,[12, 22, 23] graphite,[3, 24] alumina,[25] mica,[26] silica,[4, 19, 21] and polymers[13] have been employed as supports for interfacial chemistry. The variety of the substrates also leads to huge measurement challenge for probing the chemical structure of the interface. Coinage metals, such as gold or silver, are popular materials that have been used widely not only as electrodes,[1, 7, 8, 27-29] but also as

substrates for surface modification by self-assembly,[1, 5-7, 15-17] providing functionalized surfaces with controllable properties such as wettability,[16, 17, 30] adhesion,[9, 23] redox activity,[7, 15, 18] and biocompatibility.[7, 9, 17]

1.1.1 The metal/aqueous interface and potential modulation

Ionic and electronic processes involved at metal surfaces in contact with an aqueous solution form a charged surface, which polarizes the adjacent aqueous phase and gathers the counter ions so as to minimize the free energy of the interfacial system.[20, 27] As a direct consequence of the charged metal surface, ion accumulation, and the formation of a diffuse double-layer, the interfacial potential is one of the key factors controlling the behavior of both bound and free species at the interface. The interfacial potential, which is determined by the structure of the diffuse double-layer, decays as it propagates into solution. A well-known theory developed by Gouy and Chapman based on a statistical mechanical approach provides an expression for the interfacial potential profile $\phi$ as a function of the distance, *x*, from the electrode surface.[20, 27]

$$\frac{\tanh(ze\phi/4kT)}{\tanh(ze\phi_0/4kT)} = \exp(-\kappa x) \qquad [1.1]$$

where *z* is the magnitude of the charge on ions, *e* is the charge of the electron, *k* is the Boltzmann constant, *T* is the absolute temperature, and $\kappa$ is the reciprocal of the characteristic thickness of the diffuse layer. $1/\kappa$ is also referred to as the "Debye length." with dimensions of distance and can be calculated by,[20, 27]

$$\frac{1}{\kappa} = \left( \frac{\varepsilon\varepsilon_0 kT}{e^2 \sum n_i z_i^2} \right)^{1/2} \qquad [1.2]$$

where $\varepsilon$ is the dielectric constant of the medium, $\varepsilon_0$ is the permittivity of free space, and $n_i$ is the number concentration of ion *i* in the bulk solution. In case of a small applied potential $\phi_0$ ($\phi_0 < 50/z$ mV), the expression of the potential profile (eq 1.1) can be approximated by:

$$\phi = \phi_0 \exp(-\kappa x) \qquad [1.3]$$

For small applied potentials, the interfacial potential decays by a factor of 1/e at a distance of $1/\kappa$ from the electrode surface. The value of $1/\kappa$ is inversely proportional to the square of the electrolyte concentration and drops off very rapidly as the concentration of electrolyte increases. $1/\kappa$ also depends directly on the valency (z) of the ions involved. For a 1:1 electrolyte, $1/\kappa$ has a value of 0.3 and 30 nm for a 1.0 M and $1\times10^{-4}$ M solutions. Figure 1.1 gives the potential profile calculated from eq 1.3 for a 1:1 electrolyte at several different electrolyte concentrations. It is obvious that the higher the electrolyte concentration, the faster the decay of potential from the electrode surface.

The Poisson-Boltzmann equation (eq 1.4) predicts the activity of the ions ($a_{i,x}$) at a distance x away from a charged surface depending on the interfacial potential.[20, 27]

$$a_{i,x} = a_i^0 \exp\left(\frac{-zF\Phi_x}{RT}\right) \qquad [1.4]$$

In eq 1.4, $a_i^0$ is ion activity of the bulk solution and $\Phi_x$ is the potential at the distance x, and z is the charge of the ion. The exponential relationship of this equation shows that small variations in the potential can result in large changes in the interfacial ion activity and, thereby, perturb the binding equilibria of ionic species.

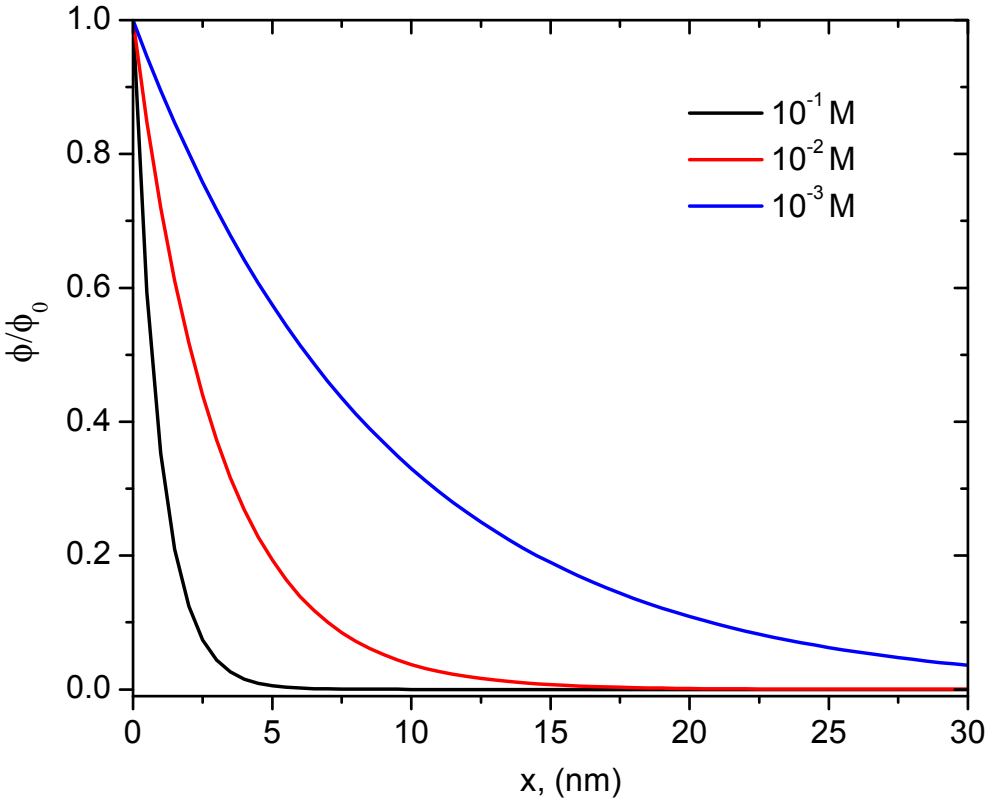


Figure 1.1 The decay of interfacial potential with distance from a surface in different electrolyte concentrations

In addition to its effect on the interfacial ion activity, the decay of interfacial potential generates an electric field that can affect the electronic structure of immobilized ligands, and consequently, their binding affinity for species in solution.[1, 2, 8, 16] The influence of the potential and electric field on interfacial processes has been widely investigated and exploited successfully for many different applications. For example, Porter et al. have demonstrated the utility of electrochemical modulation for modifying the retention of ionic species on graphite electrode surfaces.[3, 31, 32] The applied potential altered the interaction of charged analytes with the carbon surface, changing their retention. The technique was applied successfully to manipulate separations in chromatography without the need for changes in mobile phase composition. Lahann et al. have reported control of surface properties based on the conformational transition of 16-mercapto-hexadecanoic acid immobilized on gold.[16] An applied positive potential attracts the negatively charged carboxylate groups toward the gold surface, leading to a switch in surface wettability as the hydrophobic chains undergo conformational changes. The same concept has been applied successfully to manipulate the binding and unbinding of a protein on a monolayer modified surface using applied potential for control.[11] Kelley et al. found that the orientation of self-assembled DNA duplexes on the surface undergo a dramatic morphology change as a function of potential.[8] The helices stand perpendicularly or lie flat on the metal surface depending on the applied potential. Hybridization and dehybridization of DNA immobilized on electrode surfaces modulated by electric field have been demonstrated by fluorescence,[33] surface plasmon resonance,[34] and surface-enhanced Raman spectroscopy.[35] Oklejas et al. developed a probe to measure electric fields in the diffuse double-layer based on SERS detection of the vibrational

Stark effect from nitrile-terminated monolayers on silver surfaces.[36, 37] They also used the electric fields to exert control over the tautomerization of the ligand immobilized on silver surface, shifting the equilibrium of metal ion complexation.[1] Burgess et al. demonstrated that protonation/deprotonation of self-assembled monolayers of carboxylic acid-terminated thiols can be driven by electric fields as investigated with electrochemical impedance spectroscopy, cyclic voltammetry, and Fourier transform infrared spectroscopy.[38, 39] The effect of the applied potential on the charge-transfer contribution to the adsorption free energy has been utilized successfully to control the adsorption and desorption of the n-alkanethiolates on Ag surface from aqueous solution.[40-42] The electrochemical and SERS measurement provide information about the chemisorption free energy and the capability to control the accumulation of molecules on the surface using applied potentials.[40-42]

Previous studies have demonstrated the advantages of potential control by electrochemical methods for the investigation of metal/solution interfaces. With potential control, the variations in interfacial properties that would arise from an uncontrolled surface potential are minimized and more consistent and reproducible results can be obtained. Additionally, the applied potential affords an opportunity to change the activity of ions at the interface. The interfacial activities of target analytes can be adjusted *in situ* to manipulate the bulk concentration response range of an immobilized ligand. Manipulation of surface ligand electronic structure and conformation is another tool allowed by controlling the applied potential. This manipulation may shift the equilibrium to favor a desired product, or to turn a sensor on and off.[1, 11, 16, 18] By quickly and reversibly perturbing interfacial equilibria, potential control may also be used in kinetic

studies of interfacial ion-binding equilibria when combined together with time-resolved detection techniques.[1, 11, 16, 18] In short, potential control may be employed for analytical measurements at interfaces with improved sensitivity, dynamic range, speed, and reproducibility.

1.1.2 Surface enhanced Raman spectroscopy

Surface enhanced Raman spectroscopy (SERS) is a surface-sensitive technique that provides vibrational information about molecules adsorbed or bound to coinage metal surfaces with significant enhancement of Raman scatting.[43-46] The overall enhancement factor is typically observed on the order of $10^4$-$10^6$, and can be as high as $10^8$ and $10^{14}$ under favorable circumstances.[43-46] The SERS effect was first observed from the adsorption of pyridine on an electrochemically roughened silver electrode by Fleischmann et al. in 1974.[47] They attributed the huge boost of the Raman signal to the increase of surface area of Ag electrode by roughening process, which however could not account for magnitude of the signal enhancement. More credit for the SERS discovery[48, 49] was given later to Van Duyne and Creighton et al., who independently pointed out that an enhancement of the scattered intensity was involved in the adsorption process, and proposed two different theories to explain the enhancement effect. In 1978, Moskovits suggested that the unusually increased intensity of the Raman signals could be a consequence of the excitation of surface plasmons.[50] This idea led to a number of predictions about potentially SERS-active substrates, their relative enhancements, nanoscale structural features of substrates that are required for SERS to occur. These predictions were subsequently confirmed by experimental results.

Although the mechanisms leading to the phenomenal enhancement of Raman scattering intensity are still under investigation, two mechanisms are commonly cited by

the researchers to describe the enhancement effect.[43-46, 48-50] The primary one that contributes to ~$10^4$ of enhancement is electromagnetic enhancement[43-46, 49] (EM), which involves increases in the excitation and scattering field intensities as a result of plasmon resonance excitation. When interacting with a rough metal, an electromagnetic wave can excite localized plasmons on the metal surface, resulting in amplification of the electromagnetic fields near the surface. The enhancement in the EM model is a direct consequence of the interaction of adsorbed molecules with the amplified electromagnetic fields. The intensity of the Raman scattering is proportional to the square of the amplitude of the electric field of light incident on the adsorbate. Using a simplified model, the enhancement factor $E$ of the Raman signal is given by,[44, 45]

$$E = |E(\omega)|^2 |E(\omega')|^2 \qquad [1.5]$$

where $E(\omega)$ and $E(\omega')$ are the local electric-field enhancement factors at the incident frequency, $\omega$, and Stockes-shifted frequency, $\omega'$, respectively. It comes as no surprise from the above equation that a small increase in the local field can lead to such huge enhancement in the Raman scattering.

The presence of EM depends strongly on the roughness features of the metal surface. Only when the surface roughness is small in comparison to the wavelength of the incident light will excitation of the plasmon occur. In addition, visible and near-infrared radiation commonly employed for Raman spectroscopy restricts the choice of the metals to silver, copper, and gold so as to satisfy the resonance condition to provide maximal enhancement.

The electromagnetic field involved in Raman scattering that has a maximum at the metal surface decays rapidly in strength with distance from the surface. As a consequence, the enhancement falls off according to:[44, 45]

$$G = \left( \frac{r}{r+d} \right)^{12} \qquad [1.6]$$

where $r$ is the radius of the spherical of the metal roughness feature and $d$ is the distance of scattering molecules from the metal surface. Experimental results also showed that the enhancement decreases ten-fold for the analytes with a distance of 2-3 nm away from substrate surface. This distance-dependent effect of the enhancement makes SERS a surface-selective and powerful tool of for investigating on the interfacial processes with little interference from the bulk solution.

A second mechanism called chemical enhancement[43-46, 48] (CE) provides an order of magnitude or two of enhancement to the Raman scattering intensity. The CE mechanism requires direct interaction of the molecules with the metal surface to allow charge transfer between the molecules and the metal substrate to occur, which leads to an increase in the Raman scattering cross-section or polarizability of the molecules and boosts the Raman intensity. This mechanism can be explained by the resonance Raman effect,[43, 51] which assumes that the Fermi level of the metal is half way between the highest occupied orbital and lowest unoccupied orbital of the adsorbate, acting as a bridge to lower the energy required for the excitation to occur. As a result, this charge transfer interaction shifts the transition of the molecules that have lowest-lying excitation at the near ultraviolet region into the visible region, offering a possibility for resonance Raman scattering to occur in typical wavelength region of Raman excitation.

## 1.2 Overview

The applications of surface-enhanced Raman spectroscopy have grown dramatically since its discovery more than 30 years ago. The overall enhancement of Raman scattering intensity in SERS measurements can range from $10^6$ -$10^{14}$, making it sensitive enough for detection of a submonolayer coverage of molecules at an interface.[29, 35-37, 43-46] In addition, only those molecules immobilized or close enough to the substrate surface experience signal enhancement; accordingly, SERS is specific for interfacial detection.[43, 45, 46] Furthermore, SERS is compatible with measurements in aqueous solution making it especially useful for analysis of biological systems.[5-7] SERS has been widely used as a molecular probe for the detection of acid/base equilibria,[5, 6, 38] metal-ions binding reactions,[1, 2] glucose accumulation at selective surface coating,[52, 53] and protein and DNA binding to immobilized biological ligands.[7, 35, 54, 55]

In this research, SERS was employed to investigate molecular structure, properties, adsorption, and interactions at the metal/solution interface; and to investigate how an applied potential can be employed to control ion activity and the self-assembly kinetics on a surface. These studies may provide insight into the understanding of interfacial phenomena and lay groundwork for the development of new sensors with controlled sensitivity, selectivity, and reversibility.

In Chapter 2, adsorption of 11-mercaptoundecanoic acid (MUA) on silver from both aqueous and methanol solutions was monitored *in situ* by surface-enhanced Raman spectroscopy (SERS). Raman spectra reveal that in addition to the thiol group, the carboxylate group of MUA also interacts with the silver surface during the self-assembly process. Several bands including the $\nu$(C-S), $\nu_s(COO^-)$ and $\nu$(C-C) were used to describe

the evolution of the structure of adsorbed MUA on silver surfaces. The time-dependent profiles of these bands indicate a multistep process, which in the case of aqueous solutions is initiated by the binding of both carboxylate and thiol groups to the silver surface, producing a mixture of gauche and trans conformations. In a subsequent step, the COO-Ag is displaced by the S-Ag, a relatively stronger bond, leading to ordering of the resulting monolayer with formation of a complete SAM with all-trans conformations. This study also showed that the adsorption process depends strongly on the solvent, solution pH, and surface potential of the metal. These factors can significantly affect the participation and displacement of $–COO^-$ during the assembly process.

In Chapter 3, SERS was used to investigate the potential effect on acidic/basic properties of 2-mercaptobenzoic acid (2-MBA) immobilized on silver surfaces. The $COO^-$ bending mode of the benzoate form and the C-COOH stretching mode of the benzoic acid form of 2-MBA were employed to determine the relative deprotonated and protonated populations of the bound ligand, respectively. In addition, shifts in the symmetric carboxylate stretching mode of 2-MBA reveal interactions between the silver surface and benzoate group, which could be displaced by acetate and other buffer anions from solution. It was found that the applied potential has a significant effect on the proton dissociation equilibrium of immobilized 2-MBA. This effect arises from the surface potential governing the activity of protons at the interface, which changes the interfacial pH relative to bulk solution. The results were fit to a Poisson-Boltzmann model, corrected for potential distribution across monolayer and for interactions between adjacent immobilized ligands. The results show a significant increase in the intrinsic p$K_a$ of the immobilized ligand compared to the 2-MBA in free solution, which is likely due to

an increase in electron density on the benzoic acid group that occurs upon binding of the thiol group to the silver surface. The study provides a clear picture for the potential effect on protonation/deprotonation of immobilized acid/base molecules. It demonstrates control of interfacial properties using applied potential.

In Chapter 4, the adsorption of cetylpyridinium ($CP^+$) and its interaction with nitrobenzenesulfonate ($NB^-$) on 1-dodecanthiol ($C_{12}$) modified silver surface was studied by SERS. The electrolyte effect on the adsorption equilibrium of $CP^+$ on the $C_{12}$ surface was investigated. Frumkin and Langmuir isotherms can be used to describe the adsorption process in the absence and presence of KCl, respectively. The binding of the $NB^-$ to the $C_{12}$ surface relies strongly on the presence of $CP^+$, which is observed to form an ion-pair complex with $NB^-$ in the solution phase. The influence of several anions on the binding of $NB^-$ to the $C_{12}$ surface in the presence of $CP^+$ provided their binding affinity with $CP^+$. The concentration effect of $CP^+$ on the adsorbed $NB^-$ showed a bell shape dependence that is commonly observed for the effect of an ion-interaction regent on the retention of ionic analytes. The plot was quantitatively fit by a dynamic ion exchange model with the presence of ion-pairs in the solution phase. The study demonstrated SERS to be a useful technique to investigate surfactant adsorption and ion interactions at the interface, and to provide information for retention mechanism in ion-interaction chromatography.

In Chapter 5, ion pair interactions were used to concentrate $NB^-$ near a $C_{12}$ modified silver surface. Electrochemical reduction of surface-bound $NB^-$ was measured by both SERS and cyclic voltammetry. The decrease and then disappearance of the $\nu_s(NO_2)$ mode, and the shift of ring breathing mode $\nu_{12}$ are two distinctive features

observed in the reduction process. Similar to electrochemical reduction of nitrobenzene, the reduction of $NB^-$ on $C_{12}$ surface involves complex pathway and is strongly pH dependent. Differences in reversibility were observed for the reduction on $C_{12}$ surface compared to reduction on a bare Ag electrode. For the reduction of $NB^-$ on a $C_{12}$ surface with the ion-pair protocol, recovery of the adsorbate ($NB^-$) was observed upon removal of the applied potential, which was not seen for the reduction of $NB^-$ on a bare Ag surface. The study showed that protection of the hydrophobic monolayer allows repeatable measurements on the same electrode surface, because the adsorption of the analyte is reversible. In addition, selective adsorption and redox reaction at the interface is possible by using ionic surfactant with strong affinity for the target analyte.

## 1.3 References

(1) Oklejas, V.; Uibel, R. H.; Horton, R.; Harris, J. M. *Analytical Chemistry* **2008**, *80*, 1891-1901.

(2) Uibel, R. H.; Harris, J. M. *Analytical Chemistry* **2002**, *74*, 5112-5120.

(3) Keller, D. W.; Porter, M. D. *Analytical Chemistry* **2005**, *77*, 7399-7407.

(4) Deinhammer, R. S.; Shimazu, K.; Porter, M. D. *Anal. Chem.* **1991**, *63*, 1889-1894.

(5) Talley, C. E.; Jusinski, L.; Hollars, C. W.; Lane, S. M.; Huser, T. *Analytical Chemistry* **2004**, *76*, 7064-7068.

(6) Bishnoi, S. W.; Rozell, C. J.; Levin, C. S.; Gheith, M. K.; Johnson, B. R.; Johnson, D. H.; Halas, N. J. *Nano Letters* **2006**, *6*, 1687-1692.

(7) Murgida, D. H.; Hildebrandt, P. *Journal of the American Chemical Society* **2001**, *123*, 4062-4068.

(8) Kelley, S. O.; Barton, J. K.; Jackson, N. M.; McPherson, L. D.; Potter, A. B.; Spain, E. M.; Allen, M. J.; Hill, M. G. *Langmuir* **1998**, *14*, 6781-6784.

(9) Nyquist, R. M.; Eberhardt, A. S.; Silks, L. A.; Li, Z.; Yang, X.; Swanson, B. I. *Langmuir* **2000**, *16*, 1793-1800.

(10) Holmlin, R. E.; Chen, X.; Chapman, R. G.; Takayama, S.; Whitesides, G. M. *Langmuir* **2001**, *17*, 2841-2850.

(11) Liu, Y.; Mu, L.; Liu, B.; Zhang, S.; Yang, P.; Kong, J. *Chem. Commun.* **2004**, 1194-1195.

(12) Gong, D.; Subramaniam, V. P.; Highfield, J. G.; Tang, Y.; Lai, Y.; Chen, Z. *ACS Catal.*, ACS ASAP.

(13) Schreiner, E.; Nair, N. N.; Wittekindt, C.; Marx, D. *J. Am. Chem. Soc.*, *133*, 8216-8226.

(14) Feller, B. E.; Kellis, J. T.; Cascao-Pereira, L. G.; Robertson, C. R.; Frank, C. W. *Langmuir*, *27*, 250-263.

(15) Smith, R. K.; Lewis, P. A.; Weiss, P. S. *Progress in Surface Science* **2004**, *75*, 1-68.

(16) Lahann, J.; Mitragotri, S.; Tran, T.-N.; Kaido, H.; Sundaram, J.; Choi, I. S.; Hoffer, S.; Somorjai, G. A.; Langer, R. *Science* **2003**, *299*, 371-374.

(17) Schouten, S.; Stroeve, P.; Longo, M. L. *Langmuir* **1999**, *15*, 8133-8139.

(18) Matthews, J. R.; Tuncel, D. n. s.; Jacobs, R. M. J.; Bain, C. D.; Anderson, H. L. *Journal of the American Chemical Society* **2003**, *125*, 6428-6433.

(19) Gasser-Ramirez, J. L.; Harris, J. M. *Anal Chem*, *82*, 5743-5750.

(20) Myers, D. *Surface, Interface, and Colloids: Principles and Application*, 2nd ed.; Wiley-VCH: New York, 1999.

(21) Sood, S. P.; Sartori, L. E.; Wittmer, D. P.; Haney, W. G. *Anal. Chem.* **1976**, *48*, 796-798.

(22) Schulz, J. C.; Warr, G. G. *Langmuir* **2002**, *18*, 3191-3197.

(23) Bohmer, M. R.; Koopal, L. K. *Langmuir* **1992**, *8*, 2660-2665.

(24) Kiraly, Z.; Findenegg, G. H.; Klumpp, E.; Schlimper, H.; Dekany, I. *Langmuir* **2001**, *17*, 2420-2425.

(25) Fan, A.; Somasundaran, P.; Turro, N. J. *Langmuir* **1997**, *13*, 506-510.

(26) Atkin, R.; Craig, V. S. J.; Wanless, E. J.; Biggs, S. *Adv Colloid Interface Sci* **2003**, *103*, 219-304.

(27) Bard, A. J.; Faulkner, L. R. *Electrochemical Methods: Fundamentals and Applications*; Wiley: New Jersey, 2000.

(28) Gerlache, M.; Senturk, Z.; Quarin, G.; Kauffmann, J.-M. *J. Solid State Electrochem.* **1997**, *1*, 155-160.

(29) Gao, P.; Gosztola, D.; Weaver, M. J. *J. Phys. Chem.* **1988**, *92*, 7122-7130.

(30) Love, J. C.; Estroff, L. A.; Kriebel, J. K.; Nuzzo, R. G.; Whitesides, G. M. *Chemical Reviews* **2005**, *105*, 1103-1170.

(31) Deinhammer, R. S.; Ting, E.-Y.; Porter, M. D. *Anal. Chem.* **1995**, *67*, 237-246.

(32) Ting, E.-Y.; Porter, M. D. *Anal. Chem.* **1997**, *69*, 675-678.

(33) Sosnowski, R. G.; Tu, E.; Butler, W. F.; O'Connell, J. P.; Heller, M. J. *Proc. Natl. Acad. Sci. U. S. A.* **1997**, *94*, 1119-1123.

(34) Heaton, R. J.; Peterson, A. W.; Georgiadis, R. M. *Proc. Natl. Acad. Sci. U. S. A.* **2001**, *98*, 3701-3704.

(35) Mahajan, S.; Richardson, J.; Brown, T.; Bartlett, P. N. *J. Am. Chem. Soc.* **2008**, *130*, 15589-15601.

(36) Oklejas, V.; Sjostrom, C.; Harris, J. M. *J. Am. Chem. Soc.* **2002**, *124*, 2408-2409.

(37) Oklejas, V.; Sjostrom, C.; Harris, J. M. *J. Phys. Chem. B* **2003**, *107*, 7788-7794.

(38) Burgess, I.; Seivewright, B.; Lennox, R. B. *Langmuir* **2006**, *22*, 4420-4428.

(39) Rosendahl, S. M.; Burgess, I. J. *Electrochim. Acta* **2008**, *53*, 6759-6767.

(40) Hatchett, D. W.; Uibel, R. H.; Stevenson, K. J.; Harris, J. M.; White, H. S. *J. Am. Chem. Soc.* **1998**, *120*, 1062-1069.

(41) Hatchett, D. W.; Stevenson, K. J.; Lacy, W. B.; Harris, J. M.; White, H. S. *J. Am. Chem. Soc.* **1997**, *119*, 6596-6606.

(42) Uibel, R. H.; Harris, J. M. *Appl. Spectrosc.* **2004**, *58*, 934-944.

(43) Campion, A.; Kambhampati, P. *Chem. Soc. Rev.* **1998**, *27*, 241-250.

(44) Otto, A.; Mrozek, I.; Grabhorn, H.; Akemann, W. *J. Phys.: Condens. Matter* **1992**, *4*, 1143-1212.

(45) Kneipp, K.; Kneipp, H.; Moskovits, M.; Editors *Surface-Enhanced Raman Scattering: Physics and Applications*; Springer GmbH: New York, 2006.

(46) Garrell, R. L. *Anal. Chem.* **1989**, *61*, 401A-402A, 404A, 406A-408A, 410A-411A.

(47) Fleischmann, M.; Hendra, P. J.; McQuillan, A. J. *Chem. Phys. Lett.* **1974**, *26*, 163-166.

(48) Albrecht, M. G.; Creighton, J. A. *J. Am. Chem. Soc.* **1977**, *99*, 5215-5217.

(49) Jeanmaire, D. L.; Van, D. R. P. *J. Electroanal. Chem. Interfacial Electrochem.* **1977**, *84*, 1-20.

(50) Moskovits, M. *J. Chem. Phys.* **1978**, *69*, 4159-4161.

(51) Lombardi, J. R.; Birke, R. L.; Lu, T.; Xu, J. *J. Chem. Phys.* **1986**, *84*, 4174-4180.

(52) Yonzon, C. R.; Haynes, C. L.; Zhang, X.; Walsh, J. T., Jr.; Van, D. R. P. *Anal. Chem.* **2004**, *76*, 78-85.

(53) Shafer-Peltier, K. E.; Haynes, C. L.; Glucksberg, M. R.; VanDuyne, R. P. *J. Am. Chem. Soc.* **2003**, *125*, 588-593.

(54) Habuchi, S.; Cotlet, M.; Gronheid, R.; Dirix, G.; Michiels, J.; Vanderleyden, J.; De, S. F. C.; Hofkens, J. *J. Am. Chem. Soc.* **2003**, *125*, 8446-8447.

(55) Porter, M. D.; Lipert, R. J.; Siperko, L. M.; Wang, G.; Narayanan, R. *Chem. Soc. Rev.* **2008**, *37*, 1001-1011.

# CHAPTER 2

# SURFACE-ENHANCED RAMAN SCATTERING STUDY OF THE KINETICS OF SELF-ASSEMBLY OF CARBOXYLATE-TERMINATED N-ALKANETHIOLS ON SILVER

## 2.1 Introduction

N-alkanethiol self-assembled monolayers (SAMs) on metal substrates have been widely used in controlling the surface properties with numerous applications, such as corrosion inhibition, colloidal stabilization, and molecular sensors.[1-4] Understanding their structure as well as their mechanism of formation can help to control the assembly and properties of the resulting monolayers, which are crucial for their applications. Many different techniques, including scanning tunneling microscopy,[5-7] surface plasmon resonance,[8] atomic force microscopy,[9] infrared spectroscopy,[10, 11] quartz-crystal microbalance,[12] and Raman spectroscopy,[13, 14] have been utilized to elucidate the formation and structure of self-assembled monolayers. In previous studies, the assembly of n-alkanethiols on metal surface has been studied extensively, and a two-step assembly process (initial adsorption, then annealing to an organized structure) is most often reported to describe the monolayer formation.[5, 8, 9, 11, 12, 14]

Upon the formation of a monolayer, the properties of the resulting modified surface are mainly governed by the terminal function group of the organothiol used to

form the SAM.[3, 4] The widespread application of these structures is largely owing to the variety of terminal functional groups available as organothiols. Specifically, substrates with desired surface properties can be developed by varying the terminal functional groups of the monolayer and controlling solution conditions in order to produce changes in the functional-group response.[3, 4,15-21] For example, carboxylic acid-terminated thiols have been used to produce hydrophilic surfaces for many applications based on the response of $-COO^-$ group to external conditions.[16-18] Carboxylate-terminated SAMs have been employed to immobilize biological macromolecules on electrodes without denaturation by preventing direct contact of the molecules with the metal surface.[16-18] Carboxylate-terminated SAMs have also has been utilized as molecular probes to measure the pH at a solid/liquid interface or inside a living cell using a nanoparticle surface-enhanced Raman scattering probe.[22] A reversible switching surface, responsive to changes in the applied potential, has been designed based on a 16-mercaptohexadecanoic acid SAM,[23] the surface charge and wettability of which could be modulated by adjusting the applied potential relative to solution.[23] This technique has also been applied to electrochemically controlling the binding and unbinding of a protein to a surface.[24, 25]

Despite the widespread use of carboxylate-terminated SAMs in a variety of interesting applications, the formation kinetics of carboxylate-n-alkanethiol SAMs on metal surfaces have not been fully elucidated, because the role of the terminal functional group in the adsorption has not been taken into account in previous studies.[6, 9, 10] The carboxylate group has demonstrated capability of interacting with metal surfaces via the oxygen lone-pair or $\pi$ electrons,[23-27] a well characterized example of which is the adsorption of stearic-acid on silver or other metallic surfaces.[28-30] Several previous

studies have investigated the structure of carboxylate-terminated n-alkanethiol SAMs;[6, 9, 10, 31, 32] however, the participation of carboxylate groups in the adsorption and formation of the monolayer has not been reported. The techniques used in these previous studies could not detect interactions of the -$COO^-$ group with the substrate, nor were the kinetic measurements, where intermediate steps involving the carboxylate group could be observed. Investigating the role of the carboxylate group in monolayer adsorption, with control of the solution composition, pH, and the surface potential, can provide useful information for understanding the self-assembly process and for controlling the properties of the resulting monolayer.

In this work, we investigate the self-assembly of 11-mercaptoundecanoic acid (MUA) on a silver surface from both aqueous and methanol solutions. MUA was chosen because it has relatively high aqueous solution solubility, and it is reported to form compact SAMs on metal surfaces.[4] Surface-enhanced Raman scattering (SERS) spectroscopy was employed because of its interfacial selectivity, so that the measurements exhibit little interference from the bulk solution.[13, 14] In addition, the interactions of the carboxylate and thiol groups with the silver substrate and n-alkane conformational changes during the adsorption process are readily elucidated using the vibrational spectroscopic information provided by SERS. The influence of several factors, including solvent composition, solution pH, and the potential of the metal surface, on the involvement of the carboxylate group in the assembly process were investigated. Time-dependent profiles of several vibration bands including the $\nu$(C-S), $\nu$(C-C), and $\nu_s(COO^-)$ bands, which are informative of thiol binding, conformational

changes, and carboxylate-silver interactions, were used to characterize the process of adsorption and assembly of MUA monolayers on silver surfaces.

## 2.2 Experimental

### 2.2.1 Substrate pretreatment and solution preparation

All the electrodes were constructed from silver rod (99.999%, 7mm diameter, Alfa Aesar). Silver surfaces of the electrodes were polished with 800, 1500 and 2000 grit silicon carbide paper (3M, MN) and then with alumina polishing slurries (1.0 μm) on microfiber polishing cloth (Buehler Ltd., Illinois). The electrodes were then cleaned and roughened by oxidation-reduction cycles in 0.1 M KCl solution, using 3 sweeps from +0.3 V to –0.3 V and back to +0.3 V (relative to a Ag/AgCl reference) at a fixed rate of 15 mV/s, and then holding on the last cycle at –0.3 V for 2 min. The electrodes were then removed from the cell and rinsed with DI water prior to self-assembly experiments. The roughening procedures and all potential-controlled experiments were conducted in a three-electrode cell. SERS substrates on glass were prepared using metal-film-over-nanosphere (MFON) technique.[33] Specifically, glass slides coated with 220-nm carboxyl polystyrene latex nanospheres (Interfacial Dynamics Corp., Portland) by spin-coating; 20 nm of silver was then deposited on the nanosphere array using an Edwards coating system (Edwards Vacuum Ltd., England). A chamber pressure between $1 \times 10^{-5}$ to $3 \times 10^{-5}$ torr was maintained during the deposition; the silver layer was deposited at a rate of ~0.1 nm/s by heating silver shot (99.99%, Alpha Aesar) in a tungsten boat (R. D. Mathis, CA). Deposition rate and film thickness were monitored using quartz crystal microbalance and Edwards FTM5 thickness monitoring system. Using this

procedure, semitransparent substrates (AgFON), which can be used for both SERS and UV-vis adsorption measurements, are obtained.

11-Mercaptoundecanoic acid (MUA, 97%) was used as received from Sigma-Aldrich. MUA was dissolved in methanol to make a 10 mM solution, and then diluted to 0.1 mM with aqueous buffer or methanol, aqueous buffer solutions. The buffer solutions of pH 2.6 to 10.0 were prepared from the solution of 1.0mM $NaH_2PO4$ or $Na_2HPO_4$ and titrated with 1.0 M NaOH or 1.0 M $HClO_4$ solutions to a desired pH, which was measured by a pH meter (AB15, Fisher Scientific).

2.2.2 Surface-enhanced Raman spectroscopy

Surface-enhanced Raman spectra were acquired using a PI-200 Raman Analyzer (Process Instruments) with a 785-nm diode laser and fiber-optic probe. The laser power on the substrate was 260 mW, and the integration time was 10 s for all measurements. Electrochemical SERS experiments were conducted in a three-electrode cell using a potentiostat (RDE4, Pine Inc.) for potential control. An Ag/AgCl electrode (EE009, Cypress Systems Inc.) and a platinum mesh (0.1 mm diameter and 25 mm x 25 mm, Alpha Aesar) were used as reference and counter electrode, respectively.

2.2.3 UV/Vis spectrometry

UV/Vis extinction measurements were recorded on a Hitachi U-3000 spectrophotometer with a slit width of 2 nm. The spectra were measured in the 350 nm to 900 nm wavelength ranges using a 300 nm/min scan rate. The time-scan measurements on 785 nm were recorded one data point per second for 30 min.

## 2.3 Results and Discussion

### 2.3.1 Raman spectroscopy of 11-mercaptoundecanoic acid on silver

A surface-enhanced Raman scattering (SERS) spectrum of MUA on a silver surface is compared with conventional Raman spectrum of solid 11-Mercaptoundecanoic acid (MUA) in Figure 2.1. It can be seen that the SERS spectrum is different from the bulk spectrum in both the number of bands and their relative intensities. These differences arise from chemical interactions of MUA with the silver surface, which lead to frequency shifts and selective mode enhancements, where the observed SERS intensity for specific vibrational modes depends on the proximity and orientation of MUA relative to the silver surface.[34-37] Accordingly, the observed spectral differences can provide useful information about the interactions of the MUA with silver during the adsorption process.

The vibration modes of MUA and their assignments[26, 27, 38-41] are listed in Table 2.1. Several bands that are sensitive to adsorption to silver surfaces, including $\nu(C{-}S)_G$ at 630 $cm^{-1}$, $\nu(C\text{-}C)_T$ at 1099$cm^{-1}$ and $\nu_s(COO\text{-}Ag)$ at 1394 $cm^{-1}$, can be used to characterize the adsorption process. Both $\nu(C{-}S)_G$ and $\nu(C\text{-}C)_T$ give information about the conformational state of the adsorbed molecules on the silver surface, while the latter also shows the compactness of the MUA monolayer. The band at 1394 $cm^{-1}$ is assigned to the symmetric stretching mode of $COO^-$ when the carboxylate group is bound to silver (COO-Ag).[26, 27, 41, 42] The carboxylate group can interact with silver, [26, 27, 41, 42] which lowers the symmetric stretching frequency of the carboxylate group, $\nu_s(COO^-)$, from $1420 \pm 10$ $cm^{-1}$ to $1395 \pm 10$ $cm^{-1}$. As a test of this assignment, the Raman spectra of solid sodium acetate and sodium laurate are compared with their corresponding SERS spectra

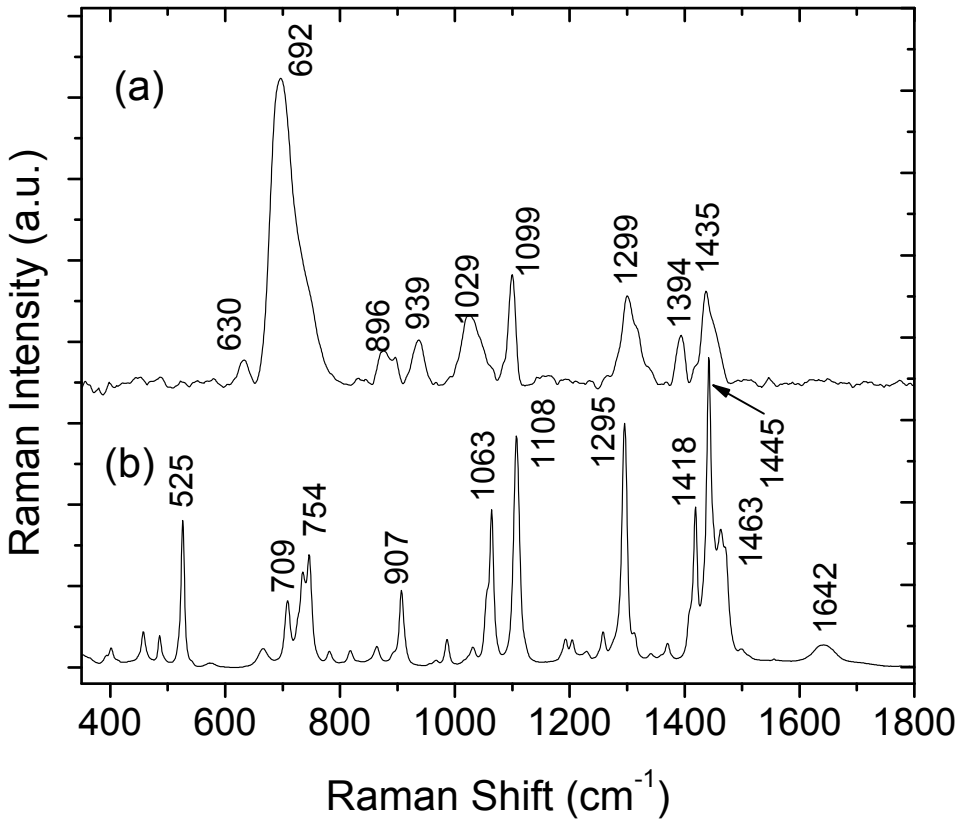


Figure 2.1. Surface-enhanced Raman scattering (SERS) spectrum of MUA on a silver surface (a), compared with an ordinary Raman spectrum of solid MUA (b).

Table 2.1.

Assignment of MUA vibrational modes for interpreting its adsorption and assembly on silver surfaces.

| Solid MUA $cm^{-1}$ | MUA on silver (SERS), $cm^{-1}$ | Assignment | Reference |
|---|---|---|---|
| 525 | | $\rho(COO)$ | 40 |
| 666 | 630 | $\nu(C\text{-}S)_G$ | 38,39,41 |
| 733 | 692 | $\nu(C\text{-}S)_T$ | 38,39,41 |
| 907 | 896 | $\nu(C\text{-}COOH)$ | 38 |
| | 939 | $\nu(C\text{-}COO^-)$ | 26,38,41,42 |
| | 1029 | $\rho(CH_3)_T$ | 39 |
| 1063 | | $\nu(C\text{-}C)_T$ | 26,39 |
| 1108 | 1099 | $\nu(C\text{-}C)_T$ | 26,39 |
| 1295 | 1299 | $\omega(CH)_2$ | 39,41 |
| | 1394 | $\nu(COO\text{-}Ag)$ | 26,27,41,42 |
| 1418 | | $\delta(CH_2)$ | 40,41 |
| 1445 | 1435 | $\delta(CH_2)$ | 40,41 |
| 1463 | | $\delta(CH_2)$ | 40,41 |
| 1642 | | $\upsilon(C=O)$ | 27,41 |

obtained from their diluted (1-mM) solutions, where only adsorbed acetate or laurate ions can be detected; see Figure 2.2. These data show that the carboxylate symmetric stretch of acetate and laurate shifts from ~1420 $cm^{-1}$ in the bulk solid to ~1398 $cm^{-1}$ when adsorbed to silver. Therefore, the band at 1394 $cm^{-1}$ from MUA in Figure 2.1 (a) is assigned to the carboxylate group of MUA interacting with silver, $\nu_s$(COO-Ag), which can provide the information about the involvement of $COO^-$ in the adsorption process. It is interesting to note that $\nu_s(COO^-)$ scattering from free carboxylate (not adsorbed on silver) is not observed in the assembly of MUA on the silver surface. While scattering is observed in a band at 1435 $cm^{-1}$, which may contain scattering from $\nu_s(COO^-)$, this band is totally insensitive to solution pH. Therefore, we assign the band at 1435 $cm^{-1}$ exclusively to $CH_2$ bending, $\delta(CH_2)$.[40] The lack of scattering from free carboxylate, even for monolayers that are thiol-bound with all-trans C-C bonding (see below), could be due to tilt of the chains, which orients the $\nu_s(COO^-)$ vibration nearly parallel to the silver surface; more likely, the distance between the carboxylate group and the silver may be too great for significant SERS enhancement compared to scattering from functional groups that are in direct contact or close proximity to the metal surface.

### 2.3.2 Time evolution of MUA Raman scattering during the self-assembly process

The monolayer self-assembly of MUA on a silver substrate was investigated for 0.1 mM solutions of the ligand prepared in water and methanol solutions. The Raman scattering intensities of the three structure-sensitive bands, $\nu(C\text{-}S)_G$, $\nu_s$(COO-Ag) and $\nu(C\text{-}C)_T$, evolved with time during the adsorption process are shown in Figure 2.3 (a) and (b), respectively. The adsorption of MUA to silver from methanol solution can be fit

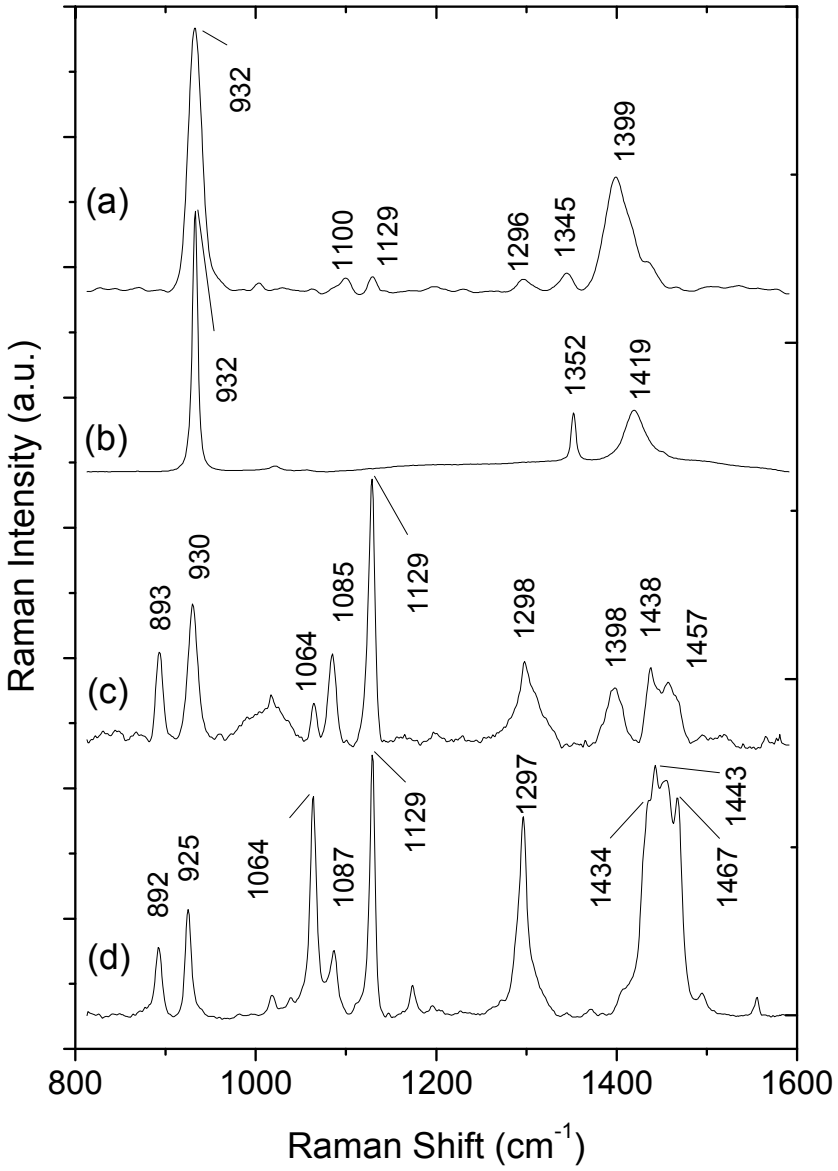


Figure 2.2. SERS spectrum of acetate ion adsorbed to a silver surface (a), ordinary Raman spectrum of solid sodium acetate (b), SERS spectrum of laurate ion adsorbed to a silver surface (c), and ordinary Raman spectrum of solid sodium laurate (d).

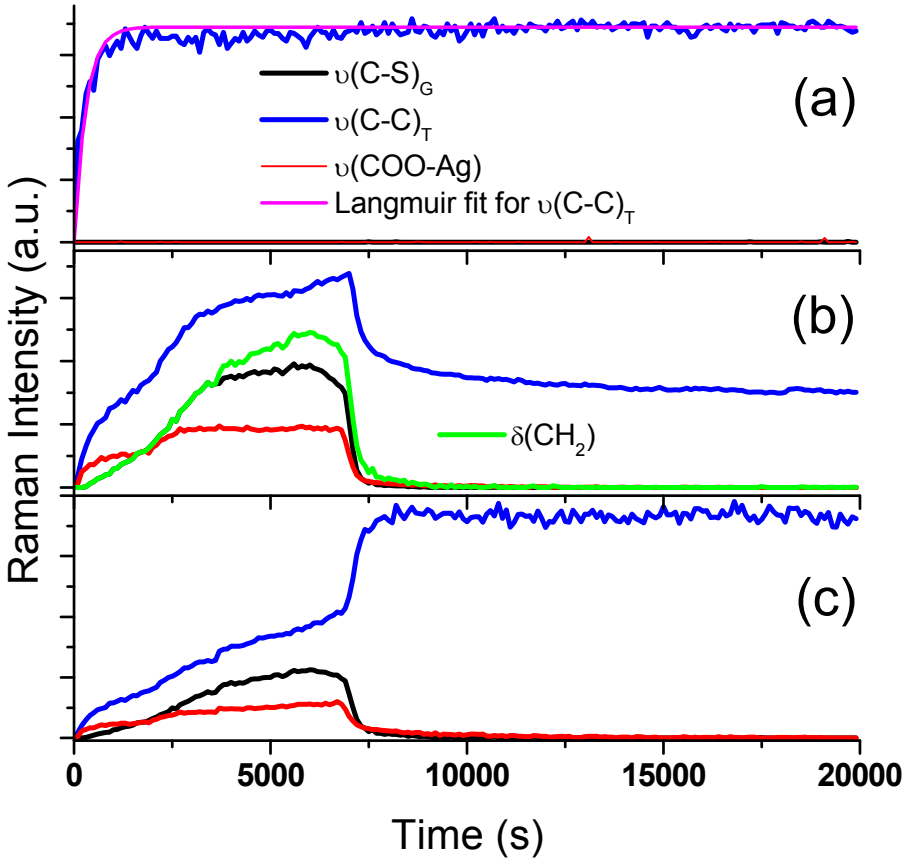


Figure 2.3. Time-dependent Raman scattering intensity from $\nu(C{-}S)_G$ (black), $\nu(C\text{-}C)_T$ (blue), and $\nu$(COO-Ag) (red) modes of MUA adsorbing to silver from methanol, fit to a Langmuir adsorption kinetic model (a), and from DI water (b). The DI water data normalized to the scattering from $\delta(CH_2)$ (c).

to a simple Langmuir adsorption kinetic model,[43, 44] $\theta(t) = [1 - \exp(-k t)]$, where $\theta$ is the surface coverage of adsorbate relative to its maximum value, and k is the rate of adsorption. This simple model fits the MUA adsorption to silver from methanol, as shown in Figure 2.3 (a), as previously observed for adsorption of alkanethiols with or without terminal functional groups.[8-12] No obvious gauche conformer or COO-Ag interaction can be seen over the entire adsorption process in methanol solution. In contrast, distinct behavior of gauche conformers and COO-Ag interactions were observed for the monolayer assembly from aqueous solution. The difference in the $COO^-$ participation and gauche conformers observed in assembly can be attributed to a stronger hydrophobic effect when the assembly of MUA was conducted in water. As a result, MUA molecules collapse onto the surface to minimize the contact with water in the first stage, where a gauche conformer with both thiol and carboxylate group bound to the silver is observed. The hydrophobic effect is less significant in methanol, and more MUA molecules can assemble on the surface assuming a trans conformation with only the stronger thiol-group binding to silver. Thus no COO-Ag interactions and gauche conformers are observed with assembly from methanol. The adsorption from methanol solution is also much faster than from aqueous solution, as shown in Figure 2.3, where the weaker hydrophobic interactions allow facile exchange of molecules with the surface and rapid annealing of the monolayer into an organized assembly.

Unlike the single-step self-assembly of MUA from methanol solution, adsorption of MUA from aqueous solution consists of at least two stages as proposed in Scheme 2.1. In the initial stage, both carboxylate and thiol groups of the MUA molecules bind to silver resulting in a mixture of gauche and trans conformers. The intensities of all three

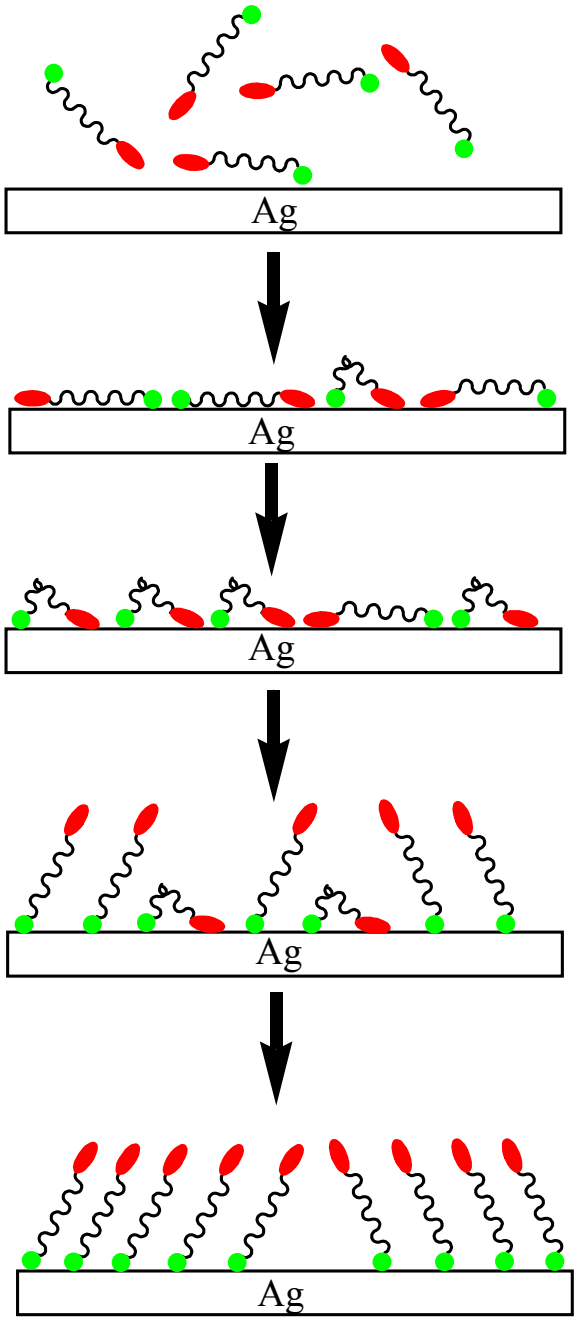


Scheme 2.1. Proposed assembly process of MUA on Ag surface from aqueous solution. Green circle and red oval are corresponding to thiol and carboxylate group, respectively.

bands $\nu(C\text{-}S)_G$, $\nu_s(COO\text{-}Ag)$, and $\nu(C\text{-}C)_T$ increase with time at this stage, as more MUA molecules arrive and stick to the surface. In the second stage, as more thiol bound MUA molecules arrive at surface, the COO-Ag interactions are displaced by S-Ag, yielding a stronger surface bond. As a result, the gauche conformers, with both functional groups bound to silver, evolve into trans conformers with only thiol groups bound to silver. This explains why gauche conformers and COO-Ag only exist as intermediates during the adsorption process. In the final stage, more MUA molecules should assemble into a well-ordered monolayer, with thiol groups bound to silver surface as a complete SAM is formed. Accordingly, the scattering intensity of trans conformers, $\nu(C\text{-}C)_T$, should increase in this final stage. However, the observed SERS intensity of the trans conformer shows an unexpected decrease in intensity.

The apparent decrease of the $\nu(C\text{-}C)_T$ intensity in the last stage of self assembly appears to be due to a loss of SERS enhancement that accompanies the unbinding of $COO^-$ from the silver surface. Evidence in support of this hypothesis derives from several observations. First, all of the Raman bands in the spectrum show a comparable fractional decrease in intensity following the loss of COO-Ag from the surface, with the notable exception of the $\nu(C\text{-}S)_G$ and $\nu_s(COO\text{-}Ag)$ which disappear (Figure 2.4). With a constant concentration of MUA in solution, it is not reasonable that the surface coverage of MUA decreases with time. As a test of this question, a silver surface with MUA adsorbed from water (after the signal decrease) is transferred to a methanol solution of MUA, and no further increase in Raman scattering intensity is observed, indicating that the final state of MUA adsorbed from water is a full monolayer. This suggests that the observed decrease in intensity in Figure 2.3 (b) is not a loss of molecules but a loss of

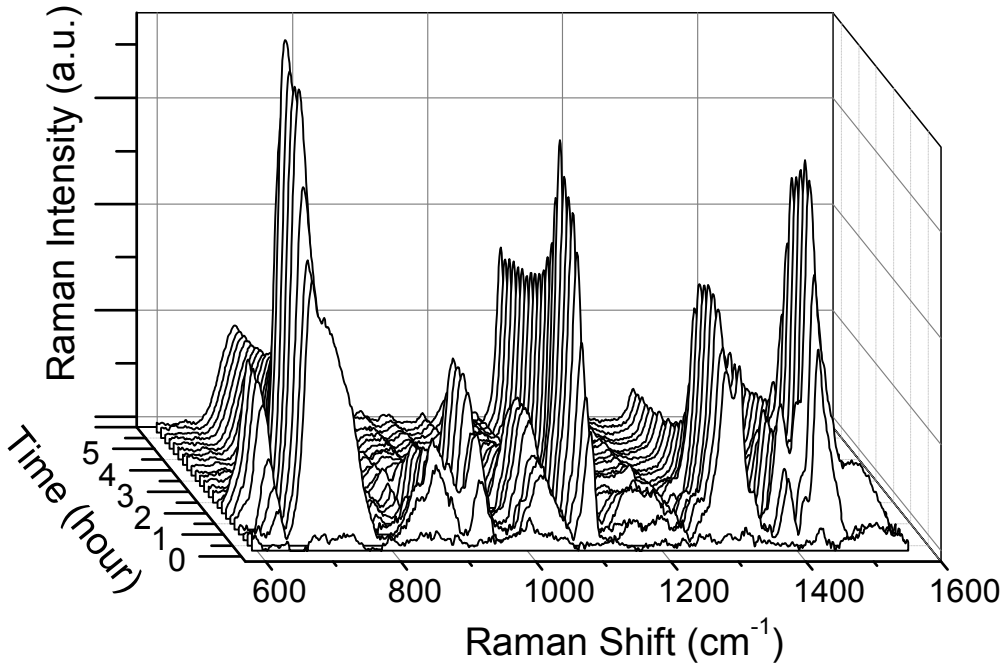


Figure 2.4. Time evolution of the Raman scattering of MUA assembling on silver surface from aqueous solution.

SERS enhancement, which affects the entire spectrum of the monolayer. The observed enhancement loss depends on assembly conditions, and it appears to accompany the unbinding of carboxylate from the silver surface. When COO-Ag is not detected, as in the adsorption of MUA from methanol, there is no decay of $\nu(C\text{-}C)_T$ or other bands in the spectrum (Figure 2.3a). To further test this dependence on formation COO-Ag, adsorption experiments were conducted for 11-mercapto-1-undecanol (MUL), 4-mercaptobenzonitrile (MBN), and 4-mercaptophenylacetic acid (MPA). We find no intensity decay for either MUL or MBN, while significant decay of SERS intensities is observed following the unbinding of COO-Ag for MPA, as shown in Figure 2.5.

The loss of SERS enhancement, accompanying the unbinding of adsorbed carboxylate, could be due to surface reconstruction of silver atoms that were interacting with carboxylate or a change in the local dielectric constant at the interface. Either mechanism should give rise to a shift in the localized surface plasmon resonance (LSPR) that provides the electromagnetic enhancement of Raman scattering. LSPR shifts due to exchange of the ligands have been previously reported for metal nanoparticles and semitransparent substrates.[45-47] To test this hypothesis, Ag-film-over-nanospheres (AgFON) substrates were prepared on glass slides so that the silver plasmon resonance could be determined in a simple UV-vis extinction measurement, and monitored during adsorption of MUA. As shown in Figure 2.6, the LSPR band exhibits a small red shift and then a blue shift, which produces changes in extinction at 785-nm where Raman scattering is excited. SERS measurements of the MUA adsorption on the AgFON substrates were also conducted so that the time-dependent changes in intensity of $\nu_s(COO\text{-}Ag)$ and $\nu(C\text{-}C)_T$ Raman scattering could be compared with changes in the

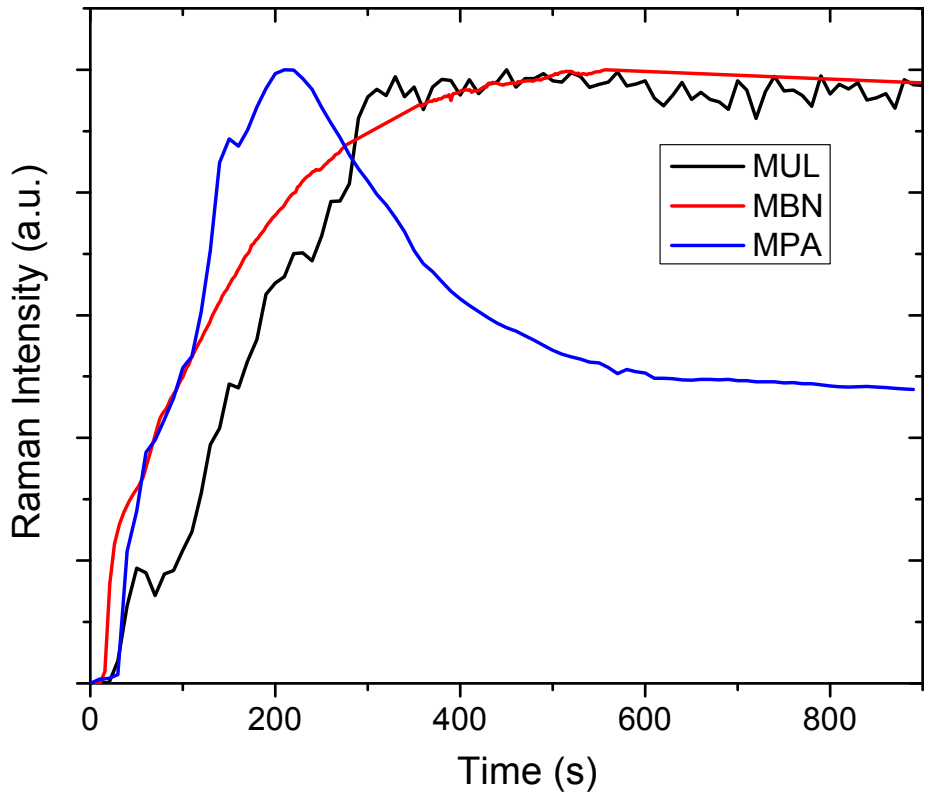


Figure 2.5. Time-dependent Raman scattering intensity of several compounds adsorbing to silver from aqueous solution. Black: $\nu(C\text{-}C)_T$ of 11-mercapto-1-undecanol (MUL), Red: $\nu_{18b}$ of 4-mercaptobenzonitrile (MBN), and blue: $\nu_{18b}$ of 4-mercaptophenylacetic acid (MPA)

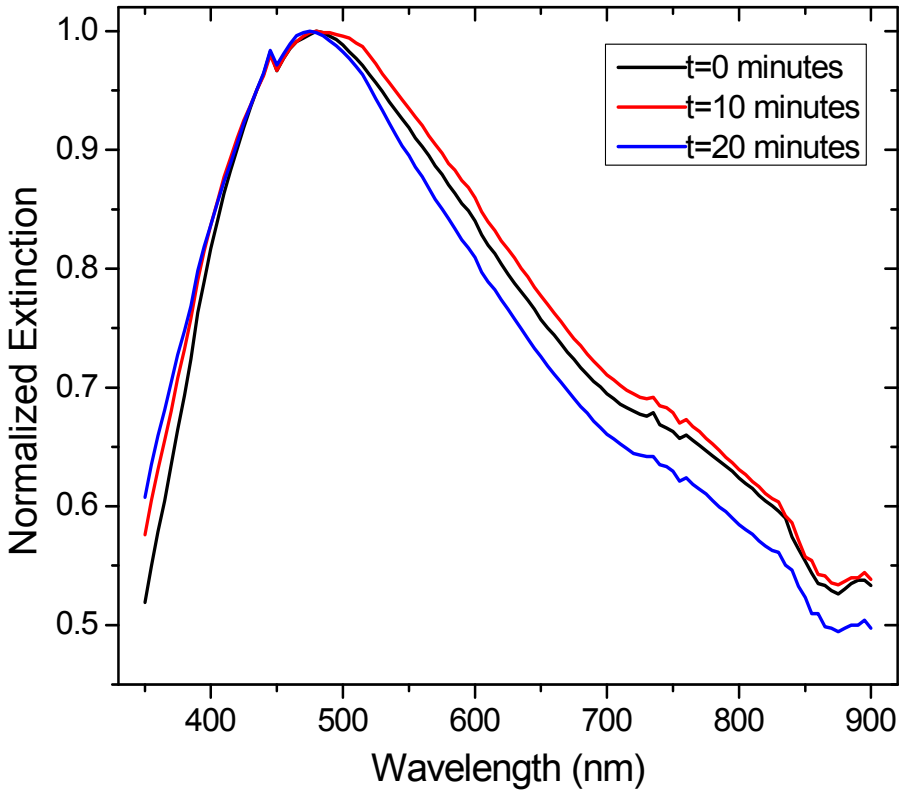


Figure 2.6. Time evolution of the plasmon resonance of an AgFON substrate exposure to 0.1-mM MUA in aqueous solution.

plasmon resonance extinction at 785 nm; see Figure 2.7. The extinction exhibits a small rise with the adsorption of MUA and then decays significantly with the loss of COO-Ag from the surface. When MUA was adsorbed from methanol solution onto the AgFON substrate, only the small rise in plasmon resonance extinction with MUA adsorption is observed, after which the LSPR is stable, as shown in Figure 2.8. Therefore, it is reasonable to assign the intensity decay of $\nu(C\text{-}C)_T$ and other bands with the loss of Ag-COO from the surface to a shift in the plasmon resonance and corresponding decrease in the SERS enhancement. Using a laser with excitation wavelength close to the plasmon resonance maximum of the substrate (~500 nm, Figure 2.6) might minimize the effect of the surface reconstruction during the assembly and produce more straightforward results, which is beyond the scope of this study.

To compensate for this change in enhancement, the intensity of a vibrational band that is insensitive to the conformation change ($\delta(CH_2)$ at 1435 $cm^{-1}$) was used as a reference. The intensities of the $\nu(C\text{-}S)_G$, $\nu_s(COO\text{-}Ag)$, and $\nu(C\text{-}C)_T$ bands were ratioed to the $\delta(CH_2)$ scattering intensity relative to its maximum so that the data are corrected for the loss in the SERS enhancement. The time-dependent profile of the band intensities thus corrected are plotted in Figure 2.3 (c), where the profiles of $\nu_s(COO\text{-}Ag)$ and $\nu(C\text{-}S)_G$ do not change significantly, whereas the intensity of $\nu(C\text{-}C)_T$ scattering increases as gauche conformers are replaced and the monolayer becomes more compact and ordered. The pronounced change of the intensity of $\nu(C\text{-}C)_T$ and $\nu(C\text{-}S)_G$ reflects a sharp transition from a high degree of gauche conformation and disorder to an all-trans conformation.[48-50] The data show that the loss of $\nu_s(COO\text{-}Ag)$ intensity corresponds to a

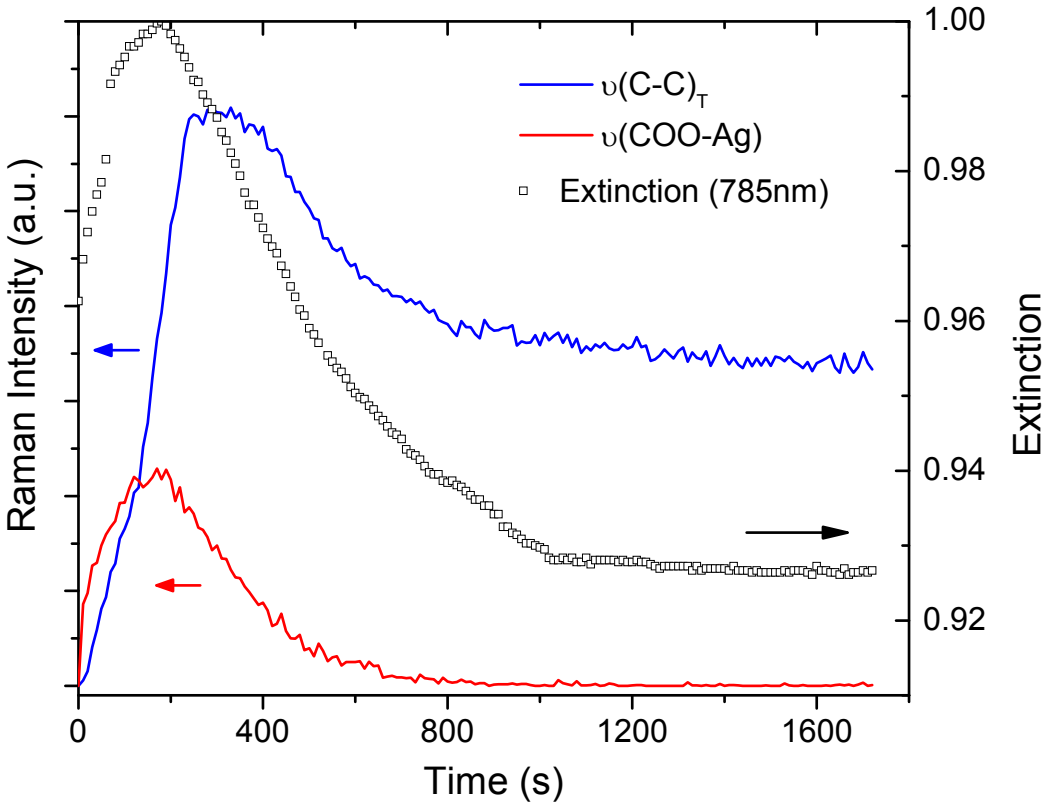


Figure 2.7. Time-dependent profiles of Raman scattering of MUA assembling on a MFON substrate, from $\nu(C\text{-}C)_T$ (blue) and $\nu(COO\text{-}Ag)$ (red) modes, are compared with the plasmon extinction at 785 nm (black square) under the same conditions.

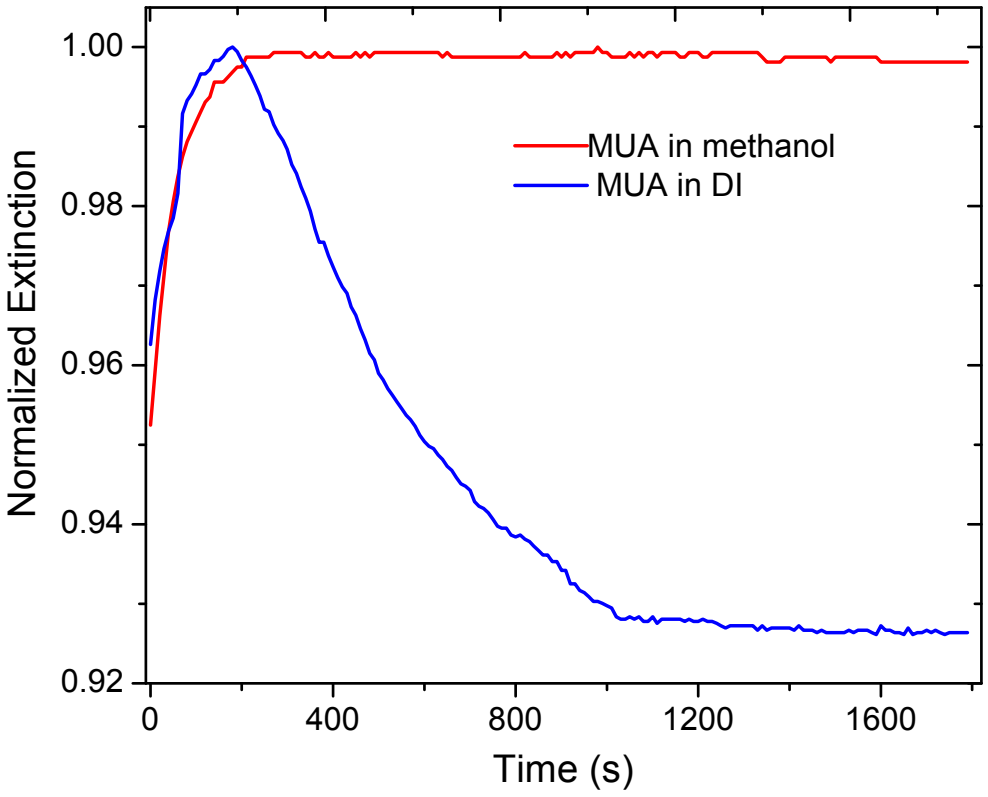


Figure 2.8. Time evolution of the plasmon extinction at 785 nm from an AgFON substrate exposure to 0.1-mM MUA in methanol solution (red) and in aqueous solution (blue).

reorganization of adsorbed MUA from a disordered state involving binding of both carboxylate and thiol to an ordered, thiol-bound monolayer.

2.3.3 The effect of pH on MUA self-assembly

The protonation state of the carboxylate group of MUA should have an effect on its interactions with a silver surface; the solution pH, which governs dissociation of the carboxylic acid, should therefore be a significant factor affecting the participation of the $COO^-$ in the assembly process. To study the influence of solution pH on the assembly process, adsorption of MUA onto silver from aqueous solutions of different pH values was investigated. Buffer solutions were 1.0 mM phosphate with 10 mM $NaClO_4$ supporting electrolyte, and the surface potential was held constant at 0.0 V relative to an Ag/AgCl reference to control for changes in surface potential that would accompany changes in solution pH.

The time-dependent Raman scattering intensity profiles of three bands $\nu(C\text{-}S)_G$, $\nu_s(COO\text{-}Ag)$ and $\nu(C\text{-}C)_T$ ratioed to the $\delta(CH_2)$ scattering intensity (see above) were acquired and are plotted in Figure 2.9. The assembly kinetics are faster than adsorption from aqueous solution at open circuit, which is likely due to the positive open-circuit potential of silver[51, 52] that hinders the assembly process (see following section). It is clear from the results that the involvement of carboxylate-silver interactions in the assembly process depends strongly on the solution pH. The higher the solution pH, the greater COO-Ag intensity is observed during assembly, which is expected since the coordination of silver would be much stronger for deprotonated carboxylate groups than for the corresponding carboxylic acid. At lower pH of 3.0 or 4.8, involvement of carboxylate bound to silver as an intermediate is small and brief, as shown in Figure 2.9

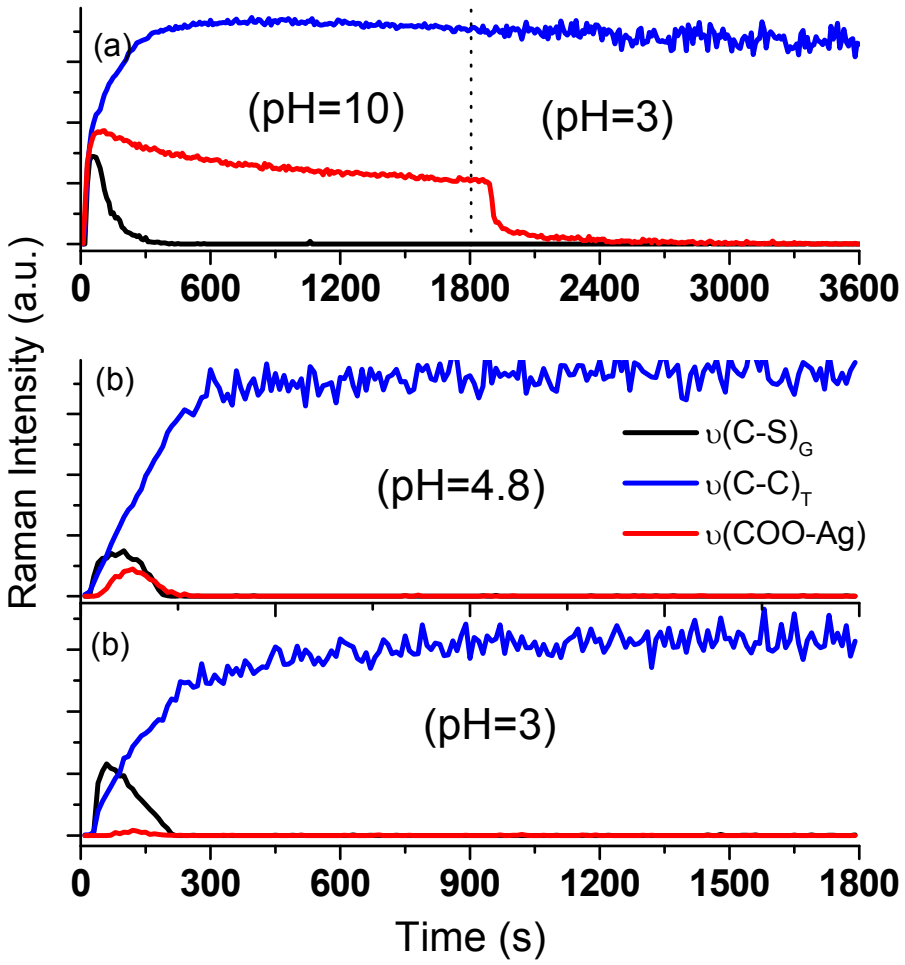


Figure 2.9. Adsorption of MUA onto silver from aqueous solutions of different pH. Time dependent SERS intensities from $\nu(C-S)_G$ (black), $\nu(C-C)_T$ (blue), and $\nu$(COO-Ag) (red) of MUA.

(b and c), nearly vanishing at pH 3.

With self-assembly from a solution of pH 10, however, the intensity of COO-Ag drops very slowly and does not completely disappear even after 24 h; here, the carboxylate activity is so great that an ordered monolayer of carboxylate-bound MUA is formed that cannot be readily displaced from the silver surface by thiol groups. Consequently, trans C-C-C conformers appear even though the silver surface is significantly populated with carboxylate groups, producing a mixture monolayer with both carboxylate and thiol bound to silver (Scheme 2.2). The displacement of COO-Ag by S-Ag is hindered not only because of the higher activity of $COO^-$, but also because of the stability of a relatively compact, ordered monolayer. Displacement of carboxylate, however, can be accelerated by changing the pH of the overlaying solution from 10 to 3. As shown in Figure 2.9 (a), the intensity of COO-Ag in the mixed monolayer decays quickly upon lowering of the solution pH. Similar transition can also be observed using buffer of pH=3 without MUA in solution, which indicates that MUA molecules can reorient from carboxylate-bound to thiol-bound on the Ag surface.

The results confirm the participation of the carboxylate group in the assembly process, which is most significant at higher solution pH where the activity of carboxylate anion is greatest.

### 2.3.4 The effect of surface potential on MUA self-assembly

Electrode potential has demonstrated the ability to control the adsorption and desorption of the alkane thiol on metal surface.[14, 53-55] A large negative potential can lead to reductive desorption of thiol-bound monolayers. The applied potential has also been proved to control the dissociation of carboxylate groups in thiol monolayer and the

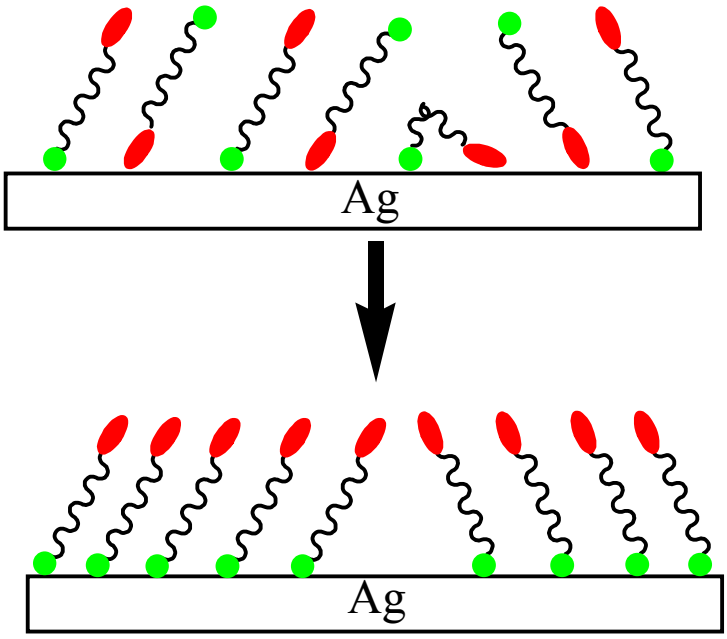


Scheme 2.2. The final stage of assembly process of MUA on Ag surface from aqueous solution with pH=10 at 0.0 V. Green circle and red oval are corresponding to thiol and carboxylate group, respectively.

affinity of the $–COO^-$ to a metal surface.[56, 57] A potential-induced switchable surface has been developed on the Au electrode covered with 16-mercaptohexadecanoic acid monolayer by driving the carboxylate to and from the Au surface with applied potential.[23] Therefore, it is reasonable to expect that the surface potential can be another factor that influences the participation of a carboxylate group in the self-assembly process. MUA adsorption experiments were carried out in pH 4.8 buffer solutions with different applied potentials, and the resulting time-dependent self-assembly profiles are shown in Figure 2.10.

From these results, the participation of $–COO^-$ in the monolayer assembly of MUA on silver clearly depends strongly on the potential of the metal surface. A more negative potential leads to much less COO-Ag involvement and corresponding gauche conformers as intermediates in the assembly process. At more positive potentials, more $–COO^-$ interactions with silver and gauche conformers are observed, and these decay much more slowly in potential. Although the electrode potential should affect the binding energy of both COO-Ag and S-Ag, a more positive surface potential attracts a greater population of $-COO^-$ into the interface and favors its interaction with silver.

In addition to greater $–COO^-$ participation as an intermediate, a positive surface potential slows the evolution of the gauche conformers to trans conformers. This is likely due to the stronger COO-Ag or S-Ag surface bonds, which must be overcome to allow annealing of the adsorbed molecules into a well-organized monolayer. At an applied potential of +0.2 V versus Ag/AgCl, the decay of gauche C-S conformers and the corresponding rise of C-C trans conformers is only ~20% over a period of 30 minutes, which is an indication of the stability of the end-group interactions with the silver

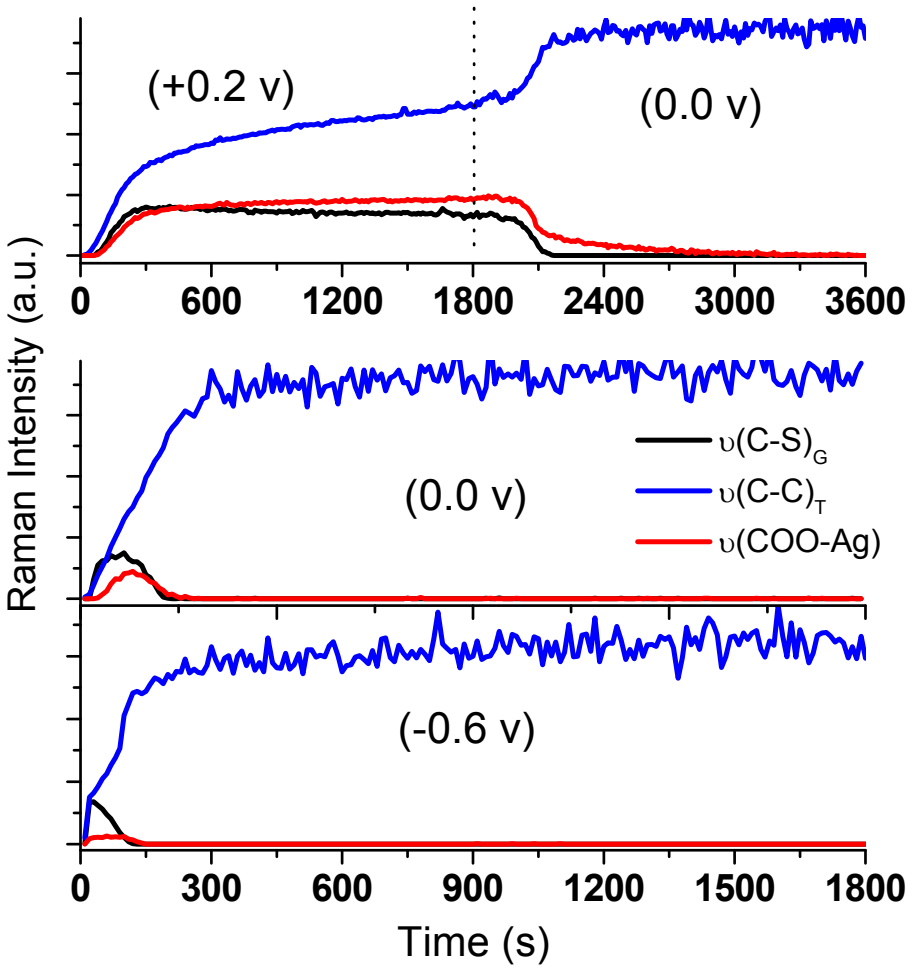


Figure 2.10. Adsorption of MUA onto silver held at different potentials versus Ag/AgCl. Time dependent SERS intensities from $\nu(C{-}S)_G$ (black), $\nu(C\text{-}C)_T$ (blue), and $\nu$(COO-Ag) (red) of MUA.

surface. The stability of these surface interactions can be disrupted when the potential is switched to 0.0 V. An abrupt increase of trans conformers can be observed along with the decay of COO-Ag and gauche species, producing a trend similar to the assembly conducted aqueous solution at open circuit (Figure 2.3c). The results demonstrate that the stability of these intermediates and assembly process can be readily controlled by changing the surface potential.

### 2.3.5 Control of self-assembly of carboxylate-terminated n-alkanethiol monolayers

One purpose of this study is to manipulate the self-assembly process to control the surface that is produced through controlled assembly conditions. Although well-ordered monolayers are most widely used in different applications, monolayers with controlled defects can be interesting for investigations of permeability, conductivity, and wettability.[23, 58-61] As demonstrated above, a complete monolayer of MUA with only thiol groups bound to silver can be assembled from methanol, mixed monolayers with both thiol or $-COO^-$ bound to silver can be obtained from aqueous solutions at high pH, while a disordered monolayer with both $-COO^-$ and thiol bound to the silver can be produced at strongly positive potentials. These mixed-binding surfaces are stable for days with relatively little evolution in their structure even when removed from their preparation conditions. For example, Figure 2.11 (a) shows the time evolution of the monolayer assembled in aqueous solution at pH 10 and 0.0 V, rinsed and stored in DI water at open circuit. While intensities of trans conformers increase somewhat over time to a steady state, the main features of the surface, absence of gauche conformer and coexistence of COO-Ag and thiol-bound molecules remain unchanged for days. Similar stability is

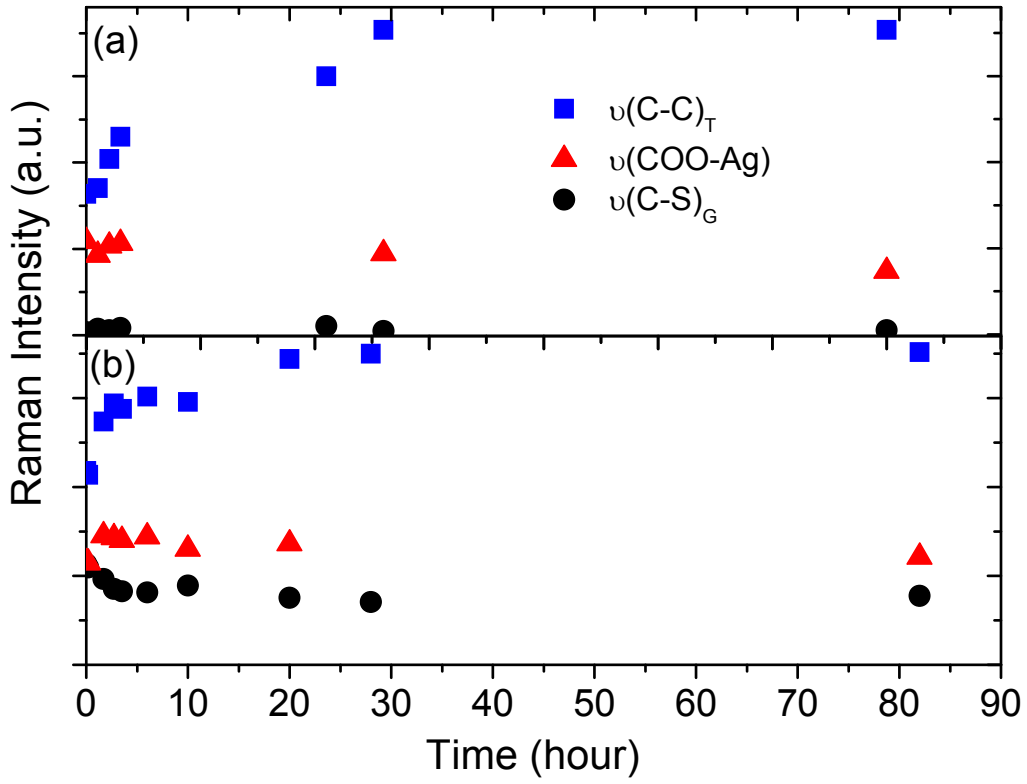


Figure 2.11. Tests of stability of mixed-mode monolayers, (a) assembled at 0.0 V versus Ag/AgCl and pH=10 and (b) assembled at 0.2 V in solution and pH=4.8. Time dependent profiles of $\nu(C-S)_G$ (black), $\nu(C-C)_T$ (blue), and $\nu$(COO-Ag) (red) after the monolayers were removed from the assembly solution, rinsed and then stored in DI water.

observed for a surface prepared at pH=4.8 and +0.2 V versus Ag/AgCl (Figure 2.11 (b)) and stored in DI water. Coexistence of the COO-Ag and both conformers is again stable for days. These surfaces might be used to develop mixed monolayers with less phase separation. The addition of a secondary ligand to fill the defect sites or to replace the MUA bound to silver by carboxylate groups might produce a more uniform mixed layer compared to the assembly from mixed solutions.

## 2.4 Conclusions

The self-assembly of monolayers of 11-mercaptoundecanoic acid on silver surfaces has been investigated *in situ* by surface-enhanced Raman spectroscopy. Spectroscopic information reveals interactions between carboxylate groups and the metal surface. Participation of $-COO^-$ in the self-assembly process depends on the solvent, solution pH, and applied potential. By varying the experimental conditions, surfaces with different MUA coverage can be obtained. More $-COO^-$ and gauche conformers appeared in the assembly in either high solution pH or more positive potential conditions, which produce a mixture monolayer and a disordered low coverage phase, respectively. These surfaces are relatively stable not only in original experimental conditions, but also when stored in DI water at open circuit. Surface-enhanced Raman spectroscopy is shown to be an informative technique for investigating the self-assembly process, which could be manipulated by changing the conditions.

## 2.5 References

(1) Zamborini, F. P.; Crooks, R. M. *Langmuir* **1998**, *14*, 3279-3286.

(2) Nyquist, R. M.; Eberhardt, A. S.; Silks, L. A.; Li, Z.; Yang, X.; Swanson, B. I. *Langmuir* **2000**, *16*, 1793-1800.

(3) Smith, R. K.; Lewis, P. A.; Weiss, P. S. *Progress in Surface Science* **2004**, *75*, 1-68.

(4) Love, J. C.; Estroff, L. A.; Kriebel, J. K.; Nuzzo, R. G.; Whitesides, G. M. *Chemical Reviews* **2005**, *105*, 1103-1169.

(5) Yamada, R.; Uosaki, K. *Langmuir* **1998**, *14*, 855-861.

(6) Petri, M.; Kolb, D. M.; Memmert, U.; Meyer, H. *Electrochimica Acta* **2003**, *49*, 175-182.

(7) Zhang, J. D.; Chi, Q. J.; Ulstrup, J. *Langmuir* **2006**, *22*, 6203-6213.

(8) Peterlinz, K. A.; Georgiadis, R. *Langmuir* **1996**, *12*, 4731-4740.

(9) Hu, K.; Bard, A. J. *Langmuir* **1998**, *14*, 4790-4794.

(10) Imae, T.; Torii, H. *Journal of Physical Chemistry B* **2000**, *104*, 9218-9224.

(11) Pan, S.; Belu, A. M.; Ratner, B. D. *Materials Science & Engineering C-Biomimetic and Supramolecular Systems* **1999**, *7*, 51-58.

(12) Pan, W.; Durning, C. J.; Turro, N. J. *Langmuir* **1996**, *12*, 4469-4473.

(13) Schoenfisch, M. H.; Pemberton, J. E. *Langmuir* **1999**, *15*, 509-517.

(14) Uibel, R. H.; Harris, J. M. *Applied Spectroscopy* **2004**, *58*, 934-944.

(15) Chi, Y. S.; Lee, K.-B.; Kim, Y.; Choi, I. S. *Langmuir* **2006**, *23*, 1209-1214.

(16) Murgida, D. H.; Hildebrandt, P. *Journal of the American Chemical Society* **2001**, *123*, 4062-4068.

(17) Murgida, D. H.; Hildebrandt, P. *Accounts of Chemical Research* **2004**, *37*, 854-861.

(18) Niki, K.; Hardy, W. R.; Hill, M. G.; Li, H.; Sprinkle, J. R.; Margoliash, E.; Fujita, K.; Tanimura, R.; Nakamura, N.; Ohno, H.; Richards, J. H.; Gray, H. B. *The Journal of Physical Chemistry B* **2003**, *107*, 9947-9949.

(19) Chirakul, P.; Perez-Luna, V. H.; Owen, H.; Hampton, G. P.; Hampton, P. D. *Langmuir* **2002**, *18*, 4324-4330.

(20) Zhu, M.; Schneider, M.; Papastavrou, G.; Akari, S.; Mohwald, H. *Langmuir* **2001**, *17*, 6471-6476.

(21) Holmlin, R. E.; Chen, X.; Chapman, R. G.; Takayama, S.; Whitesides, G. M. *Langmuir* **2001**, *17*, 2841-2850.

(22) Talley, C. E.; Jusinski, L.; Hollars, C. W.; Lane, S. M.; Huser, T. *Analytical Chemistry* **2004**, *76*, 7064-7068.

(23) Lahann, J.; Mitragotri, S.; Tran, T. N.; Kaido, H.; Sundaram, J.; Choi, I. S.; Hoffer, S.; Somorjai, G. A.; Langer, R. *Science* **2003**, *299*, 371-374.

(24) Liu, Y.; Mu, L.; Liu, B. H.; Kong, J. L. *Chemistry-a European Journal* **2005**, *11*, 2622-2631.

(25) Liu, Y.; Mu, L.; Liu, B. H.; Zhang, S.; Yang, P. Y.; Kong, J. L. *Chemical Communications* **2004**, 1194-1195.

(26) Moskovits, M.; Suh, J. S. *J. Am. Chem. Soc.* **1985**, *107*, 6826-6829.

(27) Kwon, Y. J.; Son, D. H.; Ahn, S. J.; Kim, M. S.; Kim, K. *J. Phys. Chem.* **1994**, *98*, 8481-8487.

(28) Jung Ahn, S.; Hee Son, D.; Kim, K. *Journal of Molecular Structure* **1994**, *324*, 223-231.

(29) Lee, S. J.; Kim, K. *Vibrational Spectroscopy* **1998**, *18*, 187-201.

(30) Fischer, D. A.; Hu, Z. S.; Hsu, S. M. *Tribology Letters* **1997**, *3*, 41-45.

(31) Noh, J.; Konno, K.; Ito, E.; Hara, M. *Japanese Journal of Applied Physics Part 1-Regular Papers Brief Communications & Review Papers* **2005**, *44*, 1052-1054.

(32) Rosendahl, S. M.; Burgess, I. J. *Electrochimica Acta* **2008**, *53*, 6759-6767.

(33) Dick, L. A.; McFarland, A. D.; Haynes, C. L.; Van, D. R. P. *J. Phys. Chem. B* **2002**, *106*, 853-860.

(34) Moskovits, M.; Suh, J. S. *The Journal of Physical Chemistry* **1984**, *88*, 5526-5530.

(35) Gao, X.; Davies, J. P.; Weaver, M. J. *The Journal of Physical Chemistry* **1990**, *94*, 6858-6864.

(36) Campion, A.; Kambhampati, P. *Chem. Soc. Rev.* **1998**, *27*, 241 - 250.

(37) Stiles, P. L.; Dieringer, J. A.; Shah, N. C.; Van Duyne, R. P. *Annual Review of Analytical Chemistry* **2008**, *1*, 601-626.

(38) Beata, W.; Jolanta, B.; Andrzej, K., 2005; Vol. 36, pp 1040-1046.

(39) Bryant, M. A.; Pemberton, J. E. *J. Am. Chem. Soc.* **1991**, *113*, 3629-3637.

(40) Ishioka, T.; Wakisaka, H.; Saito, T.; Kanesaka, I. 1999; Kluwer Academic Publishers; 315-316.

(41) Castro, J. L.; Lopez-Ramirez, M. R.; Arenas, J. F.; Otero, J. C. *J. Raman Spectrosc.* **2004**, *35*, 997-1000.

(42) Podstawka, E.; Ozaki, Y.; Proniewicz, L. M. *Appl. Spectrosc.* **2004**, *58*, 1147-1156.

(43) Bhugun, I.; Anson, F. C. *Journal of Electroanalytical Chemistry* **1997**, *439*, 1-6.

(44) Olson, L. G.; Harris, J. M. *Applied Spectroscopy* **2008**, *62*, 149-156.

(45) Malinsky, M. D.; Kelly, K. L.; Schatz, G. C.; Van, D. R. P. *J. Am. Chem. Soc.* **2001**, *123*, 1471-1482.

(46) Wang, W.; Chen, X.; Efrima, S. *J. Phys. Chem. B* **1999**, *103*, 7238-7246.

(47) Willets, K. A.; Van, D. R. P. *Annu. Rev. Phys. Chem.* **2007**, *58*, 267-297.

(48) Vemparala, S.; Kalia, R. K.; Nakano, A.; Vashishta, P. *J. Chem. Phys.* **2004**, *121*, 5427-5433.

(49) Himmelhaus, M.; Eisert, F.; Buck, M.; Grunze, M. *J. Phys. Chem. B* **2000**, *104*, 576-584.

(50) Badia, A.; Cuccia, L.; Demers, L.; Morin, F.; Lennox, R. B. *J. Am. Chem. Soc.* **1997**, *119*, 2682-2692.

(51) Bard, A. J.; Faulkner, L. R. *Electrochemical Methods: Fundamentals and Applications*; Wiley: New Jersey, 2000.

(52) Larkin, D.; Guyer, K. L.; Hupp, J. T.; Weaver, M. J. *J. Electroanal. Chem. Interfacial Electrochem.* **1982**, *138*, 401-423.

(53) Weisshaar, D. E.; Lamp, B. D.; Porter, M. D. *Journal of the American Chemical Society* **1992**, *114*, 5860-5862.

(54) Hatchett, D. W.; Stevenson, K. J.; Lacy, W. B.; Harris, J. M.; White, H. S. *Journal of the American Chemical Society* **1997**, *119*, 6596-6606.

(55) Hatchett, D. W.; Uibel, R. H.; Stevenson, K. J.; Harris, J. M.; White, H. S. *Journal of the American Chemical Society* **1998**, *120*, 1062-1069.

(56) Burgess, I.; Seivewright, B.; Lennox, R. B. *Langmuir* **2006**, *22*, 4420-4428.

(57) Ma, C.; Harris, J. M. *Langmuir* **2011**, *27*, 3527-3533.

(58) Patrick, D. L.; Cee, V. J.; Purcell, T. J.; Beebe, T. P., Jr. *Langmuir* **1996**, *12*, 1830-1835.

(59) Lewis, P. A.; Donhauser, Z. J.; Mantooth, B. A.; Smith, R. K.; Bumm, L. A.; Kelly, K. F.; Weiss, P. S. *Nanotechnology* **2001**, *12*, 231-237.

(60) Donhauser, Z. J.; Price, D. W.; Tour, J. M.; Weiss, P. S. *J. Am. Chem. Soc.* **2003**, *125*, 11462-11463.

(61) Chailapakul, O.; Crooks, R. M.; Tr; Order No, A.-A.; Univ. New Mexico, 1992, pp 24 pp.

# CHAPTER 3

# SURFACE-ENHANCED RAMAN SPECTROSCOPY INVESTIGATION OF THE POTENTIAL-DEPENDENT ACID-BASE CHEMISTRY OF SILVER-IMMOBILIZED 2-MERCAPTOBENZOIC ACID*

## 3.1 Introduction

Self-assembled monolayers (SAMs) are important structures for controlling the surface properties of a metal substrate which have led to numerous applications.[1-6] Among them, pH-sensitive molecules are widely used because the properties of the functionalized surfaces can be easily controlled by changing the solution conditions.[3-7] For example, the surface charge and wettability of these modified surfaces can be switched reversibly by adjusting the solution pH.[3, 4] These switchable surfaces are useful in biomolecular devices for controlling adsorption and desorption of DNA, protein, and other biomomecules.[5-7] Characterizing the acid/base chemistry of the modified surfaces, controlling surface properties, and understanding their pH-dependent responses are important for further development of these techniques and applications.

Numerous studies have been conducted to investigate the surface chemistry of the immobilized pH-sensitive molecules and determine their interfacial p$K_a$. These include contact angle measurements,[8, 9] quartz crystal microbalance,[10] atomic force

---

* Reproduced with permission from *Langmuir*, **2011**, *27* (7), pp 3527–3533 Copyright 2011 American Chemical Society

microscopy,[11, 12] capacitance titrations,[13-15] voltammetric measurements,[16-18] and infrared and Raman spectroscopy.[19-22] These studies have shown that the acid/base chemistry of surface-bound molecules can differ significantly from those in bulk solution.[8-22] Titrations of immobilized acid-base ligands generally produce a broader pH response along with a p$K_a$ shift compared to the titration in bulk solution. These differences have been ascribed in these previous studies to the interaction of the immobilized molecules with the surface and each other and the influence of the surface potential on the population of charged species at the interface.[10, 12, 14, 23, 24]

Surface-enhanced Raman scattering (SERS) is a sensitive tool that has also been used to detect the pH response of acid-base active SAMs bound to metal surfaces. That response has been exploited for the development of spectroscopic pH probes.[20-22, 25-28] Surface-enhanced Raman scattering occurs when incident radiation excites surface plasmons in the metal, which increases the local excitation intensity as well as the Raman scattering probability of surface-bound species.[29-33] The overall enhancement of the Raman scattering intensity in SERS measurements generally ranges from $10^6$ to $10^8$, making the method sufficiently sensitive for detection of submonolayer populations of molecules at an interface.[30, 32, 33] An advantage of SERS over the others techniques for the study of interfacial acid-base chemistry is that it provides *in situ* spectroscopic information on chemical structure and molecular interactions at the solid-liquid interface. While previous studies have demonstrated SERS to be capable of detecting acid-base forms of reporter molecules for the development of SERS-based pH sensors,[20-22, 25-28] the effect of the surface potential on the interfacial acid/base equilibria was not investigated. In a recent SERS study,[34] the influence of applied potential on the protonation of an

amine-terminated alkanethiolate was considered; however, the acidic and basic forms of the ligand could not be detected, so evidence of the amine protonation was inferred from changes in the intensity of perchlorate counter ions at the interface. Some potential-dependent shifting of the apparent p$K_a$ was observed in these results; however, quantitative interpretation is complicated by changes in the interfacial perchlorate ion concentration with applied potential which do not depend on protonation state of the ligand.

In this study, we employ surface-enhanced Raman spectroscopy to investigate the acid/base chemistry of immobilized 2-mercaptobenzoic acid (2-MBA) under controlled potential conditions. Raman spectra of a 2-MBA monolayer on a silver surface are recorded in solutions of varying pH, with applied potential (vs. Ag/AgCl) ranging from 0.0 to –0.6 V. The fraction of the deprotonated versus protonated 2-MBA can be readily determined from the relative intensities of the $COO^-$ bending mode, $\delta$ ($COO^-$), and the C-COOH stretching mode $\nu$(C-COOH), respectively. In addition, shifts in the symmetric carboxylate stretching mode, $\nu_s(COO^-)$, of 2-MBA reveal interactions between the silver surface and the benzoate group, which can be displaced by acetate in the buffer. It was found that the applied potential has a significant effect on the dissociation equilibrium of immobilized 2-MBA due to changes in the local activity of protons at the interface, which modulates the interfacial pH relative to bulk solution.[14, 23, 35, 36] The data are fit to a Poisson-Boltzmann model, corrected for potential distribution across monolayer and for interactions between the immobilized molecules. Differences between the intrinsic p$K_a$ of the immobilized ligand and 2-MBA in free solution are observed and attributed to changes in electron density on the benzoic acid group upon binding of the thiol to the

silver surface. Surface-enhanced Raman spectroscopy with potential control is found to be a useful tool to unravel the speciation and surface interactions of acid-base ligands immobilized to metal surfaces.

## 3.2 Experimental

### 3.2.1. Substrate and SAM preparation

All electrodes were constructed from a 7-mm diameter silver rod (99.999%, Alfa Aesar). The 2-mercaptobenzoic acid (97%, Sigma-Aldrich), 4-mercaptobenzoic acid (99%, Sigma-Aldrich), and benzoic acid (99%, Sigma-Aldrich) were used as received. The surfaces of the electrodes were polished with 800, 1500 and 2000 grit silicon carbide paper (3M) and then with alumina polishing slurries (1.0 μm) on a microfiber polishing cloth (Buehler). The electrode surfaces were then electrochemically roughened by oxidation-reduction cycles in KCl (0.1M) solution; specifically, linear sweeps from +0.3 V to -0.3 V (versus Ag/AgCl) and back to +0.3 V were applied at a sweep rate of 15 mV/s for 3 cycles, and then the potential was held at –0.3 V for 2 min.[37] Electrodes were then removed from the cell and rinsed with deionized water prior to monolayer self-assembly. The self-assembly step was conducted by immersing the Ag electrodes in 10 mM solutions of 2-mercaptobenzoic acid in methanol for 12 h.

### 3.2.2. Preparation of buffers

The buffer solutions of pH 1.0-10.0 were prepared from 0.02 M sodium acetate (NaAc) solution. The NaAc solutions were titrated with 1.0 M NaOH or 1.0 M $HClO_4$ solutions to a desired pH, which was measured with a pH meter (AB15, Fisher Scientific). Solution of 1.0 M $NaClO_4$ was added to control the final ionic strength to be 0.2 M.

3.2.3. Raman spectroelectrochemical measurements

A three-electrode potentiostat (RDE4, Pine Instrument) was used to control the applied potential. An Ag/AgCl electrode (EE009, Cypress Systems, Inc.) was used as reference and a platinum mesh (0.1 mm diameter and 25 mm x 25 mm, Alfa Aesar) was used as the counter electrode; the position of the working electrode is adjusted to be about 1 mm from the fused silica front window of the cell (see Figure 3.1). Surface enhanced Raman measurements were conducted with a fiber-optic coupled Raman spectrometer (PI-200, Process Instruments) with a frequency stabilized, 785-nm diode laser. The laser power at the sample was 200 mW, and the integration time was 10 s for all measurements.

## 3.3 Results and Discussion

### 3.3.1 Raman spectroscopy of immobilized 2-MBA

The bulk-phase Raman spectra of 2-mercaptobenzoic acid were measured in the protonated form as the solid acid and dissolved in acetonitrile, and in the deprotonated form in 0.1-M NaOH solution; these spectra are plotted in Figure 3.2, along with the surface-enhanced Raman spectra of 2-MBA immobilized on a silver surface at pH 1 and 13, respectively. There is a consistent set of bands present in the bulk-phase and immobilized 2-MBA, as listed and assigned in Table 3.1.[22, 25-27, 38, 39] Most of these bands do not change significantly with change in protonation state; however, two prominent, lower-frequency bands are good reporter vibrations for the acid and base forms of the ligand. The bending mode of the benzoate ($\delta(COO^-)$) at 840 $cm^{-1}$ of immobilized 2-MBA and the C-COOH stretching mode ($\nu$(C-COOH)) at 800 $cm^{-1}$ of immobilized 2-MBA are the most intensely scattering modes sensitive to protonation and deprotonation of the

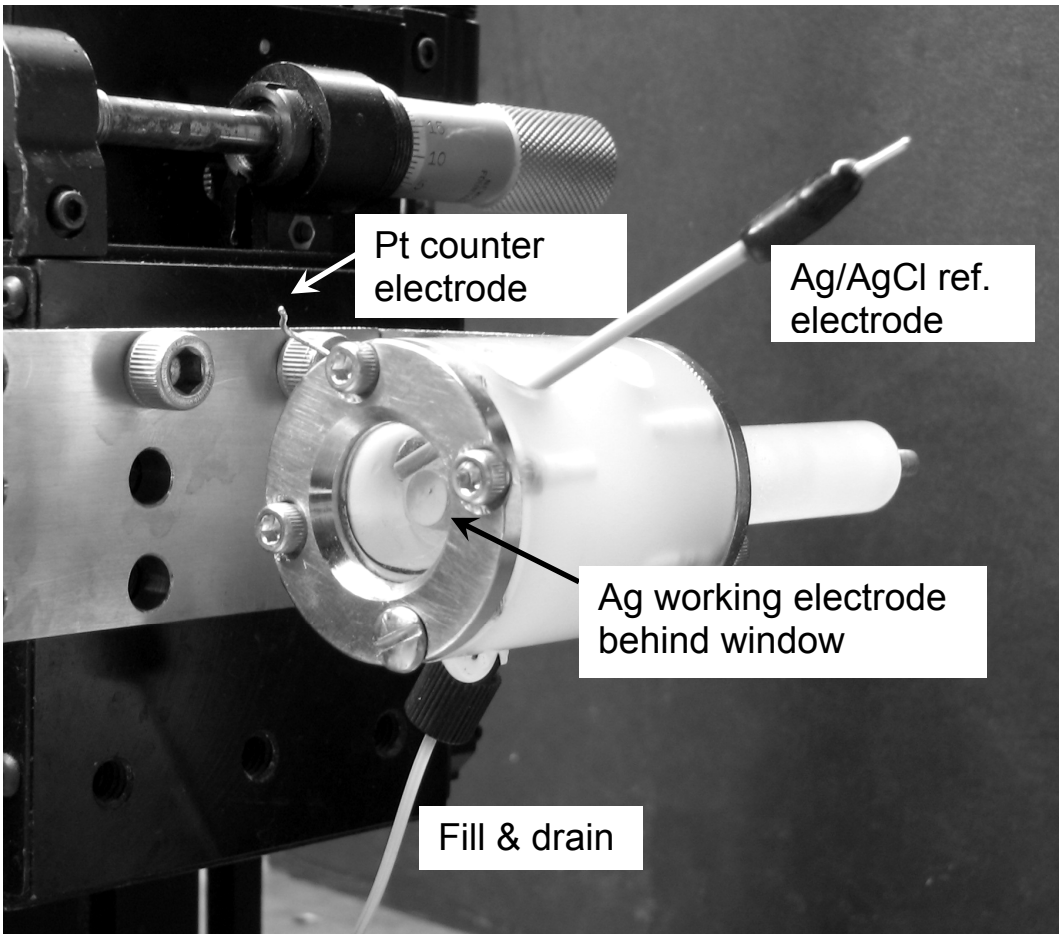


Figure 3.1. SERS spectroelectrochemical cell.

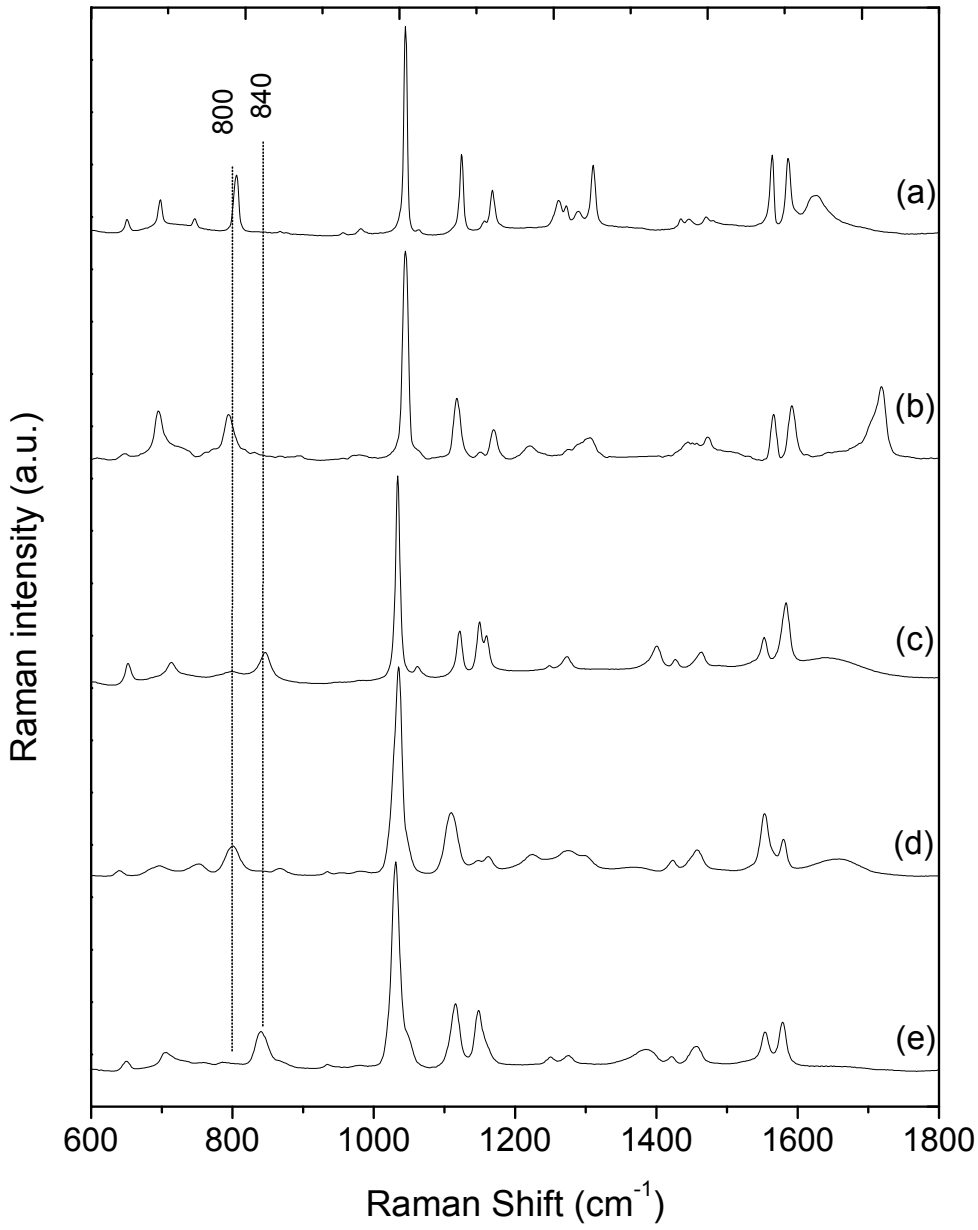


Figure 3.2. Raman spectra of solid 2-MBA (a), 2-MBA (0.05 M) dissolved in acetonitrile (b), 2-MBA (0.1 M) dissolved in basic solution, pH = 13 (c), SERS spectra of 2-MBA with applied potential as –0.6 V (vs. Ag/AgCl) in solution with pH=1 (d), and pH=13 (e).

Table 3.1.

Vibrational frequencies and band assignments for 2-MBA in bulk samples and bound to a silver surface. The bulk acid form is solid 2-MBA and the basic form is pH = 13 aqueous solution. SERS measurements are on silver electrodes held at an applied potential of -0.6 V (vs. Ag/AgCl) in pH =1 and 13 buffer, respectively.

| Raman (bulk) | | SERS | | Assignment | Reference |
|---|---|---|---|---|---|
| Acidic | Basic | Acidic | Basic | | |
| 654 | 656 | 640 | 649 | $\nu_{6a}$ | 22,38 |
| 698 | | 702 | | $\gamma$(CCC) | 22,25,38 |
| | 714 | | 706 | $\gamma(COO^-)$ | 25,38 |
| 806 | | 800 | | $\nu$(C-COOH) | 22,25 |
| | 846 | | 840 | $\delta(COO^-)$ | 22-25,38,39 |
| 1045 | 1034 | 1035 | 1031 | $\nu_{18b}$ | 22-25,38 |
| 1124 | 1122 | 1110 | 1116 | $\nu_{9b}$ | 25,38 |
| 1168 | 1150 | 1162 | 1148 | $\nu_{9a}$ | 38 |
| 1310 | 1274 | 1276 | 1275 | $\nu$(C-O) | 22,38 |
| 1430 | 1401 | | 1385 | $\nu_s(COO^-)$ | 22-25,37 |
| 1470 | 1463 | 1457 | 1457 | $\nu_{19a}$ | 22,37,38 |
| 1564 | 1553 | 1553 | 1554 | $\nu_{8a}$ | 22-25,37,38 |
| 1587 | 1584 | 1580 | 1579 | $\nu_{8b}$ | 22 |
| 1627 | 1642 | 1658 | | $\nu$(C=O) | 22,25,38 |

ligand, as shown in Figure 3.2. The relative intensity of these two bands changes monotonically and oppositely with changes in pH, as shown in Figure 3.3. As the pH is lowered and the -$COO^-$ is protonated to form -COOH, the intensities of the bands at 840 $cm^{-1}$ and 800 $cm^{-1}$ decrease and increase, respectively. The fraction of the deprotonated (benzoate) form of 2-MBA, $\beta$, can be estimated from the ratio of the relative intensities:

$$\beta = \frac{[-COO^-]}{[-COO^-]+[-COOH]} = \frac{I_{840}^{rel}}{I_{840}^{rel} + I_{800}^{rel}} \qquad [3.1]$$

where $I_{840}^{rel}$ and $I_{800}^{rel}$ are the intensities of the peak at 840 $cm^{-1}$ and 800 $cm^{-1}$ normalized to their maximum values, $I_{840}^{max}$ and $I_{800}^{max}$, which are obtained in buffer pH=10 at 0.0 V and pH= 1 at -0.6 V, respectively. $I_{840}^{max}$ and $I_{800}^{max}$ are the band intensities of the completely deprotonated and protonated 2-MBA monolayer, respectively, where the intensity of the corresponding conjugate forms are negligible. Note that by ratioing the intensities of the basic and acidic forms to report the relative fractions of the population, the effect of any variation in Raman scattering enhancement with pH or applied potential on the results will be cancelled.

3.3.2 pH response of the immobilized 2-MBA under potential control

The acid-base chemistry of the 2-MBA immobilized onto a silver surface was investigated by measuring *in situ* SERS spectra while varying the surface potential and solution pH. For each spectrum, the fraction of the deprotonated or basic form of 2-MBA, $\beta$, was determined by using Equation 3.1, and the results are plotted in Figure 3.4. It can be seen that at 0.0 V, deprotonated form (-$COO^-$) dominates even at very low pH, which is due to the low proton activity at the interface from the positively charged silver surface

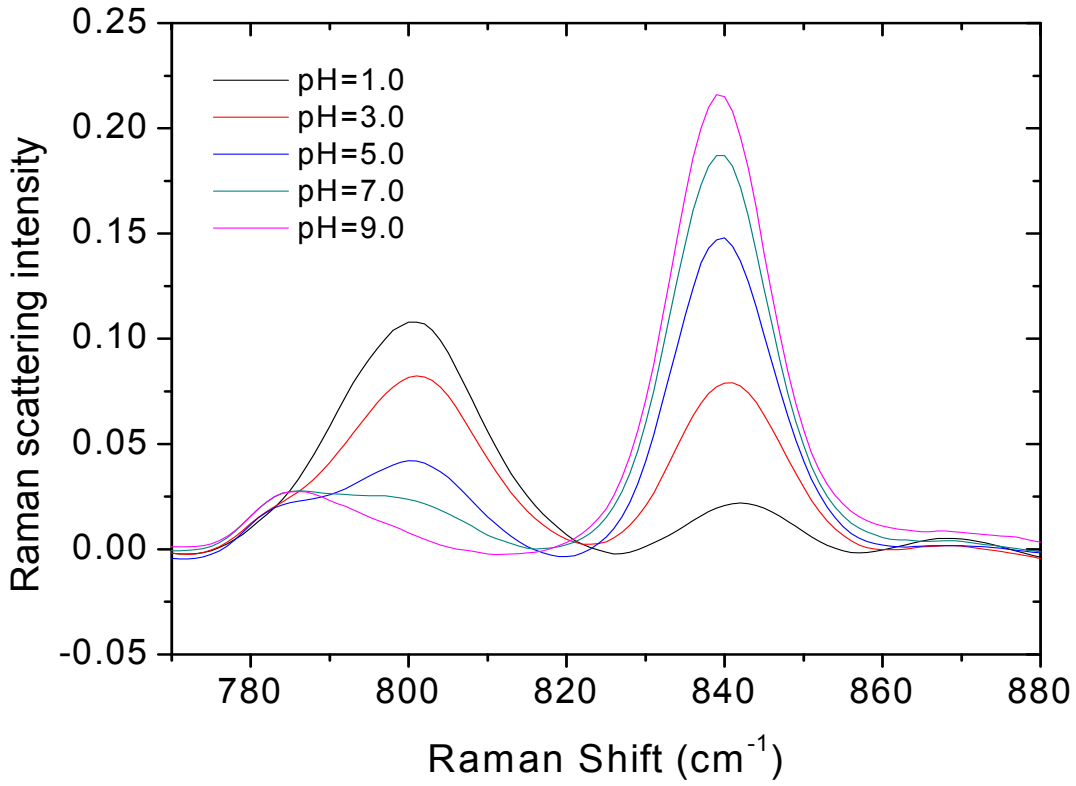


Figure 3.3. SERS spectra of 2-MBA in different solution pH with applied potential = -0.4 V (vs. Ag/AgCl).

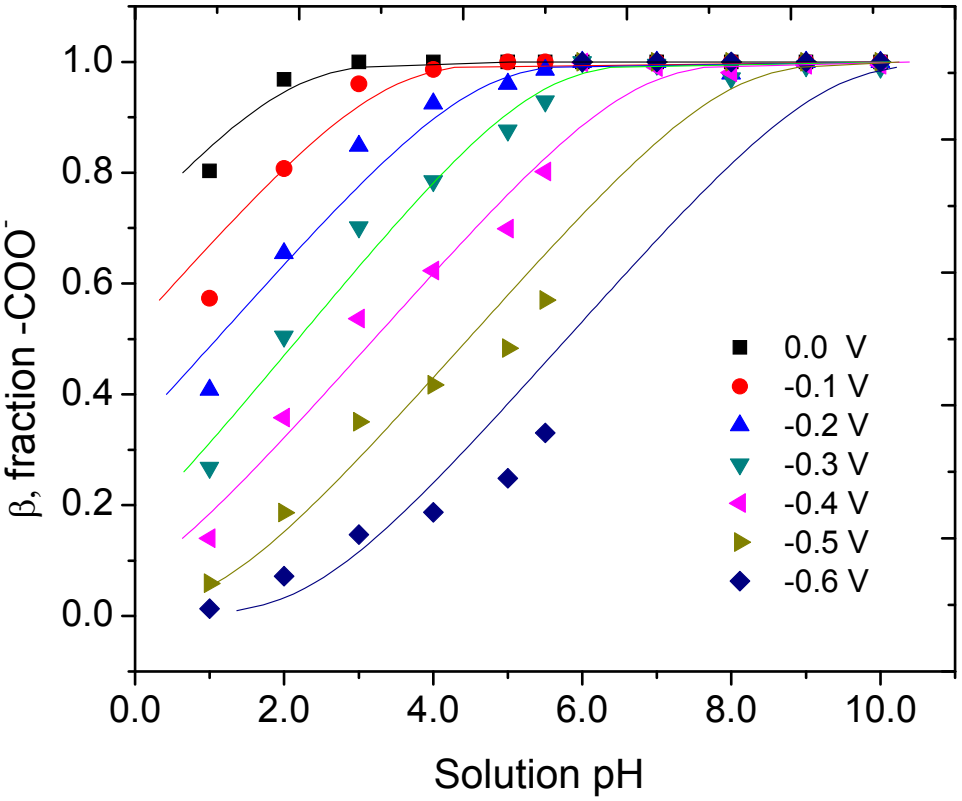


Figure 3.4. pH response of the deprotonated fraction, β, of immobilized 2-MBA under potential control with fits to Equation 3.6.

at this applied potential. At a given bulk solution pH, as the applied potential is more negative, the relative Raman scattering intensity from the bending mode of -$COO^-$ at 840 $cm^{-1}$ decreases significantly and the corresponding -COOH intensity at 800 $cm^{-1}$ increases. The protonation of the benzoate form occurs at more negative applied potentials because the local activity of protons increases at the interface, as predicted by the Poisson-Boltzmann equation for the activity of ions at a charged interface,[35]

$$a_{interface} = a_{bulk} \exp(-zF\Phi_0 / RT) \qquad [3.2]$$

where z is the charge of the ion and $\Phi_o$ is the surface potential. For protons, this equation predicts a change in the interfacial pH, $pH_{interface} = pH_{bulk} + F\Phi_o/2.303RT$, so at more negative potential, interfacial pH is lowered and the fraction of the benzoate form, β, decreases due to increased protonation.

Reversibility of the measurements on the same substrate was also tested. Figure 3.5 shows the SERS spectra of 2MBA in buffer with pH=7 before and after the 1st and 2nd potential-controlled measurement cycles. The spectra show no significant change in both band frequency and relative intensity between different bands. Some change of the absolute Raman intensity was observed, which could be due to the reconstruction of the Ag surface and change in SERS enhancement that occurs with the potential steps.

### 3.3.3 Interaction of the benzoate group of 2-MBA with silver and its displacement by acetate

A striking aspect of these data is a threshold pH that is apparent in these titration curves, above which the fraction of the benzoate form $\beta$ jumps to unity and is no longer sensitive to changes in solution pH or applied potential. This response at higher pH conditions appears to arise from an interaction of the benzoate group of immobilized

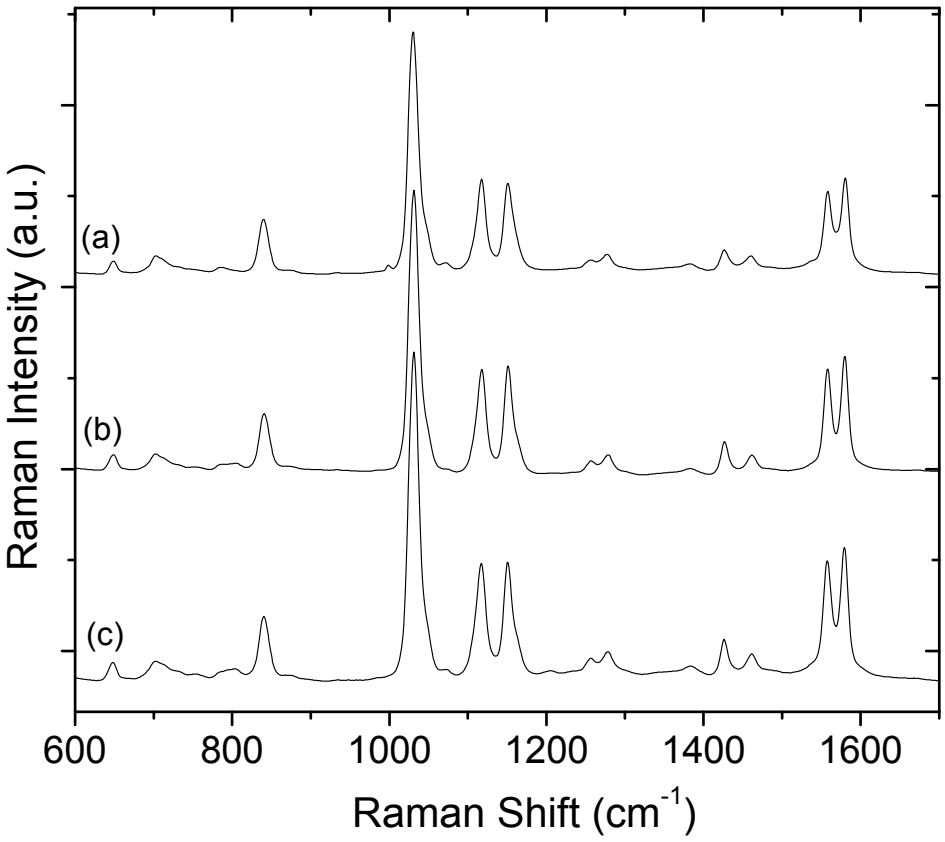


Figure 3.5. SERS spectra of immobilized 2-MBA in buffer of pH=7 at open circuit before the measurement cycle (a), after the first measurement cycle (b), and after the second measurement cycle (c). Scale of the Raman intensity of (b) is twice the others.

2-MBA with the silver surface. Because the benzoate functional group is in the ortho position relative to the thiol that immobilizes the ligand to the metal surface, the benzoate ligand is situated close to the silver surface and facilitates this interaction. The shift in the frequency of the symmetric carboxylate stretching vibrational mode, $\nu_s(COO^-)$, from 1401 $cm^{-1}$ in the basic solution to 1385 $cm^{-1}$ in the SERS spectra at higher pH is consistent with SERS spectra of carboxylate species interacting with silver surfaces as previously reported.[22, 25, 38, 39] As a check on this assignment, the SERS spectrum of benzoic acid adsorbed to silver was also measured, and it also exhibits a symmetric carboxylate stretching band at 1385 $cm^{-1}$ (see Figure 3.6).

Further evidence of benzoate interaction with the silver surface is found in the potential-dependent response of the carboxylate SERS intensity above the threshold pH of 6.0, where the silver-bound benzoate form dominates. In this higher pH range, the intensity of the symmetric carboxylate stretching mode is strongly potential dependent (see Figure 3.7(a)), which is characteristic of charge transfer interactions with the metal that contribute to the SERS enhancement;[33] these interactions require contact with the metal and can vary with applied potential which modulates the degree of charge transfer. Below the threshold pH, there is little change in the intensity of the symmetric carboxylate stretching band with applied potential; however, the band is still observed at ~1385 $cm^{-1}$ indicative of a carboxylate species interacting with the silver surface.

This apparent discrepancy is resolved by recognizing that acetate in the buffer can displace benzoate from the silver surface and lead to silver carboxylate Raman scattering when the solution pH is below the threshold. Indeed, acetate adsorbed to silver exhibits a symmetric carboxylate stretching frequency at ~1390 $cm^{-1}$. Furthermore, sodium acetate

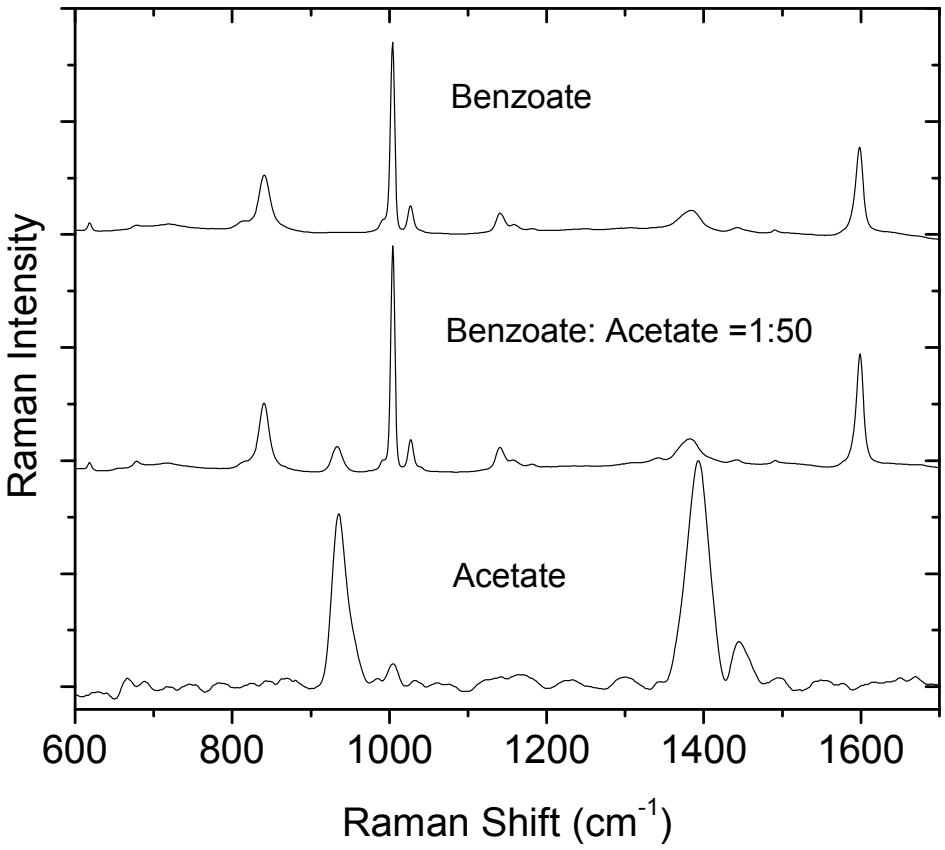


Figure 3.6. SERS spectra of sodium acetate (50mM), sodium benzoate (1mM), and mixture at the same concentrations. All spectra were taken at open circuit.

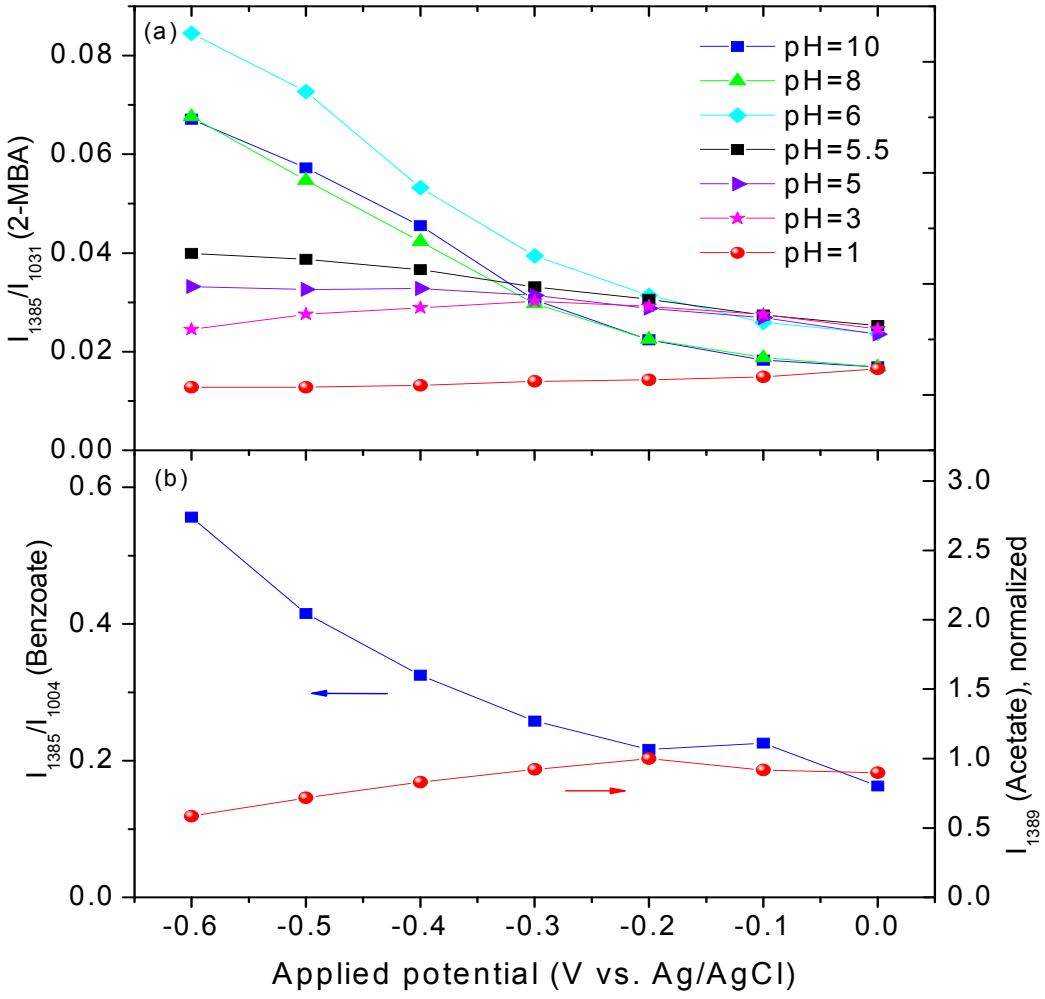


Figure 3.7. SERS intensities of ν($COO^-$) variation with applied potential. (a): immobilized 2-MBA in 20 mM acetate buffer at varying pH, and (b): sodium benzoate (1 mM) versus sodium acetate (50 mM) both at pH ~9.

can displace sodium benzoate from a silver surface when the sodium acetate solution concentration is more than 50-times that of sodium benzoate. Additional support for this hypothesis is provided by a comparison of the potential dependent SERS intensity of the symmetric carboxylate stretching mode for sodium benzoate and acetate adsorbed to a silver surface; see Figure 3.7(b). These results show a strong potential dependence for carboxylate scattering from adsorbed benzoate (similar in form to immobilized 2-MBA when the solution pH is above the threshold for benzoate-silver interaction). Adsorbed acetate, however, exhibits a much smaller carboxylate intensity change with potential, which is possible because it orients differently from benzoate on the silver surface. In addition, smaller polarizability of acetate could lead to less significant charge transfer interactions that contribute to the 'chemical' SERS enhancement. The potential variation of the adsorbed acetate scattering intensity follows the same trend as the silver-bound carboxylate band at pH values lower than the threshold for displacing 2-MBA from the silver surface (Figure 3.7(b)), which reinforces the assignment of carboxylate stretching in the low pH region to adsorbed acetate that has displaced benzoate of 2-MBA from the surface. The competition between acetate and benzoate of 2-MBA for interaction with the silver surface leads to a threshold pH that is independent of applied potential (see Figure 3.4). The reaction for displacement of silver-bound benzoate from 2-MBA (RCOOAg) to form silver-bound acetate (AgAc) must involve reaction with a neutral species, in this case acetic acid, HAc, in order for the threshold to be independent of applied potential:

$$\mathrm{RCOOAg} + \mathrm{HAc} \xleftrightarrow{K_d} \mathrm{AgAc} + \mathrm{RCOOH} \qquad [3.3]$$

where the equilibrium constant for the displacement reaction is given by:

$$K_d = \frac{[\mathrm{AgAc}][\mathrm{RCOOH}]}{[\mathrm{RCOOAg}][\mathrm{HAc}]} = \frac{[\mathrm{AgAc}][\mathrm{RCOOH}]K_a^{HAc}}{[\mathrm{RCOOAg}][\mathrm{Ac}^-][\mathrm{H}^+]} \quad [3.4]$$

where $K_a^{HAc}$ is the proton dissociation equilibrium constant for acetic acid. The displacement reaction by acetic acid leads to a threshold that is not a function of applied potential because the equilibrium depends on the product of [$Ac^-$] and [$H^+$], as indicated in the right-hand side of Equation 3.4. Because of their opposite charge, the Poisson-Boltzmann above predicts that an increase in the interfacial activity of [$H^+$] at more negative potentials is balanced by an equivalent decrease in the interfacial activity of [$Ac^-$]. There is a critical product of the two ion activities (producing a critical activity of acetic acid) that leads to displacement, and this product is independent of applied potential because of the opposite charges of the two mobile ions.

This proposed displacement of benzoate from the surface by acetic acid was further tested by measuring the threshold pH while the total acetate concentration in solution was varied. For a given total acetate concentration, $C_{NaAc}$, the threshold pH was measured by changing the solution pH from 7.0 slowly toward lower pH until a potential-sensitive benzoate fraction, $\beta$, was observed. As shown in Figure 3.8, at higher $C_{NaAc}$, a higher threshold pH for benzoate displacement is observed. Over an acetate concentration range from 5 mM to 100 mM, the threshold pH for displacement corresponds to a hydrogen ion activity which varies inversely with [$Ac^-$], as illustrated in Figure 3.8. The results show that the inverse of the proton activity, 1/[$H^+$], at the measured threshold pH, varies linearly with the acetate concentration, as predicted by the right-hand side of Equation 3.4 which describes benzoate displacement by acetic acid.

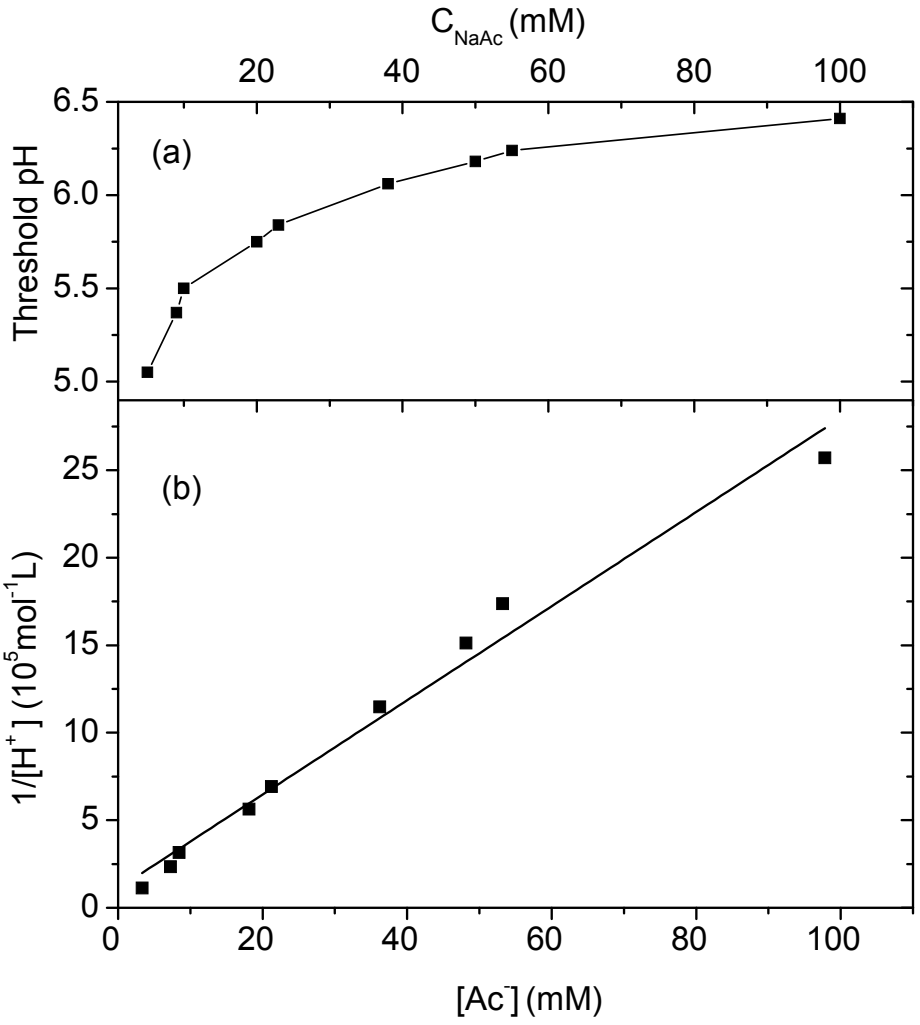


Figure 3.8. The effect of buffer concentration on threshold pH. (a): Threshold pH plotted versus total acetate concentration, $C_{NaAc}$ (upper x-axis) and (b): the inverse of the proton activity at the displacement threshold, $1/[H^+]$, plotted versus the acetate concentration, $[Ac^-]$, derived from the total acetate concentration, the solution pH, and the acetic acid dissociation constant (lower x-axis).

3.3.4 Fitting the titration curves of immobilized 2-MBA

When the solution pH is lower than the displacement threshold, the benzoate group of 2-MBA is no longer bound to silver and can, therefore, be protonated according to a usual potential-dependent pH response:

$$RCOO^- + H^+ \leftrightarrow RCOOH \qquad [3.5]$$

as shown by the results in Figure 3.4. This equilibrium can be used to determine the p$K_a$ of 2-MBA immobilized in a self-assembled monolayer, taking the surface potential into account in determining the interfacial proton activity. To determinate the p$K_a$ of the bound ligand, the pH response of 2-MBA under potential control are fitted to titration curves. Due to interactions between immobilized charged molecules and possible local variations in surface potential, titration curves of surface-immobilized ligands usually produce a broader pH response and a shift in p$K_a$ compared to a titration of the same molecule in solution.[11, 14, 15, 22, 23]

To account for interactions between charged molecules bound to a surface, Borkovec derived a model to fit interfacial titration data that includes the repulsive interaction between charged forms of the ligand on the surface,[14, 23]

$$\mathrm{pH} = \mathrm{p}K_a + \log\frac{\beta}{1-\beta} + \frac{\overline{E}\beta}{2.303RT} \qquad [3.6]$$

where $\overline{E}$ is the energy of interaction between charged ligands and $\beta$ is the fraction of the charged form of the ligand. A larger $\overline{E}$ corresponds to a greater interaction between immobilized molecules and results in a broader titration response and large p$K_a$ shift.

Figure 3.4 includes a least squares fit of the pH dependence of the benzoate fraction of 2-MBA, $\beta$, to Equation 3.6 for a single value of the repulsion energy, $\overline{E}$ = 28.1 kJ mol$^{-1}$, determined from a global fit of all seven titration curves. This energy corresponds to the repulsion of benzoate groups at complete deprotonation ($\beta$ = 1), and can be used to estimate the average distance between them, $r$, based on the repulsion energy of univalent charges on a square lattice, accounting for nearest and next-nearest neighbor interactions: $U = q^2(1 + 1/\sqrt{2})/r\ 4\pi\ \varepsilon\varepsilon_o$. Using the static dielectric constant of water for the intervening medium between the charges, the estimated average distance between bound ligands based on the repulsion energy is $r \sim 1.1$ Å, which is about an order of magnitude more closely spaced than could realistically be accommodated by the size of the 2-MBA. This result shows that there are likely additional sources of broadening of the titration and could be due to hydrogen bonds between adjacent carboxylic acid-carboxylate groups,[40] which have been invoked to explain capacitance data on the titration of carboxyl-terminated alkanethiols on gold[41] or due to a diverse population of SERS-active sites that exhibit a variation in local charge density[42] which can influence the potential-dependent interfacial p$K_a$, discussed in the following section.

3.3.5 Determination of the intrinsic p$K_a$ of immobilized 2-MBA.

The dependence of the apparent (interfacial) p$K_a$ on the applied potential can be explained by the Poisson-Boltzmann equation, which gives the dependence of the interfacial pH on the potential at the distance $x$ from the electrode surface where the ligand reacts ($\Phi_x$) and bulk solution pH,[35]

$$\mathrm{pH}_{\mathrm{interface}} = \mathrm{pH}_{\mathrm{bulk}} + \frac{F}{2.303RT}\Phi_x \qquad [3.7]$$

Substituting the interfacial pH into the definition of the p$K_a$ gives the dependence of the observed, interfacial p$K_a$ on the potential:

$$\mathrm{p}K_{a,x} = \mathrm{p}K_{a,0} - \frac{F}{2.303RT}\Phi_x \qquad [3.8]$$

where $\mathrm{p}K_{a,x}$ is the apparent (observed) interfacial p$K_a$ which depends on the interfacial potential, $\Phi_x$, and $\mathrm{p}K_{a,0}$, is the intrinsic p$K_a$ of the bound ligand at the potential of zero charge (PZC) or where $\Phi_x = 0$.

For an interface coated with dielectric monolayer, the potential distribution from the metal surface consists of a linear potential drop across the monolayer and then an approximately exponential drop of the double layer in the solution phase, where the interfacial potential at the plane of the $COO^-$ group, $\Phi_x$ is given by,[16, 17, 35, 43]

$$\Phi_x = \Phi_a - E_{\mathrm{PZC}} - \Phi_F \qquad [3.9]$$

where $\Phi_a$ is the applied potential, $E_{\mathrm{PZC}}$ is the potential of zero charge (PZC) of the Ag electrode, and $\Phi_F$ is the potential drop across the monolayer. $\Phi_F$ is proportional to the surface charge density on the metal and can be assumed to be proportional to the metal surface potential,[16, 43]

$$\Phi_F = \eta(\Phi_a - E_{\mathrm{PZC}}) \qquad [3.10]$$

where $\eta$ is the fraction of the potential drop across the dielectric monolayer. From Equations 3.8, 3.9, and 3.10, the relationship between the p$K_{a,x}$ and the applied potential, $\Phi_x$, can be obtained, where at a temperature, $T$ = 296K, $F/2.303\,RT$ = 17.0 $V^{-1}$, to yield:

$$\mathrm{p}K_{a,x} = -17.0\,\mathrm{V}^{-1}(1-\eta)\Phi_a + \mathrm{p\,K}_{a,0} + 17.0\,\mathrm{V}^{-1}(1-\eta)E_{\mathrm{PZC}} \qquad [3.11]$$

The titration curves in Figure 3.4 are fit to Equation 3.6 to obtain p$K_{a,x}$, and these results are plotted versus the applied potential, $\Phi_a$, in Figure 3.9. The data show a linear relationship between the interfacial p$K_a$ and the applied potential, given by the best fit line:

$$\mathrm{p}\,K_{a,x} = (-11.8 \pm 0.3)\,\mathrm{V}^{-1}\,\Phi_a + (-3.8 \pm 0.1) \qquad [3.12]$$

Comparing the slope of this line with the first term of Equation 3.11, gives the fraction of the applied potential that is dropped across the dielectric monolayer, $\eta$=0.31. From the intercept result at $\Phi_a$ = 0 of Equation 3.12 and substituting $\eta$=0.31, Equation 3.11 predicts the relationship between $\mathrm{p}K_{a,0}$ and PZC of the substrate,

$$\mathrm{p}K_{a,0} + 11.8\,E_{\mathrm{PZC}} = -3.8 \qquad [3.13]$$

By using the potential of zero charge ( $E_{\mathrm{PZC}} = -0.95$ V) for polycrystalline silver,[35, 44] the intrinsic p$K_a$ (which would be measured at the PZC) of the immobilized 2-MBA, $\mathrm{p}K_{a,0} = 7.4$ , is obtained. Five replicate measurements were performed to test the variation of the p$K_a$ of the electrodes prepared by the same method. The average results yield $\mathrm{p}K_{a,0} = 7.4 \pm 0.3$, which shows a significant shift compared with $\mathrm{p}K_a = 3.54$ of 2-MBA in aqueous solution.[45, 46] This shift in p$K_a$ has been corrected for surface potential as well broadening of the proton-transfer transition due to interaction between ligands on the surface (see above). It is likely that the observed shift is due to changes in electronic structure of the 2-MBA that accompany deprotonation and binding of the thiol group to

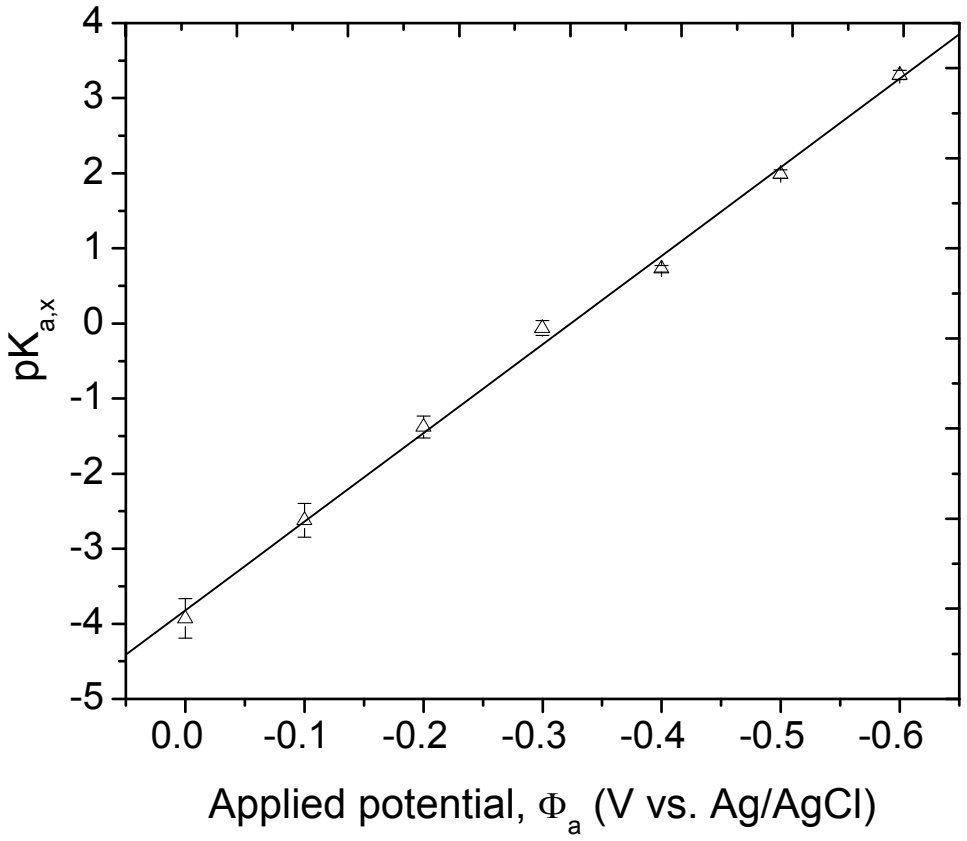


Figure 3.9. Interfacial $pK_a$ of 2-MBA varies with the applied potential (vs Ag/AgCl).

the silver surface, leading to greater electron density in the benzoic acid group than in free solution and a weaker acid for the silver-immobilized ligand.

## 3.4 Conclusions

The acid-base chemistry of 2-mercaptobenzoic acid (2-MBA) immobilized on a silver electrode was investigated by surface-enhanced Raman spectroscopy under potential control. The relative intensity of the pH-sensitive benzoate modes, $\delta(COO^-)$ and $\nu$(C-COOH), of 2-MBA were able to quantify the populations of the basic and acidic forms of the ligand, while the carboxylate symmetric stretching mode, $\nu_s(COO^-)$, revealed interactions between the benzoate group and the silver surface, which dominated at high pH conditions. This benzoate surface binding could be displaced by acetic acid at a pH threshold, below which ordinary titration behavior by the immobilized ligand was observed. This displacement threshold is not unique to acetate; phosphate buffer also yielded a similar threshold at higher pH values than acetate at an equivalent solution concentration, indicating the expected stronger interactions by phosphate with the silver surface. Having the carboxylate in the ortho position relative to the thiol group in 2-MBA greatly increases the likelihood of its interaction with the silver surface; however, this particular substitution is not required for these interactions, which were also observed with the para-substituted, 4-MBA when the surface coverage was low, where the ligand could apparently lie down on the metal surface. A systematic coverage- and potential-dependent study of the interactions of 4-MBA with silver surfaces is currently in progress.

Fitting of the 2-MBA titration curves below the displacement threshold pH provided information about interactions between the ligands that lead to broadening of

the pH response. In addition, the potential-dependence of the interfacial p$K_a$ was analyzed using the Poisson-Boltzmann equation to determine the intrinsic p$K_a$ of immobilized 2-MBA at the PZC of the metal substrate. This result showed decrease in the acidity of the benzoate group compared to the same molecule in free solution, which likely arises from changes in electronic structure when the ligand binds to the metal surface through the thiol group.

These results suggest that one should exercise care in the interpretation of the pH response of carboxylate ligands as SERS pH probes, either immobilized on metal particles or bound to fiber-optic sensors. Carboxylate reporter groups were found to interact with metal surfaces, the degree to which can vary with the presence of other metal-active molecules in solution. Ligands should, therefore, be chosen to have a conformation and surface coverage that prevents the carboxylate or other pH sensitive functional groups from finding the metal surface. Furthermore, the results show the significant influence of the surface potential on the activity of protons at the interface, which changes the interfacial pH relative to the bulk solution. This effect can occur even in open-circuit situations when ions in solution adsorb to the surface and change its potential relative to free solution.[36] When possible, SERS studies of proton- or other ion-binding ligands should be performed under potential control, to avoid having the observed equilibria depend not only on the target ion activity but also on other ions that may adsorb and accumulate at the sensor surface. While potential control is not possible for SERS nanoparticle sensor applications, it might be possible to incorporate an inert but strongly dipolar probe molecule in the self-assembled monolayer that responds to changes in surface potential by Stark-tuning of the vibrational transition. This concept

has been successfully applied using mixed monolayers with nitrile-terminated thiols to probe electric fields in the diffuse double layer[47-49] and could be useful as a means to monitor and correct the effects of surface potential on SERS-active probes for ionic species in solution.

## 3.5 References


(1) Love, J. C.; Estroff, L. A.; Kriebel, J. K.; Nuzzo, R. G.; Whitesides, G. M. *Chemical Reviews* **2005**, *105*, 1103-1170.

(2) Lahann, J.; Mitragotri, S.; Tran, T.-N.; Kaido, H.; Sundaram, J.; Choi, I. S.; Hoffer, S.; Somorjai, G. A.; Langer, R. *Science* **2003**, *299*, 371-374.

(3) Jiang, Y.; Wang, Z.; Yu, X.; Shi, F.; Xu, H.; Zhang, X.; Smet, M.; Dehaen, W. *Langmuir* **2005**, *21*, 1986-1990.

(4) Matthews, J. R.; Tuncel, D. n. s.; Jacobs, R. M. J.; Bain, C. D.; Anderson, H. L. *Journal of the American Chemical Society* **2003**, *125*, 6428-6433.

(5) Liu, Y.; Mu, L.; Liu, B.; Zhang, S.; Yang, P.; Kong, J. *Chem. Commun.* **2004**, 1194-1195.

(6) Schouten, S.; Stroeve, P.; Longo, M. L. *Langmuir* **1999**, *15*, 8133-8139.

(7) Murgida, D. H.; Hildebrandt, P. *Journal of the American Chemical Society* **2001**, *123*, 4062-4068.

(8) Creager, S. E.; Clarke, J. *Langmuir* **1994**, *10*, 3675-3683.

(9) Liu, Y.-J.; Navasero, N. M.; Yu, H.-Z. *Langmuir* **2004**, *20*, 4039-4050.

(10) Sugihara, K.; Shimazu, K.; Uosaki, K. *Langmuir* **2000**, *16*, 7101-7105.

(11) Smith, D. A.; Wallwork, M. L.; Zhang, J.; Kirkham, J.; Robinson, C.; Marsh, A.; Wong, M. *The Journal of Physical Chemistry B* **2000**, *104*, 8862-8870.

(12) Sheikh, K. H.; Evans, S. D.; Christenson, H. K. *Langmuir* **2007**, *23*, 6893-6895.

(13) Bryant, M. A.; Crooks, R. M. *Langmuir* **1993**, *9*, 385-387.

(14) Kakiuchi, T.; Iida, M.; Imabayashi, S.-i.; Niki, K. *Langmuir* **2000**, *16*, 5397-5401.

(15) Leopold, M. C.; Black, J. A.; Bowden, E. F. *Langmuir* **2002**, *18*, 978-980.

(16) Smith, C. P.; White, H. S. *Langmuir* **1993**, *9*, 1-3.

(17) White, H. S.; Peterson, J. D.; Cui, Q.; Stevenson, K. J. *J. Phys. Chem. B* **1998**, *102*, 2930-2934.

(18) Burgess, I.; Seivewright, B.; Lennox, R. B. *Langmuir* **2006**, *22*, 4420-4428.

(19) Pope, J. M.; Buttry, D. A. *J. Electroanal. Chem.* **2001**, *498*, 75-86.

(20) Mullen, K. I.; Wang, D.; Crane, L. G.; Carron, K. T. *Analytical Chemistry* **1992**, *64*, 930-936.

(21) Yu, H.-Z.; Xia, N.; Liu, Z.-F. *Analytical Chemistry* **1999**, *71*, 1354-1358.

(22) Lee, S. B.; Kim, K.; Kim, M. S. *J. Raman Spectrosc.* **1991**, *22*, 811-817.

(23) Borkovec, M. *Langmuir* **1997**, *13*, 2608-2613.

(24) Gershevitz, O.; Sukenik, C. N. *Journal of the American Chemical Society* **2003**, *126*, 482-483.

(25) Michota, A.; Bukowska, J. *Journal of Raman Spectroscopy* **2003**, *34*, 21-25.

(26) Talley, C. E.; Jusinski, L.; Hollars, C. W.; Lane, S. M.; Huser, T. *Analytical Chemistry* **2004**, *76*, 7064-7068.

(27) Bishnoi, S. W.; Rozell, C. J.; Levin, C. S.; Gheith, M. K.; Johnson, B. R.; Johnson, D. H.; Halas, N. J. *Nano Letters* **2006**, *6*, 1687-1692.

(28) Lim, J. K.; Joo, S.-W. *Applied Spectroscopy* **2006**, *60*, 847-852.

(29) Jeanmaire, D. L.; Van Duyne, R. P. *Journal of Electroanalytical Chemistry* **1977**, *84*, 1-20.

(30) Haynes, C. L.; McFarland, A. D.; Duyne, R. P. V. *Analytical Chemistry* **2005**, *77*, 338 A-346 A.

(31) Fleischmann, M.; Hendra, P. J.; McQuillan, A. J. *Chemical Physics Letters* **1974**, *26*, 163-166.

(32) Otto, A.; Mrozek, I.; Grabhorn, H.; Akemann, W. *J. Phys.: Condens. Matter* **1992**, *4*, 1143-1212.

(33) Campion, A.; Kambhampati, P. *Chem. Soc. Rev.* **1998**, *27*, 241-250.

(34) Cao, X. W. *Journal of Raman Spectroscopy* **2005**, *36*, 250-256.

(35) Bard, A. J.; Faulkner, L. R. *Electrochemical Methods: Fundamentals and Applications*; Wiley: New Jersey, 2000.

(36) Uibel, R. H.; Harris, J. M. *Analytical Chemistry* **2002**, *74*, 5112-5120.

(37) Lecomte, S.; Ricoux, R.; Mahy, J. P.; Korri-Youssoufi, H. *J Biol Inorg Chem* **2004**, *9*, 850-858.

(38) Jung Sang, S.; Jurae, K. *Journal of Raman Spectroscopy* **1998**, *29*, 143-148.

(39) Kwon, Y. J.; Son, D. H.; Ahn, S. J.; Kim, M. S.; Kim, K. *J. Phys. Chem.* **1994**, *98*, 8481-8487.

(40) Meot-Ner, M.; Elmore, D. E.; Scheiner, S. *J. Am. Chem. Soc.* **1999**, *121*, 7625-7635.

(41) Aoki, K.; Kakiuchi, T. *Journal of Electroanalytical Chemistry* **1999**, *478*, 101-107.

(42) Oklejas, V.; Harris, J. M. *Applied Spectroscopy* **2004**, *58*, 945-951.

(43) Smith, C. P.; White, H. S. *Anal. Chem.* **1992**, *64*, 2398-2405.

(44) Larkin, D.; Guyer, K. L.; Hupp, J. T.; Weaver, M. J. *J. Electroanal. Chem. Interfacial Electrochem.* **1982**, *138*, 401-423.

(45) Buckingham, J. *Dictionary of Organic Compounds, 6th Edition*; Chapman & Hall, 1996.

(46) Armarego, W. L. F.; Chai, C. *Purification of Laboratory Chemicals, 5th Edition*; Butterworth-Heinemann: Oxford, England, 2003.

(47) Oklejas, V.; Sjostrom, C.; Harris, J. M. *The Journal of Physical Chemistry B* **2003**, *107*, 7788-7794.

(48) Oklejas, V.; Sjostrom, C.; Harris, J. M. *Journal of the American Chemical Society* **2002**, *124*, 2408-2409.

(49) Oklejas, V.; Harris, J. M. *Langmuir* **2003**, *19*, 5794-5801.

# CHAPTER 4

# SURFACE-ENHANCED RAMAN SPECTROSCOPY STUDIES OF SURFACTANT ADSORPTION AND ION-INTERACTION ON A HYDROPHOBIC SURFACE

## 4.1 Introduction

The interactions between surfactants and solid surface are of increasing interest in research because they play a key role in many important applications[1] including ore floatation, lubrication, adhesion, detergency, emulsification, and ion interaction chromatography (IIC).[2, 3] Understanding of interactions between a surfactant and the hydrophobic surface is essential for controlling retention in IIC, which employs a surfactant or ion-interaction reagent to modify the retention and separation of ionized species.[2, 3] By forming an ion pair with an oppositely charged surfactant, ionic analytes can be strongly retained by the stationary phase, resulting in enhanced resolution and better selectivity in chromatographic separations.[2, 3]

Knowledge of the surfactant adsorption at the stationary phase/solution interface and their interaction with ionic species is important for understanding retention mechanism and optimizing experimental conditions, which contributes to advances in separation using IIC.[2, 3] Researchers have made considerable effort to investigate the mechanism of ion retention in IIC and different models have been proposed. In the "ion-pair" model,[2-5] a complex of surfactant and ionic analytes is assumed to be formed

in the mobile phase, and then adsorbed onto the stationary phase with sufficient stability to influence the analyte retention. In contrast, in the "dynamic ion-exchange" model,[2, 3, 6, 7] researchers suggested that the surfactant adsorbed to the stationary phase forming a dynamic ion exchanger, which allows the ionic species to be retained and eluted from the surface. Many studies also suggested that both mechanisms can occur under certain experimental conditions.[2, 3, 6, 8-10]

Most previous studies of IIC were based on chromatographic retention measurements,[4-7, 11] which do not provide *in situ* information about the interactions occurring stationary phase/solution interface. *In situ* probing of molecules adsorbed at the interface is a challenge, especially when the surface coverage is much less than a monolayer, because it is difficult to separate the signals of surface-bound species from those in the bulk solvent, which can be a significant interference. A variety of techniques such as quartz crystal microbalance,[12, 13] contact angle measurement,[14] ellipsometry,[15, 16] atomic force microscopy,[17-20] cyclic voltammetry,[21-23] surface plasmon resonance spectroscopy,[24-28] and attenuated total reflection Fourier transform infrared spectroscopy[26, 29-34] have been used to characterize the n-alkane chain functionalized surface and *in situ* investigate the adsorption/desorption of surfactants at the interface. However, few of these studies have addressed ion interactions at the interface, which are fundamental for understanding the retention mechanism of IIC. Fluorescence spectroscopy[8, 35] has been demonstrated to be a useful tool to *in situ* study the interaction of ionic species with the hydrophobic surface in the presence of a surfactant. This approach is, however, restricted to fluorescent active ionic species, which are not common analytes studied by IIC.

Recently, confocal Raman microscopy has been used to study the ion interaction of cetylpyridinium ion ($CP^+$) and nitrobenzenesulfonate ($NB^-$) at n-alkane chain ($C_{18}$) functionalized stationary phase.[36] Preadsorption of $CP^+$ at the $C_{18}$ surface was observed, which was increased by the addition of supporting electrolyte or $NB^-$. Quantitative analysis of the Raman scattering data confirmed the formation of a surface ion-pair complex between $CP^+$ and $NB^-$. Another tool for investigating molecules adsorbed on metal surface is surface-enhanced Raman scattering (SERS), which occurs when incident radiation excites surface plasmons in the metal, increasing the local excitation intensity as well as the Raman scattering probability of surface-bound species.[37-41] With an enhancement factor ranging from $10^6$ to $10^8$, the method is sufficiently sensitive for detection of submonolayer populations of molecules at an interface.[37-41] Interaction of surfactants with bare metal surfaces and monolayer-modified hydrophobic surface has been studied using SERS technique.[42-48] In this latter study,[48] the adsorption of the cetylpyridinium on a $C_{18}$-modified gold colloid surface was investigated with SERS, and the adsorption equilibrium was observed to follow a Frumkin isotherm.

In this work, the accumulation of $CP^+$ on the 1-dodecanthiol modified silver ($C_{12}$) surface and the effect of supporting electrolyte KCl on the adsorption equilibria were investigated by SERS. A second goal of this work is to examine the retention of $NB^-$ to the $C_{12}$ surface and the participation of $CP^+$ in this process. The competition of several anions, perchlorate, chloride, and sulfate with the adsorption of $NB^-$ onto the $C_{12}$ surface in the presence of $CP^+$ was studied, which provided the relative binding affinity of these anions with the $CP^+$ at the interface. SERS results showed significant enrichment of $NB^-$ on the $C_{12}$ surface with the addition of $CP^+$. However, a reduction in $NB^-$ intensity was

observed with further addition of the $CP^+$. This observation is consistent with the effect of surfactant concentration on the retention data from IIC measurements. The adsorption equilibrium of $CP^+$ and the coadsorption of $NB^-$ on the $C_{12}$ surface were fit to a Langmuir model and "dynamic ion-exchange" model, respectively. The study demonstrated that SERS can be an effective technique to investigate the adsorption of surfactants and ion interactions at a hydrophobic modified metal electrode surface.

## 4.2 Experimental

### 4.2.1 Materials

1-dodecanthiol (98%, Sigma-Aldrich), cetylpyridinium chloride (CPC) (98%, Sigma-Aldrich), sodium nitrobenzenesulfonate (98%, Sigma-Aldrich), Triton X-100 (Sigma-Aldrich), potassium chloride (GR, Merck), sodium perchlorate (98%, Sigma-Aldrich), and sodium sulfate (AR, Mallinckrodt) were used as received.

### 4.2.2 Substrate preparation

All electrodes were constructed from a 7-mm diameter silver rod (99.999%, Alfa Aesar). The surfaces of the electrodes were polished with 800, 1500 and 2000 grit silicon carbide paper (3M) and then with alumina polishing slurries (1.0 μm) on a microfiber polishing cloth (Buehler). The electrode surfaces were then electrochemically roughened by oxidation-reduction cycles in KCl (0.1 M) solution; specifically, linear sweeps from +0.3 V to -0.3 V (vs. Ag/AgCl) and back to +0.3 V were applied at a sweep rate of 15 mV/s for 3 cycles, and then the potential was held at –0.3 V for 2 min.[49] Electrodes were then removed from the cell and rinsed with deionized water prior to monolayer self-assembly.

4.2.3 SAM preparation

The self-assembly step was conducted by immersing the Ag electrodes in 0.1 mM solutions of 1-dodecanthiol in methanol for 12 h.

4.2.4 Raman scattering measurements

Surface-enhanced Raman measurements were conducted with a fiber-optic coupled Raman spectrometer (PI-200, Process Instruments) with a frequency stabilized, 785-nm diode laser. The laser power at the sample was 260 mW, and the integration time was 20 s for all measurements. The position of the working electrode is adjusted to be about 1 mm from the fused silica front window of the cell to minimize the interference from the bulk solution.

## 4.3 Results and Discussion

### 4.3.1 Adsorption of $CP^+$ to the $C_{12}$ surface

Figure 4.1 shows the Raman spectrum of 0.1 M CPC in aqueous solution and SERS spectra of 1-dodecanthiol monolayer and adsorption of 0.1 mM CPC onto the $C_{12}$ surface. The most intensely scattering mode observed at 1031~1032 $cm^{-1}$ for CPC, which is corresponding to the symmetric trigonal ring breathing mode ($\upsilon_1$) of the pyridinium,[36, 45, 46, 48] is used to identify the presence of $CP^+$ and to calculate its intensity at the interface. For the spectrum of $C_{12}$ monolayer, the broad band at 705 $cm^{-1}$ is the characteristic of a trans conformers of S-C-C chain, while bands at 1082 $cm^{-1}$ and 1127 $cm^{-1}$ are assigned to the stretching modes of trans C-C-C.[50, 51] As indicated by Figure 4.1, the adsorption of 100 $\mu$M CPC to the $C_{12}$ surface leads to a slight shift of $\upsilon_1$ mode and a significant increase in the band intensity. It is clear that this Raman intensity of the CPC originates

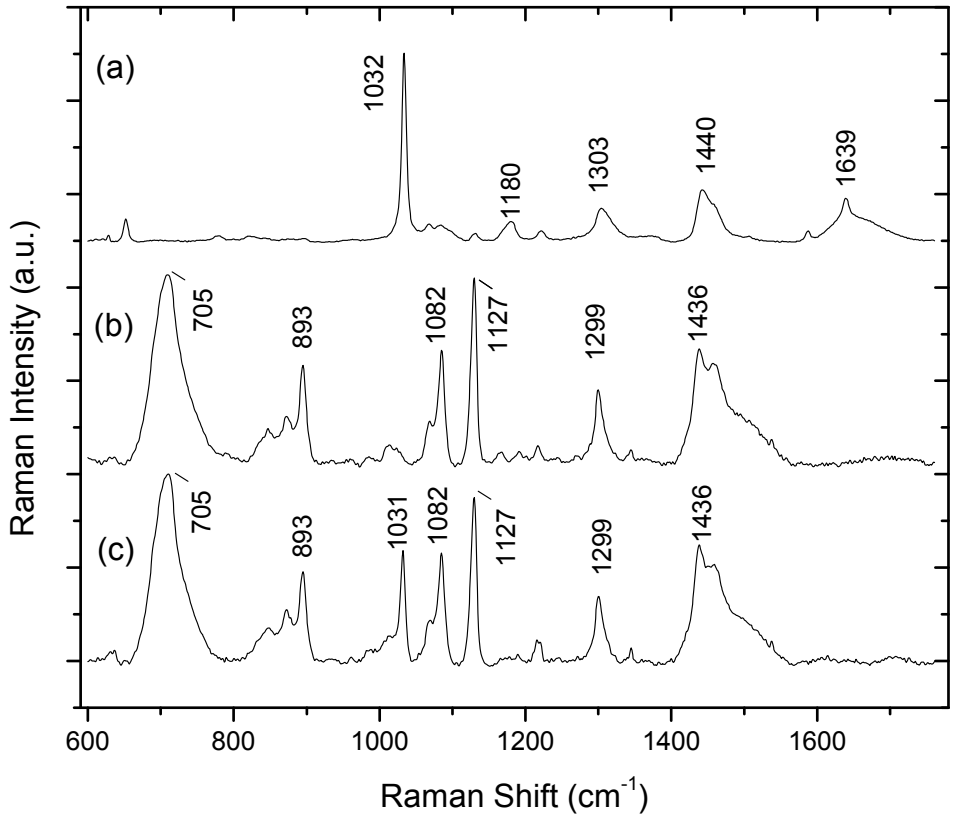


Figure 4.1. Raman spectrum of CPC (50 mM) in aqueous solution (a), SER spectrum of $C_{12}$ on Ag surface (b), and SER spectrum of $C_{12}$ in the presence of 0.5 mM CPC (c).

from the surface-bound molecules, instead of the molecules in bulk solution, which are not detectable at 100 μM concentration.

To measure the adsorption equilibrium of the $CP^+$ on $C_{12}$ surface, the intensity of $\upsilon_1$ mode of pyridinium ($I_{1031}$) was used to determine the relative surface coverage, which is plotted as a function of CPC concentration (Figure 4.2). Similar to the results reported in a previous study,[48] the adsorption data are not well fit by a Langmuir model.[52] This was attributed to repulsive interactions of the adsorbed charged molecules limiting their accumulation on the $C_{12}$ surface. Therefore, to account for this interaction, a Frumkin isotherm was employed to fit the adsorption equilibrium,[48, 53]

$$\frac{\theta}{1-\theta} = KC\exp(2g\theta) \qquad [4.1]$$

where $\theta$ is the relative surface coverage, $C$ is the bulk CPC concentration, $K$ is the equilibrium constant, and $g$ is the Frumkin interaction parameter. A positive or negative value of $g$ can be observed when the interaction between the adsorbate is attractive or repulsive, respectively. In the limiting case, when $g = 0$, the adsorption equilibrium is equivalent to a Langmuir model.[52]

The fitting of the $I_{1031}$ as a function of CPC concentration with Frumkin isotherm, optimized by iterative nonlinear least squares, is shown in Figure 4.2. The data fitting yields $K = (2.9 \pm 2) \times 10^5 M^{-1}$ and $g = -1.7 \pm 0.4$, which indicates a repulsion between the adsorbed molecules. This observation is expected because of charge repulsion of the head groups of adsorbed $CP^+$.

In order to verify that the deviation of the adsorption from the Langmuir isotherm is due to the repulsion of the charged molecules, adsorption of $CP^+$ on $C_{12}$ surface was

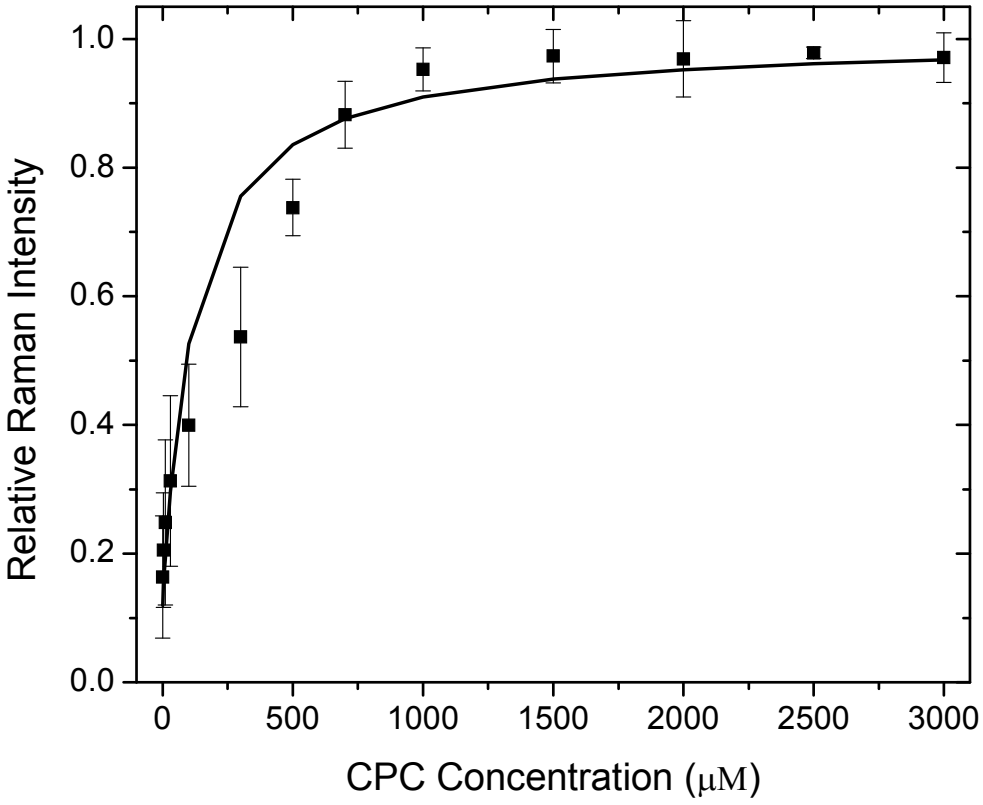


Figure 4.2. Adsorption isotherm of $CP^+$ on the $C_{12}$ surface without supporting electrolyte and the Frumkin isotherm fit of the data set to eq 4.1.

investigated with the addition of supporting electrolyte, which can screen the surface accumulated charge and decrease the repulsion of the adsorbates. As shown in Figure 4.3, equilibrium intensity of $CP^+$ increases to maximum with the increase of KCl concentration. This is likely due to the shielding of the charge of the pyridinium head group by the $Cl^-$ ions, allowing more $CP^+$ to accumulate on the $C_{12}$ surface. The adsorption equilibrium of the $CP^+$ in the presence of 3 mM KCl was also measured. As shown in Figure 4.4, the isotherm looks more Langmuir-like compared to the adsorption without added supporting electrolyte (Figure 4.2). The fitting of the data to a Langmuir isotherm yields an adsorption equilibrium constant $K = (1.4 \pm 0.6) \times 10^4 \, \mathrm{M}^{-1}$. The results demonstrated that the addition of supporting electrolyte has a significant effect on the adsorption of surfactants to the hydrophobic surface.

4.3.2 Ion interaction measurement

The existence or nonexistence of ion pairs in the solution phase is a critical question to address in order to understand the mechanism of ion interaction chromatography. Previous studies have shown that ion-pairs can forms in either mobile phase or stationary phase, leading to different retention mechanisms proposed for IIC.[2, 3] Ion-pair complexes in solution have been identified previously using conductivity measurement based on the plot of the conductance of the mixture solution as a function of the surfactant concentration.[3, 54] A straight line of the plot indicates that no ion interaction occurs, while deviation from the straight line reflects the formation of ion-pair complexes.

In this study, sodium nitrobenzenesulfonate (NBS) was used as the ionic analyte to study its ion interaction with $CP^+$. As shown in Figure 4.5 (a), the Raman spectrum of

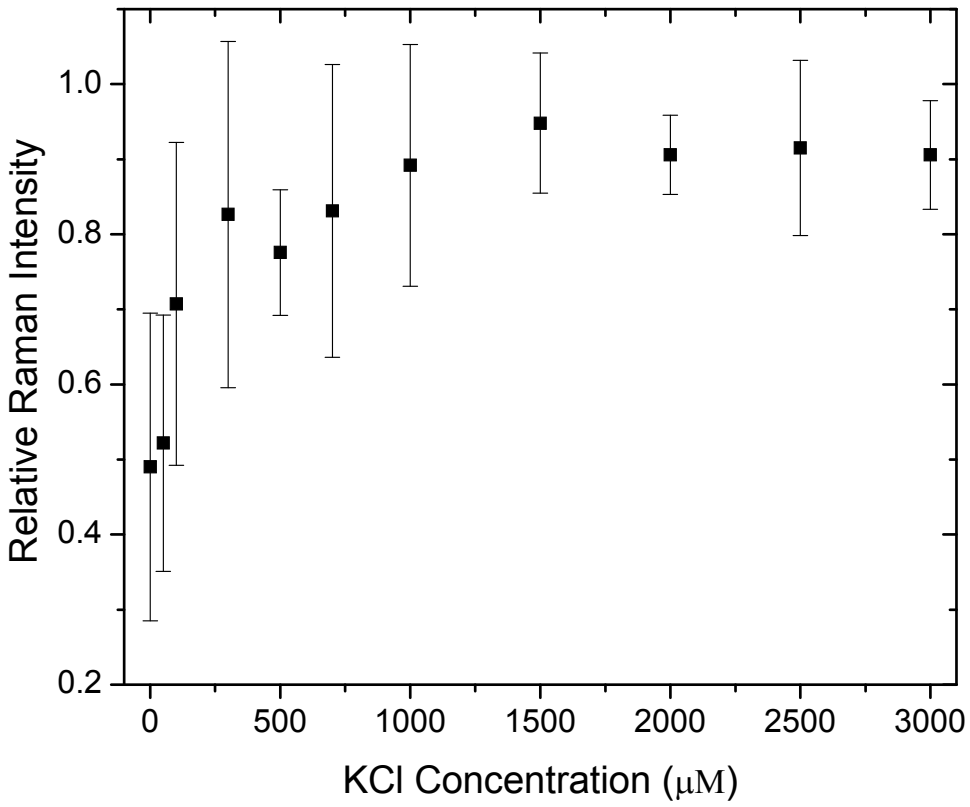


Figure 4.3. The effect of KCl concentration on the adsorption of $CP^+$ (0.3 mM) to the $C_{12}$ surface.

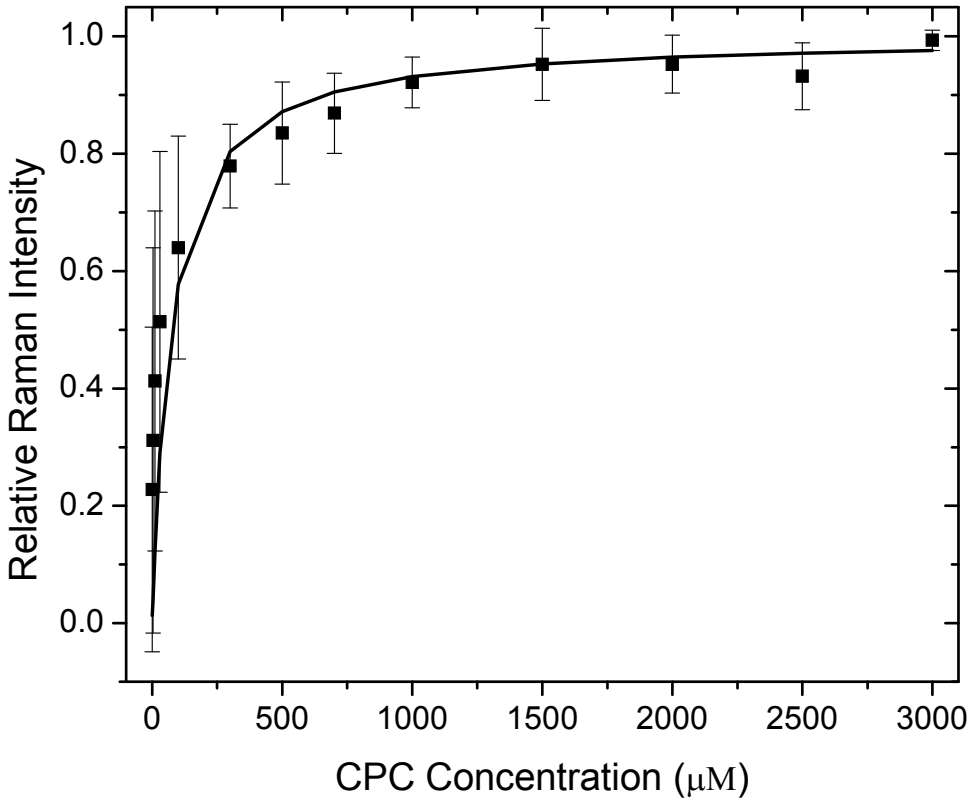


Figure 4.4. Adsorption isotherm of $CP^+$ on the $C_{12}$ surface in the presence of 3 mM KCl and the Langmuir fit of the data set.

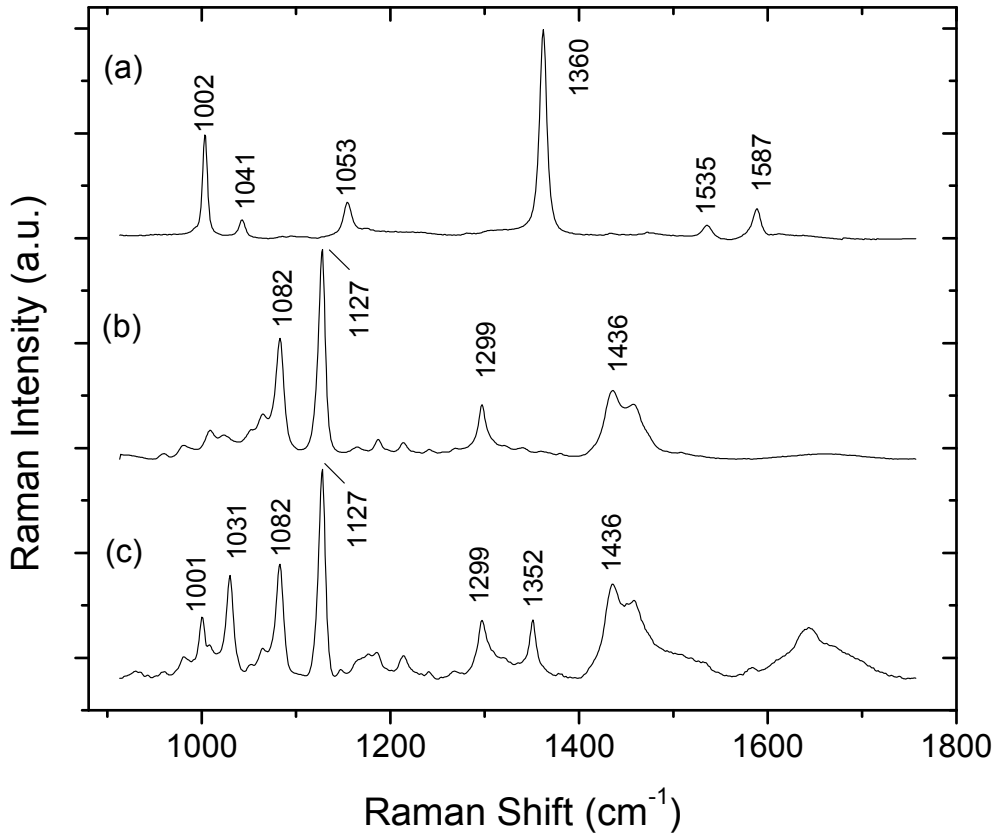


Figure 4.5. Raman spectrum of NBS (50 mM) in aqueous solution (a), SER spectrum of $C_{12}$ surface in the presence of 0.5 mM NBS (b), and SER spectrum of $C_{12}$ in the presence of 0.5 mM CPC and 0.5 mM NBS (c).

NBS in aqueous solution exhibits two major bands at 1002 $cm^{-1}$ and 1360 $cm^{-1}$, which correspond to the ring breathing mode and symmetry stretching mode of $NO_2$ group,[55] $\upsilon(NO_2)$, respectively. The strongest band, $\upsilon(NO_2)$ is used to identify the presence of $NB^-$ and to calculate its intensity. Interaction between $CP^+$ and $NB^-$ in solution was investigated based on the Raman spectra of their mixture solutions, as shown in Figure 4.6. Addition of CPC to the NBS solution leads to a shift of the $\upsilon(NO_2)$ band to a lower wavenumber, which indicates formation of a complex, changing the electronic structure of the $NB^-$ and shifting the vibrational band. The shift of $\upsilon(NO_2)$ depends strongly on the molar ratio of CPC vs NBS. This observation shows that the band shifting results from the ion interaction equilibrium (eq 4.2),

$$NB^- + CP^+ \xleftrightarrow{K_{b1}} IP \qquad [4.2]$$

where IP is the ion-pair complex of $CP^+$ and $NB^-$, and $K_{b1}$ is the binding constant of $NB^-$ with $CP^+$, which can be obtained by:

$$K_{b1} = \frac{[IP]}{([NB]_0 - [IP]) * ([CP]_0 - [IP])} \qquad [4.3]$$

where $[NB]_0$ and $[CP]_0$ are the total concentration of $NB^-$ and $CP^+$, respectively. Increasing the CPC concentration moves the equilibrium toward the right, and results in a larger shift of the $\upsilon(NO_2)$ band. When molar ratio of CPC vs NBS is 10 times or higher, the $\upsilon(NO_2)$ band was observed at 1352 $cm^{-1}$, which can be ascribed to the $\upsilon(NO_2)$ band of the ion-pair form. The equilibrium constant is estimated from the band intensities at 1360 $cm^{-1}$ and 1352 $cm^{-1}$, which are used to estimate the concentration of free $NB^-$ and

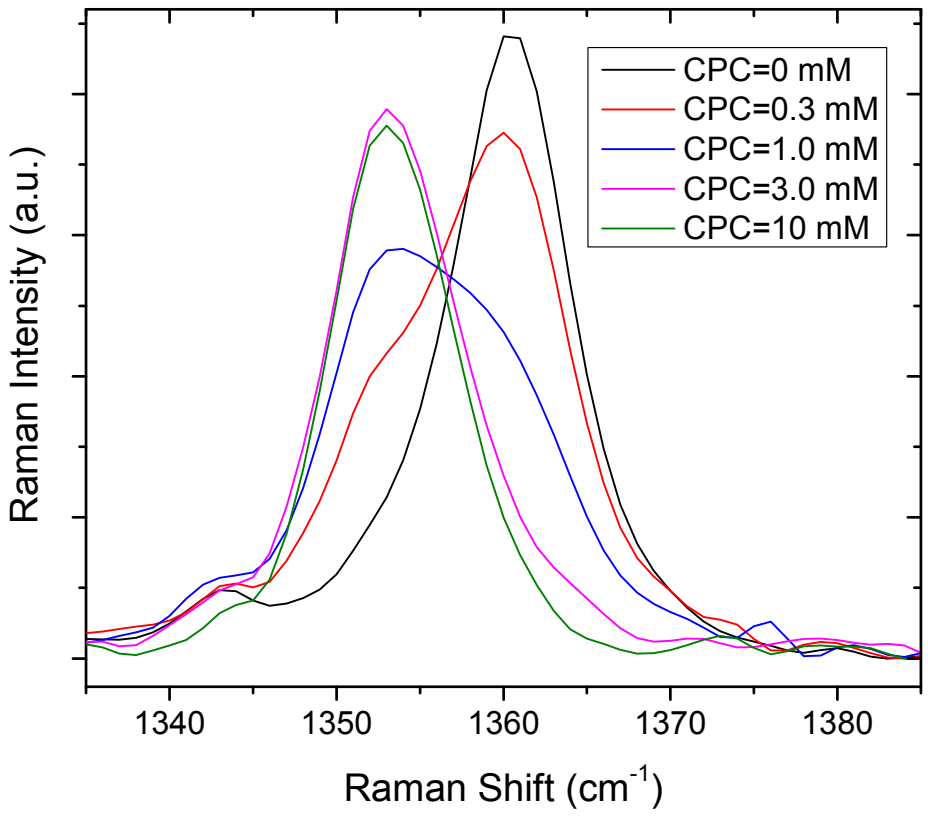


Figure 4.6. Raman band $\upsilon(NO_2)$ of NBS (1.0 mM) mixed with CPC of different concentrations.

ion-paired $NB^-$ in the mixture solutions, respectively. Figure 4.7 shows the [IP] changing as a function of $CP^+$ concentration, and fitting of the data to eq 4.3 by least squares, which yields a binding constant for the ion pair $K_{b1} = 2.9 \pm 1.4 \times 10^3\ M^{-1}$.

The adsorption of the $NB^-$ on the $C_{12}$ surface with and without the presence of CPC was also measured by SERS. As showed in Figure 4.5 (b), the adsorption of the $NB^-$ to $C_{12}$ is negligible in the absence of CPC, which is most likely due to strong hydrophobicity of the $C_{12}$ surface, prohibiting the accumulation of ionic species. Obvious features can be observed at 1031 $cm^{-1}$ for $CP^+$ together with 1352 $cm^{-1}$ and 1002$cm^{-1}$ for $NB^-$ when CPC is presented in the solution. The absence of band at 1360 $cm^{-1}$ indicates that the adsorbed $NB^-$ is exclusively in the ion-pair form.

In order to test whether the adsorption of $NB^-$ on the $C_{12}$ is due to the change the surface wettability by a surfactant or because of ion interactions, the effect of a nonionic surfactant Triton X-100 on the $NB^-$ adsorption was also investigated. As shown in Figure 4.8, no obvious shift can be observed for band $\upsilon(NO_2)$ in $NB^-$ solution with the addition of Triton X-100. As expected, adsorbed $NB^-$ on the $C_{12}$ is negligible in the presence of Triton X-100, although adsorption of Triton to the $C_{12}$ surface can be observed. This result further demonstrates that accumulation of $NB^-$ to the hydrophobic surface is driven by ion-pairing interactions between the $NB^-$ and $CP^+$.

Electrolytes are used in the ion chromatography and IIC as eluents based on their competition with the retained analytes to the charged surface or adsorbed surfactant. In addition, IIC systems often contain various buffer salts in addition to pairing ions, it is therefore important to examine the electrolyte effect on the ion-pairing. The influence of several anions $Cl^-$, $SO_4^{2-}$, and $ClO_4^-$ on the ion-pairing of $CP^+$ and $NB^-$ on the $C_{12}$ surface

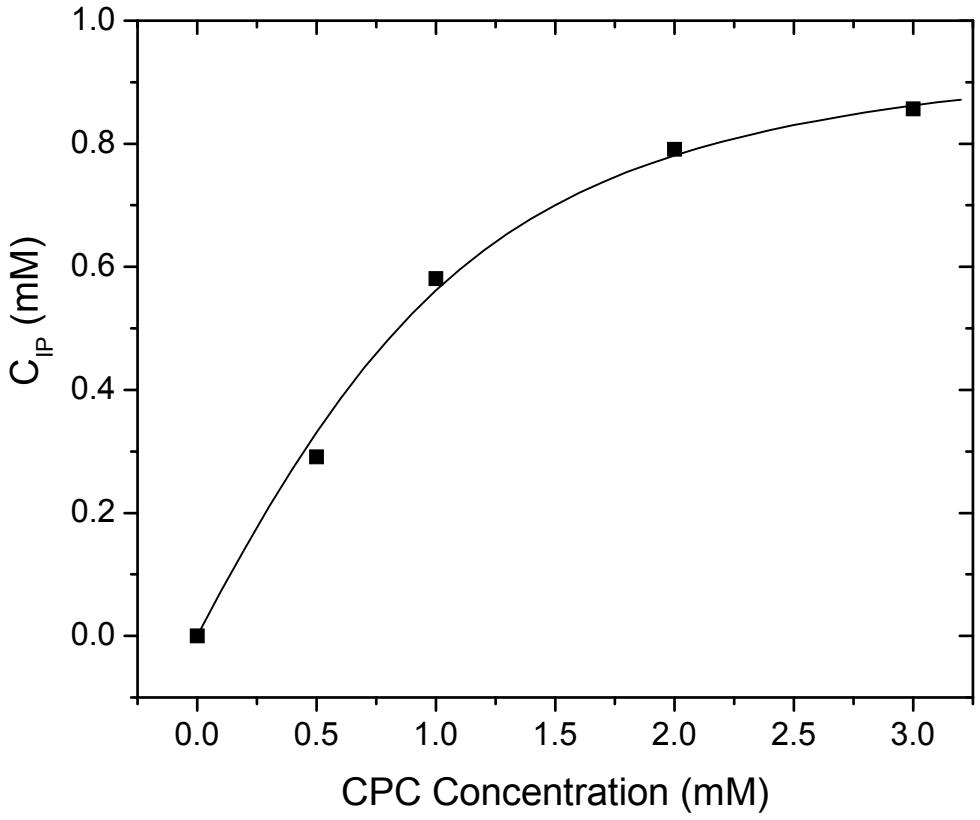


Figure 4.7. Concentration of ion-pairing $NB^-$ changes as a function of CPC concentration in 1 mM $NB^-$ solution, and the least squares fitting of the data.

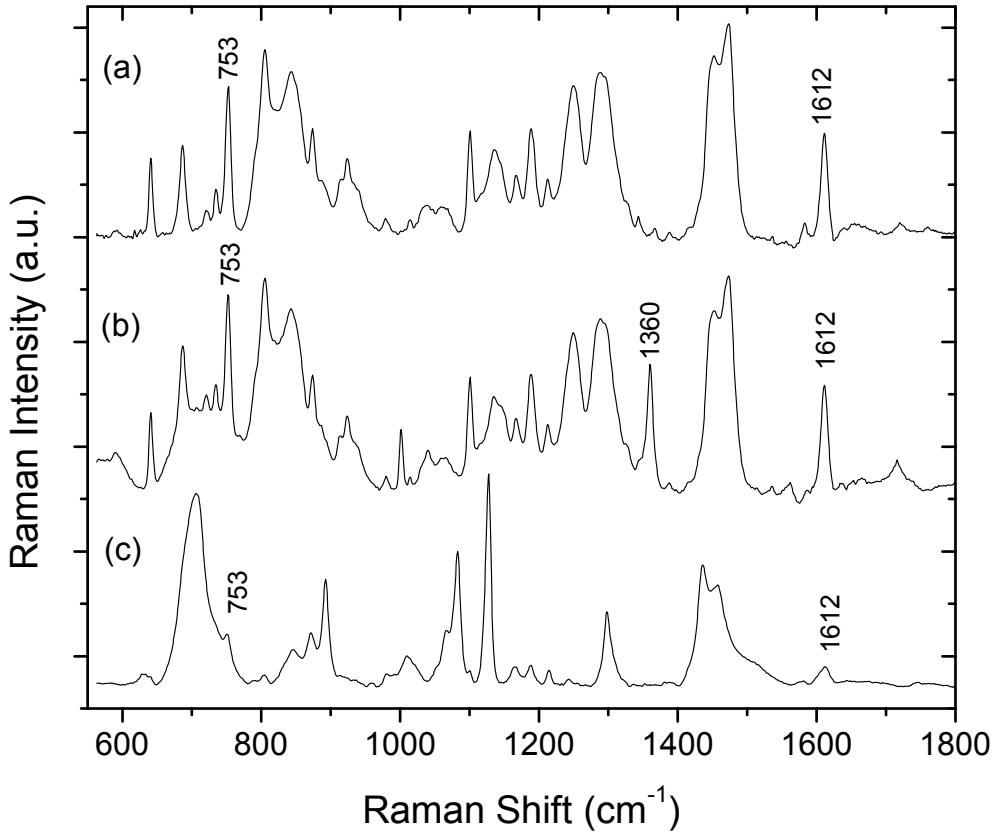


Figure 4.8. Raman spectra of Triton Tx-100 (50 mM) in aqueous solution (a), and mixture solution of NBS (5 mM) and Triton (5 mM) (b), SER spectrum of $C_{12}$ surface in the presence of 1.0 mM Triton and 1.0 mM NBS.

was investigated, and the results were plotted in Figure 4.9. In general, a decrease of the $NB^-$ intensity ($I_{NB}$) is observed as the concentration of the electrolyte is increased, which is attributed to the competition of additional anions with the $NB^-$ for the formation of ion pair with $CP^+$. However, the effects of these ions on ion-pairing differ significantly from each other as shown in Figure 4.9. No obvious change in $I_{NB}$ was observed even at very high concentration of $SO_4^{2-}$, ($Na_2SO_4$, 1.0 M), whereas $I_{NB}$ drops significantly with the addition of either $Cl^-$ or $ClO_4^-$. The concentration ratios of the anions versus $NB^-$ needed to decrease by half the adsorbed $NB^-$ on the $C_{12}$ surface are 136 and 1.2 for $Cl^-$ and $ClO_4^-$, respectively. Although it is not yet possible to predict quantitatively the influence of these ions may cause on the ion-pairing, it can be deduced from the results that their binding affinity with $CP^+$ is in the sequence of $NB^- \approx ClO_4^- > Cl^- > SO_4^{2-}$, which is consistent with chromatographic separation results reported previously.[2, 3, 7] This measurement can be a more convenient method compared to chromatography in providing information on the affinity between ionic species and the surfactants, which could be useful for predicting the retention selectivity, and optimizing experimental conditions.

As discussed above, the adsorption of the $NB^-$ to the $C_{12}$ surface relies strongly on the presence of $CP^+$. The concentration of the surfactant has been demonstrated to govern the retention of the ionic species in IIC measurement. Bell shaped plots of the retention as a function of surfactant concentration are generally observed.[3] Retention of ionic species increases at low surfactant concentrations, and levels off once the surface becomes saturated with the surfactant. The effect of the CPC concentration on the accumulation of $NB^-$ on the $C_{12}$ surface was also studied, and the result is plotted in Figure 4.10. Similar

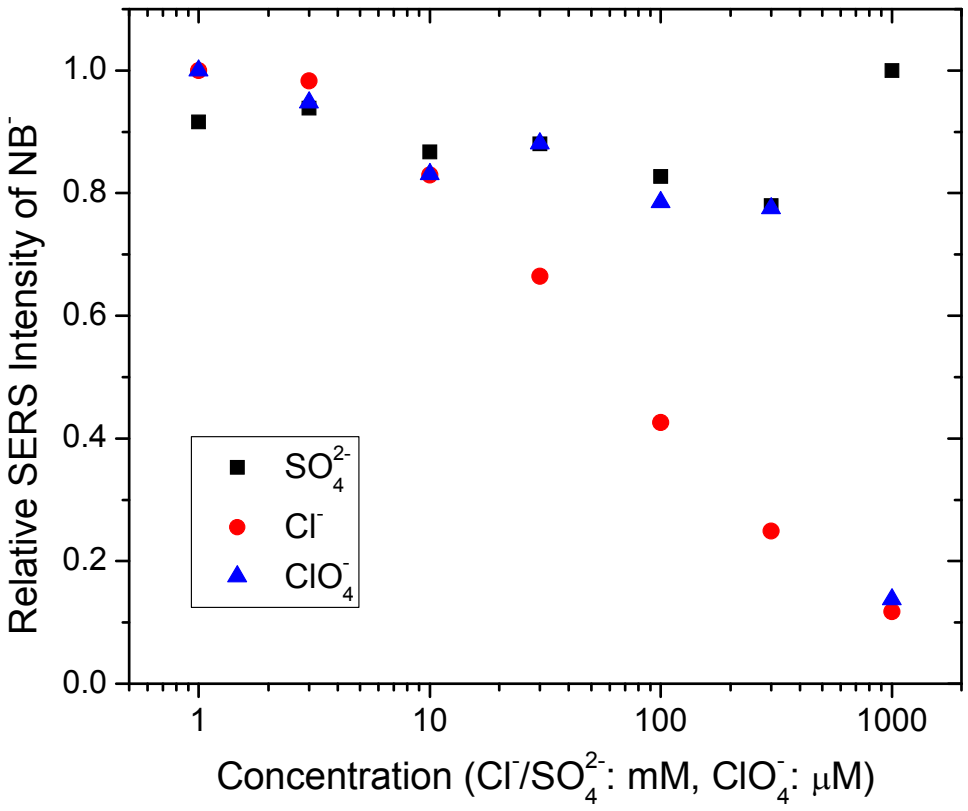


Figure 4.9. Anion effect on the SER intensity of $NB^-$ in the presence of CPC.

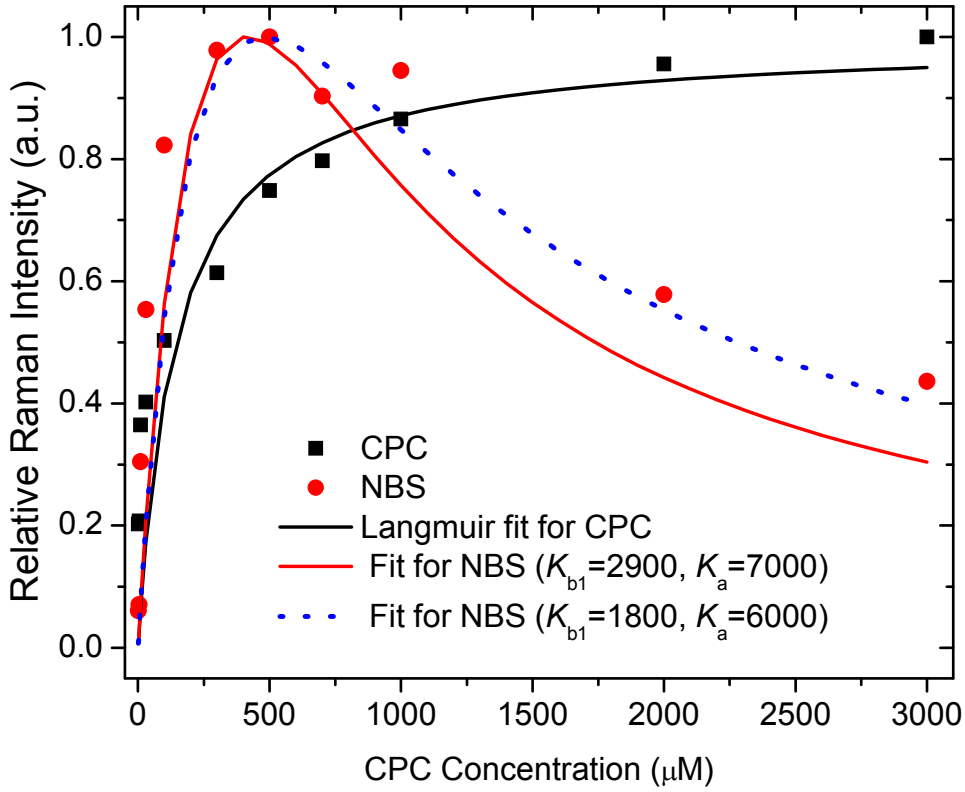


Figure 4.10. Adsorption isotherm of $CP^+$ on the $C_{12}$ surface in the presence of 0.5 mM NBS (black square), and the Langmuir isotherm fit of the data set (black line), Adsorption isotherm of $NB^-$ (0.5 mM) as a function of CPC concentration (red circle) and fitting of the data set by eq 4.9 with $K_{b1} = 2900 M^{-1}$ (red line) and $K_{b1} = 1800\ M^{-1}$ (blue dot).

to the results of the surfactant concentration on the retention of the ionic analytes reported previously, a bell shaped curve is observed for the adsorption of $NB^-$ as a function of CPC concentration. The adsorbed $NB^-$ decays at high CPC concentrations. This decay has been ascribed to the increase of counter ions $Cl^-$ as the CPC concentration is increased.[3] This explanation, however, does not account for the observation in this study, that the desorption of $NB^-$ from the $C_{12}$ surface by the 3.0 mM $Cl^-$ is negligible as shown in Figure 4.9.

The bell shaped curve confirms the existence of ion-pairs formed in the solution phase. Without forming ion-pairs in solution, the decay of $I_{NB}$ at high CPC concentration would not occur for a fixed NBS concentration, because $I_{NB}$ would depend only surface coverage of $CP^+$, which increases to a steady state as CPC concentration is increased (Figure 4.10). The effect of the surfactant concentration on analyte retention can be qualitatively explained by either "dynamic ion exchange" or "ion-pair formation in the mobile phase" retention mechanisms, both of which predict a similar trend for the analyte retention as a function of surfactant concentration. The model of "dynamic ion exchange" with the presence of ion-pairs in mobile phase was used to describe and fit the data set in Figure 4.10.

Several equilibria coexist according this model: the formation of ion-pairs in solution (eq 4.2), adsorption of $CP^+$ to the $C_{12}$ surface (eq 4.4), and the formations of $NB^-$ complexes with $CP^+$ that is bound to the $C_{12}$ surface (eq 4.5).

$$CP_m^+ \xleftrightarrow{K_a} CP_s^+ \qquad [4.4]$$

$$NB^- + CP_s^+ \xleftrightarrow{K_{b2}} IP_s \qquad [4.5]$$

where subscript m and s are used to denote the mobile phase and surface-bound species, respectively. The relative coverage of $CP^+$ on the $C_{12}$ surface can be simplified to a Langmuir isotherm (eq 4.6),

$$[CP_s^+] = \frac{K_a[CP_m^+][CP_s^+]^*}{1 + K_a[CP_m^+]} \quad [4.6]$$

where $[CP_s^+]^*$ is the maximum concentration of surface-bound $CP^+$. This simplification is reasonable for the adsorption of $CP^+$ on the $C_{12}$ surface in the presence of $NB^-$ because the isotherm is very similar to that obtained in 3.0 mM KCl. As demonstrated in Figure 4.10, the adsorption is well fit by a Langmuir isotherm, yielding $K_a = 7.0 \pm 3.0 \times 10^3 M^{-1}$. The $[NB^-]$ in the solution can derived from the equilibrium in eq 4.4 and is obtained by eq 4.7

$$[NB^-] = \frac{[NB]_0}{1 + K_{b1}[CP_m^+]} \quad [4.7]$$

where $[NB]_0$ is the total concentration of NBS. Surface-bound $NB^-$ is exclusively in the ion pair form and equals to $[IP_s]$, which can be calculated by the combination of eqs 4.5, 4.6, and 4.7.

$$[IP_s] = K_{b2}[NB^-][CP_s^+] = \frac{K_a K_{b2}[NBS]_0[CP_m^+][CP_m^+]^*}{(1 + K_{b1}[CP_m^+])(1 + K_a[CP_m^+])} \quad [4.8]$$

Given that $K_a$, $K_{b2}$, $[NBS]_0$, and $[CP_m^+]^*$ are all constants, the above equation can be rewritten as:

$$[\mathrm{IP_s}] = \frac{K[\mathrm{CP_m^+}]}{(1 + K_{\mathrm{b1}}[\mathrm{CP_m^+}])(1 + K_{\mathrm{a}}[\mathrm{CP_m^+}])} \qquad [4.9]$$

where $K = K_a K_{b2}[\mathrm{NBS}]_0[\mathrm{CP}_m^+]$*. The plot of $I_{\mathrm{NB}}$, which is proportional to [$\mathrm{IP_s}$], as a function of $[\mathrm{CP_m^+}]$ was fit by least-squares to above equation using $K_{\mathrm{b1}} = 2.9 \times 10^3\ \mathrm{M^{-1}}$ and $K_a = 7.0 \times 10^3 \mathrm{M}^{-1}$ obtained above. It can be seen that the eq 4.9 predicts the shape of the isotherm for surface binding of $\mathrm{NB^-}$. The deviation of the data from the fit could be due to the simplification of the $\mathrm{CP^+}$ adsorption isotherm or from the uncertainty in adsorption constant of $\mathrm{CP^+}$ ($K_{\mathrm{a}}$) and the ion-pair binding constant of $\mathrm{CP^+}$ and $\mathrm{NB^-}$ ($K_{\mathrm{b1}}$). In fact, as shown in Figure 4.10, a better fit can be obtained when using $K_{\mathrm{b1}} = 1.8 \times 10^3\ \mathrm{M^{-1}}$ and $K_a = 6.0 \times 10^3 \mathrm{M}^{-1}$, which are both within the uncertainties of their independently measured values.

## 4.4 Conclusions

The adsorption of cetylpyridinium ($\mathrm{CP^+}$) and its interaction with nitrobenzenesulfonate ($\mathrm{NB^-}$) on 1-dodecanthiol ($\mathrm{C_{12}}$) modified silver surface was studied by SERS. Addition of electrolyte has a significant effect on the adsorption equilibria. A Frumkin isotherm is observed for the adsorption of $\mathrm{CP^+}$ on the $\mathrm{C_{12}}$ surface without supporting electrolyte, while Langmuir isotherm can describe the adsorption in the presence of KCl or $\mathrm{NB^-}$. Ion-pairing of $\mathrm{CP^+}$ and $\mathrm{NB^-}$ can be observed in the solution, which facilitates the binding $\mathrm{NB^-}$ to the $\mathrm{C_{12}}$ surface. The effects of several anions on the adsorption of $\mathrm{NB^-}$ onto the $\mathrm{C_{12}}$ surface in the presence of $\mathrm{CP^+}$ gave their binding affinity with $\mathrm{CP^+}$ in the sequence: $\mathrm{NB^-} \approx \mathrm{ClO_4^-} > \mathrm{Cl^-} > \mathrm{SO_4^{2-}}$. Competition of $\mathrm{Cl^-}$ and $\mathrm{ClO_4^-}$ with the $\mathrm{NB^-}$ in formation of ion pair with $\mathrm{CP^+}$ leads to the desorption of $\mathrm{NB^-}$ from the $\mathrm{C_{12}}$

surface, while surface-bound ion-pair of $NB^-$ and $CP^+$ is sufficiently stable to persist in the presence of $Na_2SO_4$. The adsorption of $NB^-$ to the $C_{12}$ surface relies strongly on the presence of the CPC. A bell shape plot is observed for the intensity of surface-bound $NB^-$ as a function of CPC concentration, which is consistent with the effect of the surfactant on the retention of ionic analytes reported previously. This trend can be quantitatively explained by the retention theory of "dynamic ion exchange" with the presence of ion-pair in the mobile phase. The study demonstrated that SERS is a well suited technique to study the adsorption of surfactants and ion interactions on hydrophobic surfaces, which is important for understanding the mechanism of ion-interaction chromatography. In addition, the binding of the ionic species to the monolayer modified electrode surface through ion interactions allows potential control and electrochemical measurements, details of which will be discussed in next chapter.

## 4.5 References


(1) Myers, D. *Surface, Interface, and Colloids: Principles and Application*, 2nd ed.; Wiley-VCH: New York, 1999.

(2) Cecchi, T. *Crit. Rev. Anal. Chem.* **2008**, *38*, 161-213.

(3) Milton, H. *Ion-Pair Chromatography*; Marcel Dekker, Inc: New York, 1985.

(4) Wittmer, D. P.; Nuessle, N. O.; Haney, W. G., Jr. *Anal. Chem.* **1975**, *47*, 1422-1423.

(5) Sood, S. P.; Sartori, L. E.; Wittmer, D. P.; Haney, W. G. *Anal. Chem.* **1976**, *48*, 796-798.

(6) Bidlingmeyer, B. A.; Warren, F. V., Jr. *Anal. Chem.* **1982**, *54*, 2351-2356.

(7) Iskandarani, Z.; Pietrzyk, D. J. *Anal. Chem.* **1982**, *54*, 1065-1071.

(8) Dowling, S. D.; Seitz, W. R. *Anal. Chem.* **1985**, *57*, 602-605.

(9) Liu, H.; Cantwell, F. F. *Anal. Chem.* **1991**, *63*, 993-1000.

(10) Liu, H.; Cantwell, F. F. *Anal. Chem.* **1991**, *63*, 2032-2037.

(11) Zappoli, S.; Bottura, C. *Anal. Chem.* **1994**, *66*, 3492-3499.

(12) Caruso, F.; Serizawa, T.; Furlong, D. N.; Okahata, Y. *Langmuir* **1995**, *11*, 1546-1552.

(13) Ryu, D. Y.; Free, M. L. *Colloids Surf., A* **2003**, *226*, 17-23.

(14) Haidara, H.; Vonna, L.; Schultz, J. *Langmuir* **1996**, *12*, 3351-3355.

(15) Brinck, J.; Joensson, B.; Tiberg, F. *Langmuir* **1998**, *14*, 1058-1071.

(16) Tiberg, F.; Landgren, M. *Langmuir* **1993**, *9*, 927-932.

(17) Grant, L. M.; Ederth, T.; Tiberg, F. *Langmuir* **2000**, *16*, 2285-2291.

(18) Schulz, J. C.; Warr, G. G. *Langmuir* **2002**, *18*, 3191-3197.

(19) Atkin, R.; Craig, V. S. J.; Biggs, S. *Langmuir* **2001**, *17*, 6155-6163.

(20) Liu, J.-F.; Min, G.; Ducker, W. A. *Langmuir* **2001**, *17*, 4895-4903.

(21) Masadome, T.; Ueda, A.; Kawakami, M. *Anal. Lett.* **2004**, *37*, 225-233.

(22) Gerlache, M.; Senturk, Z.; Quarin, G.; Kauffmann, J.-M. *J. Solid State Electrochem.* **1997**, *1*, 155-160.

(23) Brahimi, B.; Labbe, P.; Reverdy, G. *Langmuir* **1992**, *8*, 1908-1918.

(24) Sigal, G. B.; Mrksich, M.; Whitesides, G. M. *Langmuir* **1997**, *13*, 2749-2755.

(25) Levchenko, A. A.; Argo, B. P.; Vidu, R.; Talroze, R. V.; Stroeve, P. *Langmuir* **2002**, *18*, 8464-8471.

(26) Artyukhin, A. B.; Burnham, K. J.; Levchenko, A. A.; Talroze, R. V.; Stroeve, P. *Langmuir* **2003**, *19*, 2243-2248.

(27) Norman, L. L.; Badia, A. *Langmuir* **2007**, *23*, 10198-10208.

(28) Oskarsson, H.; Holmberg, K. *J. Colloid Interface Sci.* **2006**, *301*, 360-369.

(29) Almanza-Workman, A. M.; Raghavan, S.; Sperline, R. P. *Langmuir* **2000**, *16*, 3636-3640.

(30) Xing, R.; Rankin, S. E. *J. Phys. Chem. B* **2006**, *110*, 295-304.

(31) Sander, L. C.; Callis, J. B.; Field, L. R. *Anal. Chem.* **1983**, *55*, 1068-1075.

(32) Montgomery, M. E., Jr.; Wirth, M. J. *Langmuir* **1994**, *10*, 861-869.

(33) Praus, P.; Pospisil, M. *Mater. Struct. Chem., Biol., Phys. Technol.* **2008**, *15*, 32-37.

(34) Kung, K. H. S.; Hayes, K. F. *Langmuir* **1993**, *9*, 263-267.

(35) Rigas, P. G.; Pietrzyk, D. J. *Anal. Chem.* **1988**, *60*, 1650-1654.

(36) Gasser-Ramirez, J. L.; Harris, J. M. *Anal. Chem. (Washington, DC, U. S.)*, *82*, 5743-5750.

(37) Jeanmaire, D. L.; Van Duyne, R. P. *Journal of Electroanalytical Chemistry* **1977**, *84*, 1-20.

(38) Haynes, C. L.; McFarland, A. D.; Duyne, R. P. V. *Analytical Chemistry* **2005**, *77*, 338 A-346 A.

(39) Fleischmann, M.; Hendra, P. J.; McQuillan, A. J. *Chemical Physics Letters* **1974**, *26*, 163-166.

(40) Otto, A.; Mrozek, I.; Grabhorn, H.; Akemann, W. *J. Phys.: Condens. Matter* **1992**, *4*, 1143-1212.

(41) Campion, A.; Kambhampati, P. *Chem. Soc. Rev.* **1998**, *27*, 241-250.

(42) Suga, K.; Bradley, M.; Rusling, J. F. *Langmuir* **1993**, *9*, 3063-3066.

(43) Foucault, R.; Birke, R. L.; Lombardi, J. R. *Langmuir* **2003**, *19*, 8818-8827.

(44) Koglin, E.; Tarazona, A.; Kreisig, S.; Schwuger, M. J. *Colloids Surf., A* **1997**, *123-124*, 523-542.

(45) Kreisig, S. M.; Tarazona, A.; Koglin, E.; Schwuger, M. J. *Langmuir* **1996**, *12*, 5279-5288.

(46) Sun, S.; Birke, R. L.; Lombardi, J. R. *J. Phys. Chem.* **1990**, *94*, 2005-2010.

(47) Fanigliulo, A.; Bozzini, B. *Electrochim. Acta* **2002**, *47*, 4511-4521.

(48) Olson, L. G.; Harris, J. M. *Appl. Spectrosc.* **2008**, *62*, 149-156.

(49) Lecomte, S.; Ricoux, R.; Mahy, J. P.; Korri-Youssoufi, H. *J Biol Inorg Chem* **2004**, *9*, 850-858.

(50) Moskovits, M.; Suh, J. S. *J. Am. Chem. Soc.* **1985**, *107*, 6826-6829.

(51) Bryant, M. A.; Pemberton, J. E. *J. Am. Chem. Soc.* **1991**, *113*, 3629-3637.

(52) Langmuir, I. *J. Am. Chem. Soc.* **1918**, *40*, 1361-1402.

(53) Frumkin, A. *Z. physik. Chem.* **1925**, *116*, 466-484.

(54) Bracko, S.; Span, J. *Dyes Pigm.* **2001**, *50*, 77-84.

(55) Gao, P.; Gosztola, D.; Weaver, M. J. *J. Phys. Chem.* **1988**, *92*, 7122-7130.

# CHAPTER 5

# ADSORPTION AND ELECTROCHEMICAL REDUCTION OF IONIC ANALYTES ON A HYDROPHOBIC SURFACE THROUGH ION INTERACTION WITH CETYLPYRIDINIUM CHLORIDE

## 5.1 Introduction

Adsorption and reaction at solid/liquid interfaces are fundamental processes for chemical and biochemical sensing, which usually involve selective interactions of target analytes at a solid substrate.[1-4] Self-assembled monolayers (SAMs) are an excellent approach to anchoring molecules to the substrate surface, because SAMs provide a flexible and tailorable system for different species.[5-8] In fact, molecules can be physically adsorbed to,[9-16] electrostatically attached to,[3, 7, 9, 17-24] or covalently bound to[25-27] the monolayer, owning to the variety of SAMs which can be used. For example, ionic solutes can be attracted to the surface modified by monolayer with oppositely charged head group,[9, 18, 23, 24] whereas nonionic solutes can be accumulated on hydrophilic or hydrophobic monolayer modified surfaces,[10, 12, 14-16] respectively, depending on their water solubility.

An interesting example is an ionic surfactant, which can be adsorbed on both a hydrophobic surface and a charged surface.[13, 24, 28-30] Similar to other ionized compounds, ionic surfactants can adsorb onto oppositely charged surfaces from aqueous solution

through electrostatic interactions of their head groups with the substrate.[22, 24, 29] Given a substrate covered with a hydrophobic SAM, the ionic surfactant interacts with the monolayer through its hydrophobic chain, exposing its charged head group toward the aqueous solution.[13, 29, 30] As a consequence, the resulting surface shows strong affinity to ionic species, which can be electrostatically bound to the surface by interacting with the head group of the adsorbed surfactant.[29, 30] This technique has been widely used in ion interaction chromatography to modify the separation of ionic solutes on hydrophobic stationary phases by the addition of amphiphilic molecules to the mobile phase.[31-33] Ion interaction of 3-nitrobenzenesulfonate ($NB^-$) with cetylpyridinium ($CP^+$) and their adsorption to a $C_{18}$ modified silica surface have been demonstrated previously by confocal Raman spectroscopy.[30] The results in Chapter 4 showed that with the addition of $CP^+$, the $NB^-$ can be strongly accumulated onto a $C_{12}$ modified Ag surface.

In this work, surface-enhanced Raman spectroscopy (SERS) and cyclic voltammetry (CV) were employed to examine the electrochemical reduction of adsorbed $NB^-$ on a $C_{12}$ surface using the same immobilization method as developed in Chapter 4. Reduction of nitrobenzene was identified based on changes in the adsorbate Raman spectra with applied potential and comparison to the Raman spectrum of 3-aminobenzenesulfonate ion (ABS). Similar to the electrochemical reduction of nitrobenzene on a bare electrode surface,[34] the decrease and then disappearance of the $\nu_s(NO_2)$ mode, and the shift of the ring breathing mode $\nu_{12}$ can be observed for the reduction of $NB^-$ coadsorbed with $CP^+$ to a $C_{12}$ modified surface. The influence of the solution pH on the reduction of $NB^-$ was investigated. The reductions of $NB^-$ on both $C_{12}$ and bare Ag surface were compared, which show similar product formation but different

reversibility. Removal of the potential results in the recovery of the $NB^-$ on $C_{12}$ surface, which was not observed for the reduction on a bare Ag surface.

The ion interaction protocol demonstrates the capability of bringing an ionic analyte to a hydrophobic electrode surface, providing an alternative for spectroelectrochemical measurements. Protecting by the $C_{12}$ monolayer, the surface can avoid the irreversible adsorption of analytes or their corresponding redox forms, allowing repeatable measurement on the same electrode. In addition, hydrophobic monolayer surface blocks nonspecific adsorption and provides selectivity for species that have high affinity to the ionic surfactant. As a consequence, selective binding and redox reaction can be realized by using ionic surfactants with head groups that have strongly affinity for a target analyte.

## 5.2 Experimental

### 5.2.1 Materials

1-dodecanthiol (98%, Sigma-Aldrich), cetylpyridinium chloride (CPC) (98%, Sigma-Aldrich), sodium nitrobenzenesulfonate (98%, Sigma-Aldrich), 3-aminobenzenesulfonic acid (97%, Sigma-Aldrich), and sodium sulfate (AR, Mallinckrodt) were used as received.

### 5.2.2 Substrate preparation

All electrodes were constructed from a 7-mm diameter silver rod (99.999%, Alfa Aesar). The surfaces of the electrodes were polished with 800, 1500 and 2000 grit silicon carbide paper (3M) and then with alumina polishing slurries (1.0 μm) on a microfiber polishing cloth (Buehler). The electrode surfaces were then electrochemically roughened by oxidation-reduction cycles in KCl (0.1 M) solution; specifically, linear sweeps from

+0.3 V to -0.3 V (vs Ag/AgCl) and back to +0.3 V were applied at a sweep rate of 15 mV/s for 3 cycles, and then the potential was held at –0.3 V for 2 min.[35] Electrodes were then removed from the cell and rinsed with deionized water prior to monolayer self-assembly.

5.2.3 SAM preparation

The self-assembly step was conducted by immersing the Ag electrodes in 0.1 mM solutions of 1-dodecanthiol in methanol for 12 h.

5.2.4 Raman spectroelectrochemical measurements

A three-electrode potentiostat (RDE4, Pine Instrument) was used to control the applied potential. A Ag/AgCl electrode (EE009, Cypress Systems, Inc.) was used as reference and a platinum mesh (0.1 mm diameter and 25 mm x 25 mm, Alfa Aesar) was used as the counter electrode; the position of the working electrode is adjusted to be about 1 mm from the fused silica front window of the cell. Surface-enhanced Raman measurements were conducted with a fiber-optic coupled Raman spectrometer (PI-200, Process Instruments) with a frequency stabilized, 785-nm diode laser. The laser power at the sample was 260 mW, and the integration time was 20 s for all measurements.

5.2.5 Cyclic voltammetry measurements

Cyclic voltammetry (CV) was performed on a potentiostat (AFRDE5, Pine Instrument) controlled by Labview 2010 program, using a scan rate of 10 mV/s. The surface area of the silver electrodes used for CV measurements are around 2 $\mu m^2$. All solutions are purged with $N_2$ for ~30 min before the measurements.

## 5.3 Results and Discussion

### 5.3.1 Reduction of $NB^-$ on bare Ag surface

Surface-enhanced Raman scattering (SERS) has been demonstrated to be an excellent tool for examining the electrochemical process on electrode surfaces, owning to its surface-sensitivity and low bulk-phase interference.[3, 11, 21, 34, 36] Electrochemical reactions on both bare metal surfaces[34, 36] and monolayer modified surfaces[3, 11, 21, 36] have been previously measured by SERS. The reduction of nitrobenzene on Au surface studied by SERS in conjunction with cyclic voltammetry (CV) indicated an irreversible multi-step process involving several intermediates, as shown in scheme 5.1 and 5.2.[34]

$$C_6H_5NO_2 \xrightarrow{2e^-} C_6H_5NO \xrightarrow{2e^-} C_6H_5NHOH \xrightarrow{2e^-} C_6H_5NH_2 \qquad [5.1]$$

A coupling step was also observed in basic or neutral condition producing azoxybenzene, which could be further reduced to azobenzene or hydrazobenzene.[34]

$$C_6H_5NO + C_6H_5NHOH \longrightarrow C_6H_5N = N(O)C_6H_5 \qquad [5.2]$$

Reduction of $NB^-$ on bare Ag in both acidic and basic solutions was first measured by SERS in this work. Figure 5.1 shows a series of SERS spectra of the $NB^-$ on bare Ag at different potentials in basic solution (NaOH, 1 mM). Raman intensities of the absorbed $NB^-$ are very weak at 0 V or -0.2 V and become intense at more negative potentials. This is likely due to the increase in the chemical (charge-transfer) SERS enhancement as the potential becomes more negative.[37, 38] Potential dependence of 3-aminobenzenesulfonic acid **(**ABS) on Ag surface showed similar results although no further reduction was observed, as shown in Figure 5.2. Spectra in Figure 5.1 show that

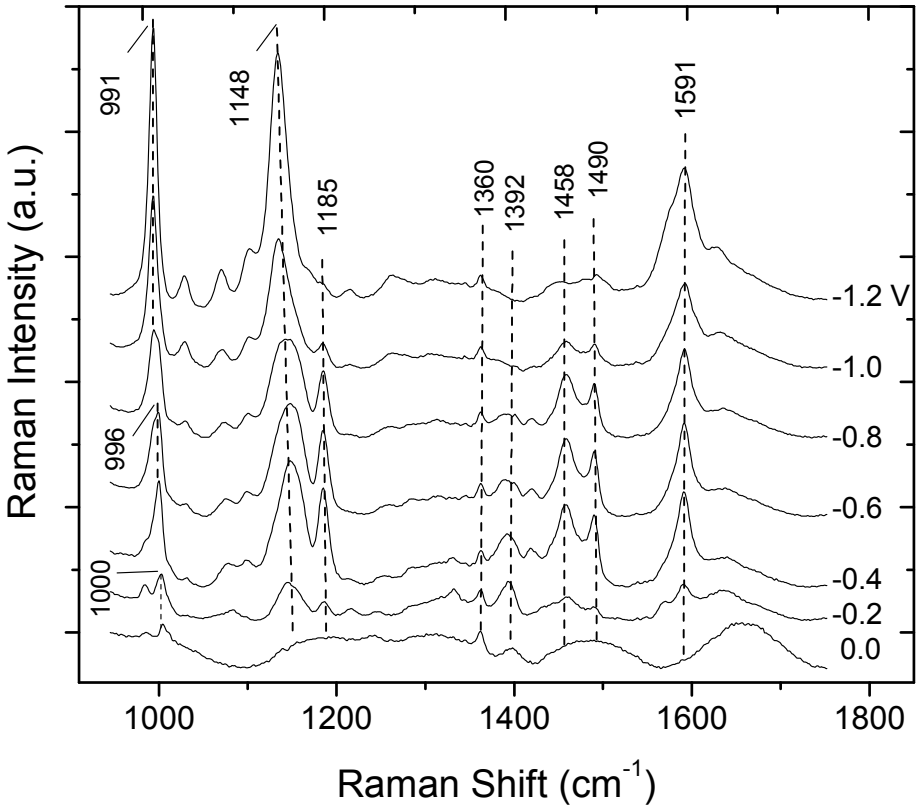


Figure 5.1. Sequence of SERS spectra obtained for the reduction of $NB^-$ on bare Ag surface in basic solution. (NBS=10 mM, $Na_2SO_4$=10 mM, and NaOH=1 mM) Potential are relative to a Ag/AgCl reference.

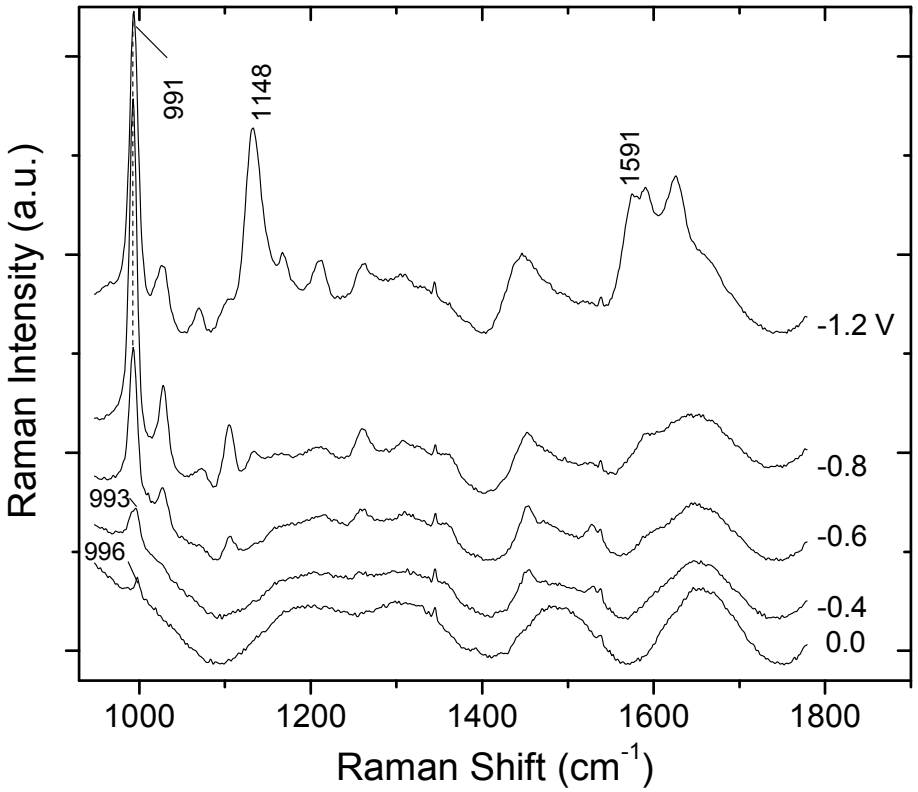


Figure 5.2. Potential dependence of SERS spectra of 3-aminobenzensulfonic acid (ABS). (ABS=10 mM, $Na_2SO_4$=10 mM, and NaOH=10 mM) Potential are relative to a Ag/AgCl reference.

intensities of several bands increase with negative potential and remain intense even at -1.2 V. These include bands at around 1000, 1148, and 1591 $cm^{-1}$, which are assigned to the ring breathing mode ($\nu_{12}$), Ph-N stretching mode, and ring stretching mode ($\nu_{8a}$), respectively. These vibrations remain mostly unchanged during the reduction process, although the reduction of $–NO_2$ group leads to a shift in their frequencies. However, different characteristics can be observed for several other bands. The N-O stretching mode $\nu$(NO), at 1390 $cm^{-1}$ that appears at 0 V becomes intense at -0.2 V, and weakens and then disappears at more negative potential. This observation indicates the involvement of the $C_6H_5NO$ or $C_6H_5NHOH$ in the reduction process[34] (Scheme 5.1). Similarly, features of azo compound observed at 1185, 1458, and 1490 $cm^{-1}$ appear at -0.2 V and then disappear at -1.2 V, revealing the presence of an azobenzene intermediate (Scheme 5.2).

Figure 5.3 shows the results of $NB^-$ reduction in acidic solution ($H_2SO_4$, 1 mM). The reduction product (spectrum at -1.2 V) is similar to that obtained in basic solution, although smaller $\nu$(NO) and no features of the azo compound can be observed. The pH effect on the reduction of $NB^-$ is consistent with the reduction of nitrobenzene reported previously. It should be mentioned that the $\nu_s(NO_2)$ at 1360 $cm^{-1}$ is very small and does not show obvious change with the applied potential in either acidic or basic solution, although reduction of $–NO_2$ should lead to the disappearance of this vibrational mode. The small band observed at 1360 $cm^{-1}$ in both Figure 5.1 and 5.3 could be from the $NB^-$ ions in bulk solution. This assumption is supported by the fact that band $\nu_s(NO_2)$ disappears upon removal of the solution from the Ag surfaces, while other bands representing surface adsorbed species remain unchanged. The absence of $\nu_s(NO_2)$ from

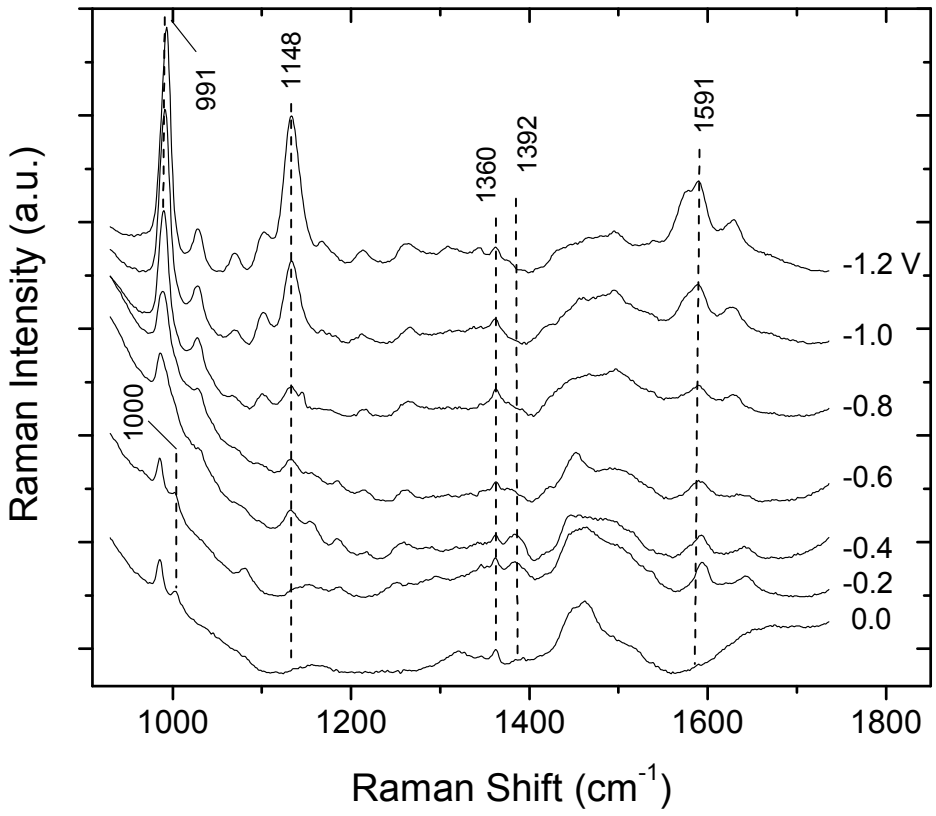


Figure 5.3. Sequence of SERS spectra obtained for the reduction of $NB^-$ on bare Ag surface in acidic solution. (NBS =10 mM, $Na_2SO_4$=10 mM, and $H_2SO_4$=1 mM) Potential are relative to a Ag/AgCl reference.

the surface-bound $NB^-$ is possible because the $–NO_2$ group lies flat on the silver surface, giving no SERS enhancement to $\nu_s(NO_2)$ because the polarizability change lies in the plane of a conductor. As shown in Figure 5.1, 5.2, and 5.3, the reduction of $NB^-$ in both basic and acidic solution on Ag surface results in a product that is very similar to the ABS adsorbed on Ag at -1.2 V.

5.3.2 Reduction of $NB^-$ on $C_{12}$ modified Ag surface

As discussed in Chapter 4 and shown in Figure 4.5, the addition of $CP^+$ increases the surface-bound $NB^-$ significantly, which is otherwise negligible on the $C_{12}$ surface. Figure 5.4 shows a series of SERS spectra of $NB^-$/ $CP^+$ coadsorbed on $C_{12}$ surface under different potentials in basic solution (NaOH, 10 mM). Band assignments for the $C_{12}$ monolayer, $CP^+$, and $NB^-$ have been discussed in Chapter 4. As expected, the features for the $C_{12}$ monolayer located at 1082, 1127, 1297, and 1435 $cm^{-1}$ are not sensitive to applied potential. In contrast, increase in intensity with negative potential can be observed for the bands of $CP^+$ at 1030, 1212, and 1622 $cm^{-1}$, which could be due to the accumulation or orientation change of $CP^+$ on the surface, as the potential becomes more negative. In the case of $NB^-$, a decrease and then disappearance of $\nu_s(NO_2)$ at 1352 $cm^{-1}$, and shift of $\nu_{12}$ from 1000 $cm^{-1}$ to 991 $cm^{-1}$ with negative potential was observed. In addition, features of the azo intermediate at 1458 and 1486 $cm^{-1}$ appear at -0.6 V and then disappear at -0.8 V. These observations are consistent with the electrochemical reduction of $NB^-$ on Ag surface[34] discussed above and also reduction of nitrobenzene on Au surface reported previously. Reduction of $NB^-$ to ABS was further confirmed by the spectrum of ABS coadsorbed with $CP^+$ on $C_{12}$ surface, which produces a similar band of $\nu_{12}$ at 991 $cm^{-1}$ at

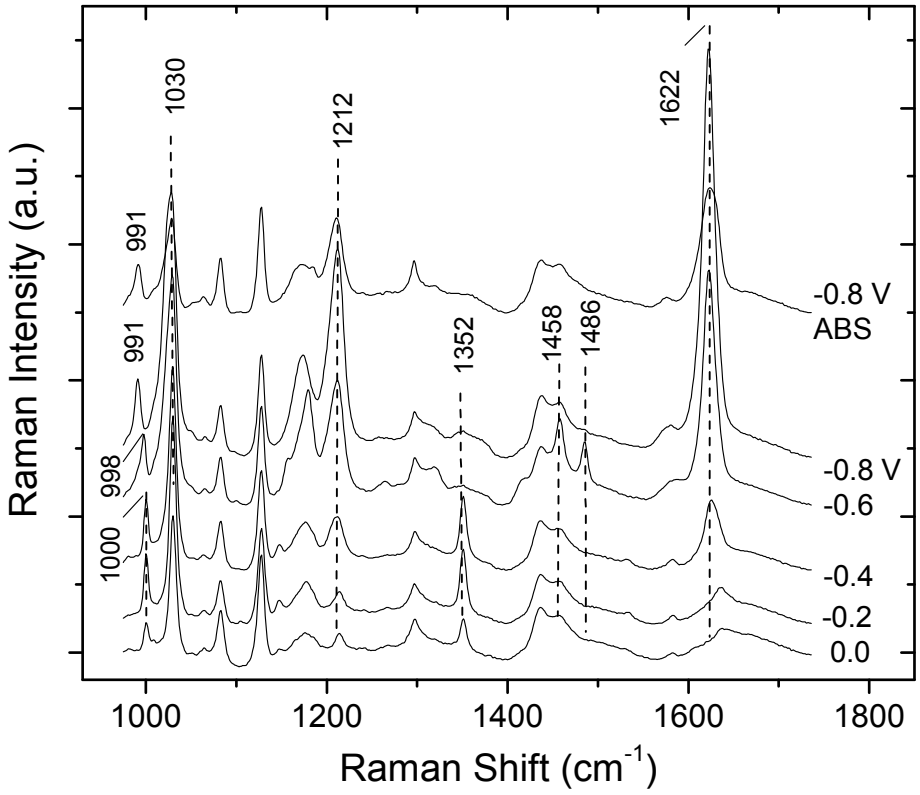


Figure 5.4. Sequence of SERS spectra obtained for the reduction of $NB^-$ on $C_{12}$ modified Ag surface in basic solution, (NBS =1 mM, CPC=1 mM, $Na_2SO_4$=10 mM, and NaOH=10 mM) and SERS spectrum of ABS at -0.8 V (vs Ag/AgCl) on $C_{12}$ surface (ABS =1 mM, CPC=1 mM, $Na_2SO_4$=10 mM, and NaOH=10 mM)

-0.8 V (Figure 5.4). As shown in Figure 5.5, reduction of $NB^-$ on a $C_{12}$ surface in acidic solution gives similar observations for the $\nu_s(NO_2)$ and $\nu_{12}$ bands, although no intermediate of azo compound was detected. These results agree with the reduction of $NB^-$ and nitrobenzene on a bare electrode surface in acidic solution.

5.3.3 Reversibility of reduction of $NB^-$

One of the disadvantages of using a bare electrode for redox measurements is irreversible adsorption, which could result in serious interferences for SERS measurements. For example, reduced product or intermediates of $NB^-$, such as amino or azo compounds, can bind strongly and irreversibly to bare silver, resulting in a non-renewable electrode surface. In order to examine the reusability of the bare Ag electrode in $NB^-$ reduction, SERS spectra were recorded by switching the potential between -0.8 V and 0 V for five cycles. As shown in Figure 5.6, spectra obtained at 0 V change significantly from the second cycle, indicating irreversible adsorption. Although it is difficult to identify the specific adsorbates from these spectra, the bands observed 1185, 1454, and 1488 $cm^{-1}$ reveal the binding of the azo compound.

Similarity of the spectra obtained at -0.8 V in different cycles suggests that these irreversible adsorbed species are intermediates of reduced $NB^-$, which can be further reduced to similar products at -0.8 V. The Raman intensity decreases about 50% from sequence 0.5 to 1.5, which could be due to change of the Ag surface in SERS enhancement after one redox cycle. Incomplete reduction of the adsorbed $NB^-$ at sequence 0.5 might account for this intensity drop, given that the intensities of $\nu_{12}$ can vary significantly for different intermediates. This argument is also supported by the difference of the spectrum between sequence 0.5 and other cycles (1.5-4.5). These results

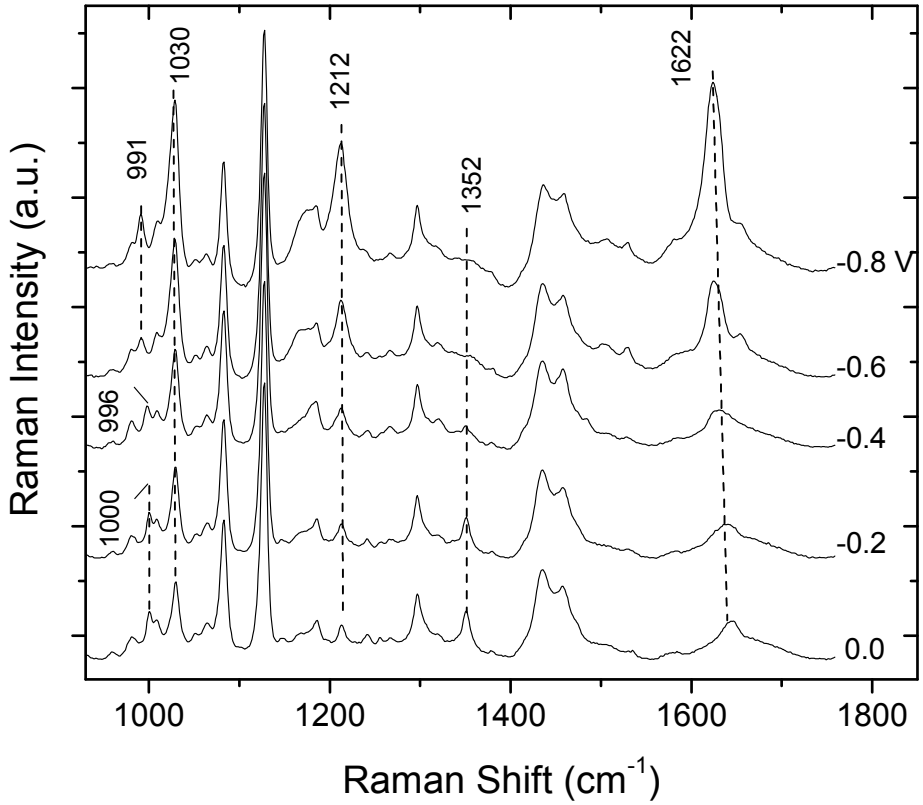


Figure 5.5. Sequence of SERS spectra obtained for the reduction of $NB^-$ on $C_{12}$ modified Ag surface in acidic solution. (NBS=1 mM, CPC=1 mM, $Na_2SO_4$=10 mM, and $H_2SO_4$=10 mM) Potential are relative to a Ag/AgCl reference.

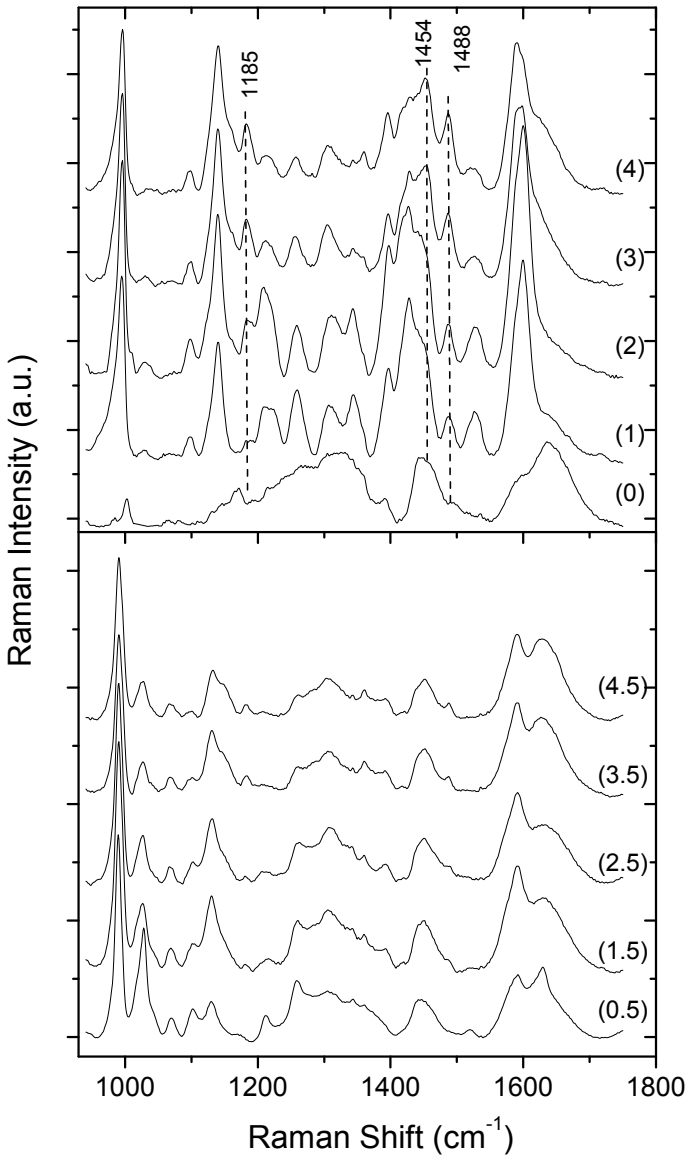


Figure 5.6. Potential dependence of SERS spectra of $NB^-$ switching between 0 V and -0.8 V (vs Ag/AgCl) in basic solution on bare Ag surface. The legend numbers (#) are corresponding to the sequence of the measurements. Potentials are 0 V for #0, 1, 2, 3, and 4, and -0.8 V for #0.5, 1.5, 2.5, 3.5, and 4.5. (NBS =10 mM, $Na_2SO_4$=10 mM, and NaOH=1 mM). Scale of Raman intensity for #0.5 is twice the others.

demonstrate that a bare Ag electrode is not renewable for measuring $NB^-$ reduction. In fact, reduction of $NB^-$ from the second cycle can no longer be identified because the SERS signal is overwhelmed by those species other than $NB^-$.

Similar experiments were conducted on the $C_{12}$ surface to examine its reversibility for investigating reduction of $NB^-$. Figure 5.7 shows the spectra obtained by switching between at 0 V and -0.8 V for 5 cycles. It can be seen that spectra obtained at the same potential (either 0 or -0.8 V) show no obvious difference in both band frequencies and intensities with measurement cycle. As shown in Figure 5.7 and 5.8, recovery of the adsorbed $NB^-$ that is lost at -0.8 V is repeatedly observed when negative potential is removed. Similarly, disappearance of $\nu_s(NO_2)$ and the shift of $\nu_{12}$ from 1000 $cm^{-1}$ to 991 $cm^{-1}$ are repeatable seen at -0.8 V. This recovery of surface-bound $NB^-$ is, however, not due to the reversibility of its redox reaction, but rather due to the displacement of the reduction product (ABS) by the $NB^-$ from solution. This repeatable displacement suggests the reversibility of the adsorption/desorption of the $NB^-$ and ABS, and their similar affinities to $CP^+$ on the $C_{12}$ surface. In short, $C_{12}$ hydrophobic monolayer prevents irreversible adsorption on the Ag electrode surface, allowing repeatable measurements on the same electrode surface without further treatment.

### 5.3.4 Selectivity of the electrode surface

As discussed in Chapter 4, the adsorption of $NB^-$ on the $C_{12}$ surface relies strongly on the presence of $CP^+$. Without addition of $CP^+$, the adsorbed $NB^-$ is negligible even in 10 mM solution. Cyclic voltammetry was also used to examine the $C_{12}$ modified surface. As shown in Figure 5.9, in the solution without $CP^+$, no obvious reduction of $NB^-$ can be observed on a $C_{12}$ surface, compared with the strong cathodic waves obtained on a bare

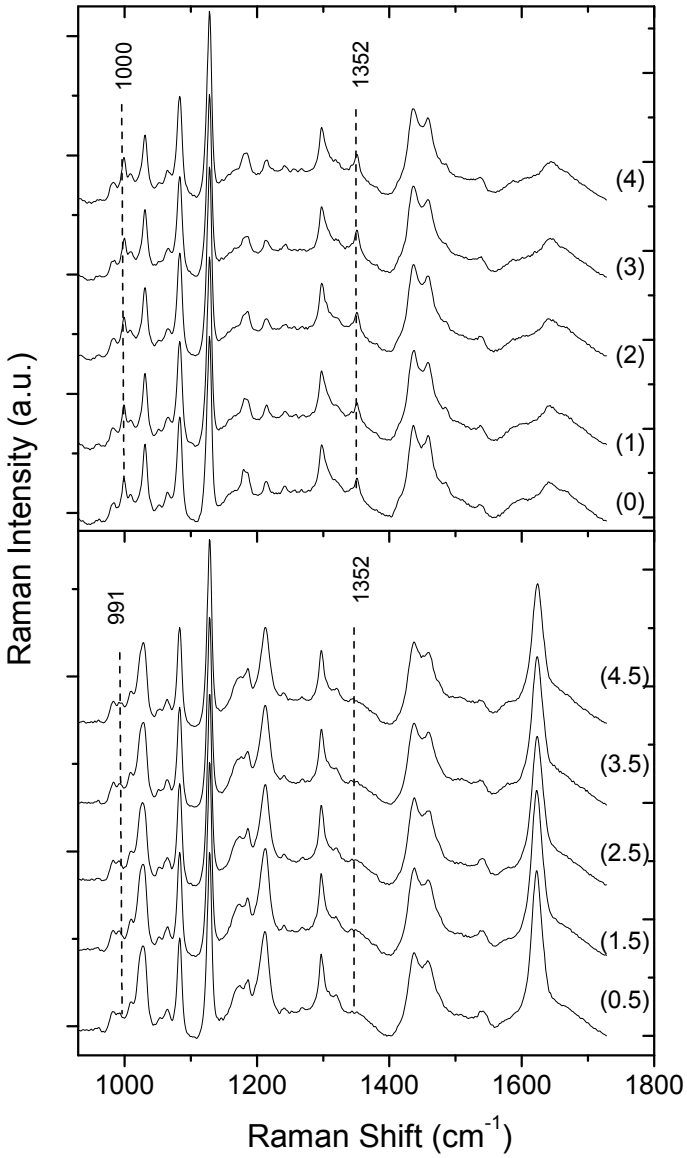


Figure 5.7. Potential dependence of SERS spectra of $NB^-$ switching between 0 V and -0.8 V (vs Ag/AgCl) in basic solution on $C_{12}$ modified Ag surface. The legend numbers (#) are corresponding to the sequence of the measurements. Potentials are 0 V for #0, 1, 2, 3, and 4, and -0.8 V for #0.5, 1.5, 2.5, 3.5, and 4.5. (NBS =1 mM, CPC=1 mM, $Na_2SO_4$=10 mM, and NaOH=1 mM)

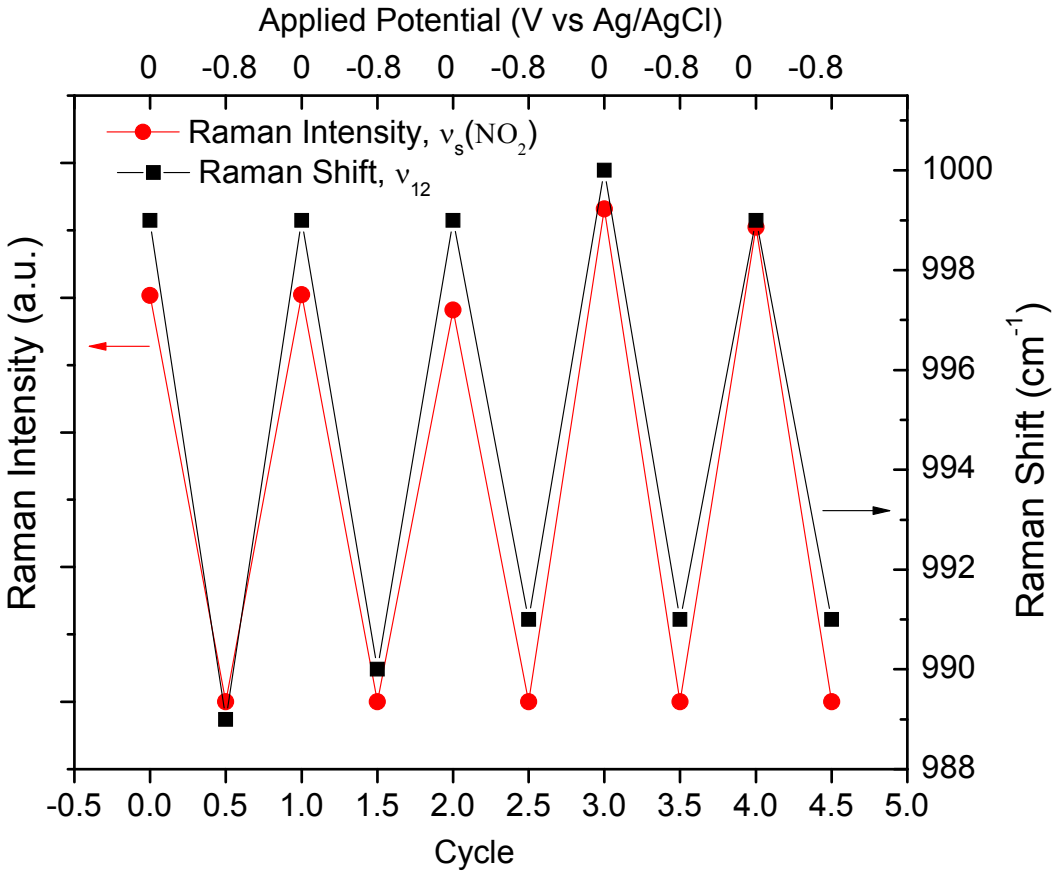


Figure 5.8. SERS intensities of $\nu_s(NO_2)$ and band frequencies of $\nu_{12}$ vary with applied potential between 0 and -0.8 V (vs Ag/AgCl). Potentials are 0 V for #0, 1, 2, 3, and 4, and -0.8 V for #0.5, 1.5, 2.5, 3.5, and 4.5. (NBS =1 mM, CPC=1 mM, $Na_2SO_4$=10 mM, and NaOH=1 mM)

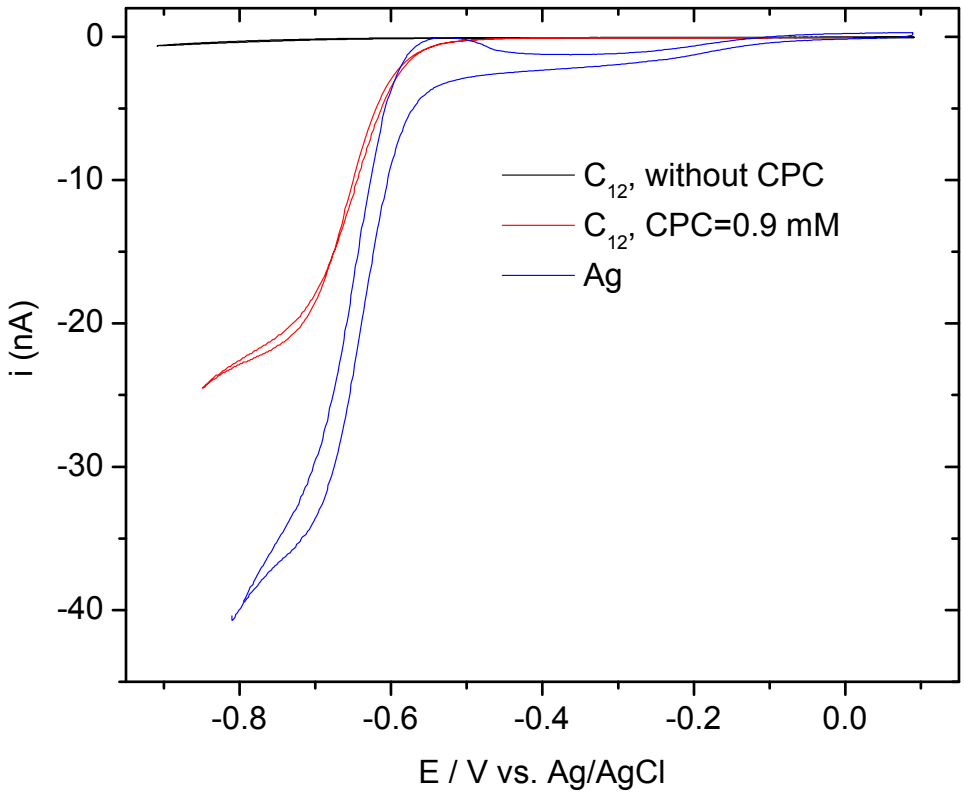


Figure 5.9. Cyclic voltammograms of NBS (2 mM) on a bare Ag surface and on a $C_{12}$ modified Ag surface with and without CPC (0.9 mM). ($Na_2SO_4$=100 mM for all measurements)

Ag surface. This result suggests that the Ag surface is well protected by the $C_{12}$ monolayer, avoiding nonspecific adsorption or reduction. With the addition of $CP^+$ to the $NB^-$ solution, around 50% of the reduction current can be obtained on $C_{12}$ surface as compared to the reduction of $NB^-$ on bare Ag surface, demonstrating the significance of the $CP^+$ in accumulating the $NB^-$ to the $C_{12}$ surface. Using $C_{12}$ modification and ionic surfactants, the adsorption and reduction no longer depend on the affinity of the molecules to the Ag surface. Instead, the affinities of the molecules to the ionic surfactant govern their binding to the surface, which allows selective adsorption and reduction on the surface.

## 5.4 Conclusions

Ion interaction was used to accumulate the ionic analyte, nitrobenzenesulfonate ($NB^-$) to a 1-dodecanthiol modified silver surface ($C_{12}$). With $CP^+$ in solution, significant accumulation of $NB^-$ can be observed on the $C_{12}$ surface, and the immobilization is stable enough to allow its reduction to be studied by CV and SERS. Repeatable measurement on the same electrode is realized because adsorption/desorption of $NB^-$ and its reduction products on the $C_{12}$ surface is fully reversible. Protected by the hydrophobic monolayer, nonspecific adsorption can be avoided on the electrode surface, which provides high selectivity for reduction of analytes that show strong affinity to the ionic surfactant.

## 5.5 References

(1) Strehlitz, B.; Gruendig, B.; Schumacher, W.; Kroneck, P. M. H.; Kotte, H. *Anal. Chem.* **1996**, *68*, 807-816.

(2) Murgida, D. H.; Hildebrandt, P. *Journal of the American Chemical Society* **2001**, *123*, 4062-4068.

(3) Murgida, D. H.; Hildebrandt, P. *Accounts of Chemical Research* **2004**, *37*, 854-861.

(4) Yantasee, W.; Lin, Y.; Fryxell, G. E.; Busche, B. J. *Anal. Chim. Acta* **2004**, *502*, 207-212.

(5) Chaki, N. K.; Vijayamohanan, K. *Biosens. Bioelectron.* **2002**, *17*, 1-12.

(6) Matthews, J. R.; Tuncel, D. n. s.; Jacobs, R. M. J.; Bain, C. D.; Anderson, H. L. *Journal of the American Chemical Society* **2003**, *125*, 6428-6433.

(7) Liu, Y.; Mu, L.; Liu, B. H.; Zhang, S.; Yang, P. Y.; Kong, J. L. *Chemical Communications* **2004**, 1194-1195.

(8) Love, J. C.; Estroff, L. A.; Kriebel, J. K.; Nuzzo, R. G.; Whitesides, G. M. *Chemical Reviews* **2005**, *105*, 1103-1169.

(9) Oskarsson, H.; Holmberg, K. *J. Colloid Interface Sci.* **2006**, *301*, 360-369.

(10) Grant, L. M.; Ederth, T.; Tiberg, F. *Langmuir* **2000**, *16*, 2285-2291.

(11) Yuan, S.; Hu, C.; Hu, S. *Electrochim. Acta* **2006**, *51*, 5274-5285.

(12) Jones, C. L.; Bantz, K. C.; Haynes, C. L. *Anal. Bioanal. Chem.* **2009**, *394*, 303-311.

(13) Olson, L. G.; Harris, J. M. *Appl. Spectrosc.* **2008**, *62*, 149-156.

(14) Olson, L. G.; Uibel, R. H.; Harris, J. M. *Appl. Spectrosc.* **2004**, *58*, 1394-1400.

(15) Shafer-Peltier, K. E.; Haynes, C. L.; Glucksberg, M. R.; VanDuyne, R. P. *J. Am. Chem. Soc.* **2003**, *125*, 588-593.

(16) Yonzon, C. R.; Haynes, C. L.; Zhang, X.; Walsh, J. T., Jr.; Van, D. R. P. *Anal. Chem.* **2004**, *76*, 78-85.

(17) Pedrosa, V. A.; Caetano, J.; Machado, S. A. S.; Freire, R. S.; Bertotti, M. *Electroanalysis* **2007**, *19*, 1415-1420.

(18) Kim, J. M.; Park, J. Y.; Song, S. H.; Lee, B. J.; Muramatsu, H.; Chang, S. M. *Sens. Actuators, B* **2001**, *B76*, 74-79.

(19) Jordon, C. E.; Frey, B. L.; Kornguth, S.; Corn, R. M. *Langmuir* **1994**, *10*, 3642-3648.

(20) Zhu, M.; Schneider, M.; Papastavrou, G.; Akari, S.; Mohwald, H. *Langmuir* **2001**, *17*, 6471-6476.

(21) Niki, K.; Hardy, W. R.; Hill, M. G.; Li, H.; Sprinkle, J. R.; Margoliash, E.; Fujita, K.; Tanimura, R.; Nakamura, N.; Ohno, H.; Richards, J. H.; Gray, H. B. *The Journal of Physical Chemistry B* **2003**, *107*, 9947-9949.

(22) Schouten, S.; Stroeve, P.; Longo, M. L. *Langmuir* **1999**, *15*, 8133-8139.

(23) Oklejas, V.; Uibel, R. H.; Horton, R.; Harris, J. M. *Analytical Chemistry* **2008**, *80*, 1891-1901.

(24) Masadome, T.; Ueda, A.; Kawakami, M. *Anal. Lett.* **2004**, *37*, 225-233.

(25) Chrisey, L. A.; Lee, G. U.; O'Ferrall, C. E. *Nucleic Acids Res.* **1996**, *24*, 3031-3039.

(26) Smith, E. A.; Wanat, M. J.; Cheng, Y.; Barreira, S. V. P.; Frutos, A. G.; Corn, R. M. *Langmuir* **2001**, *17*, 2502-2507.

(27) Brockman, J. M.; Frutos, A. G.; Corn, R. M. *J. Am. Chem. Soc.* **1999**, *121*, 8044-8051.

(28) Goloub, T. P.; Koopal, L. K. *Langmuir* **1997**, *13*, 673-681.

(29) Gerlache, M.; Senturk, Z.; Quarin, G.; Kauffmann, J.-M. *J. Solid State Electrochem.* **1997**, *1*, 155-160.

(30) Gasser-Ramirez, J. L.; Harris, J. M. *Anal. Chem. (Washington, DC, U. S.)*, *82*, 5743-5750.

(31) Iskandarani, Z.; Pietrzyk, D. J. *Anal. Chem.* **1982**, *54*, 1065-1071.

(32) Milton, H. *Ion-Pair Chromatography*; Marcel Dekker, Inc: New York 1985.

(33) Cecchi, T. *Crit. Rev. Anal. Chem.* **2008**, *38*, 161-213.

(34) Gao, P.; Gosztola, D.; Weaver, M. J. *J. Phys. Chem.* **1988**, *92*, 7122-7130.

(35) Lecomte, S.; Ricoux, R.; Mahy, J. P.; Korri-Youssoufi, H. *J Biol Inorg Chem* **2004**, *9*, 850-858.

(36) Tognalli, N. G.; Fainstein, A.; Vericat, C.; Vela, M. E.; Salvarezza, R. C. *J. Phys. Chem. B* **2006**, *110*, 354-360.

(37) Kreisig, S. M.; Tarazona, A.; Koglin, E.; Schwuger, M. J. *Langmuir* **1996**, *12*, 5279-5288.

(38) Osawa, M.; Matsuda, N.; Yoshii, K.; Uchida, I. *J. Phys. Chem.* **1994**, *98*, 12702-12707.